UCRL-10865

University of California

Ernest O. Lawrence Radiation Laboratory

I. TENSOR-FORCE EFFECTS IN THE NUCLEAR SHELL THEORY

II. NUCLEAR SPECTROSCOPIC STUDIES OF ISOMERIC STATES IN ODD-ODD YTTRIUM NUCLEI

TWO-WEEK LOAN COPY

This is a Library Circulating Copy which may be borrowed for two weeks. For a personal retention copy, call Tech. Info. Division, Ext. 5545

DISCLAIMER

This document was prepared as an account of work sponsored by the United States Government. While this document is believed to contain correct information, neither the United States Government nor any agency thereof, nor the Regents of the University of California, nor any of their employees, makes any warranty, express or implied, or assumes any legal responsibility for the accuracy, completeness, or usefulness of any information, apparatus, product, or process disclosed, or represents that its use would not infringe privately owned rights. Reference herein to any specific commercial product, process, or service by its trade name, trademark, manufacturer, or otherwise, does not necessarily constitute or imply its endorsement, recommendation, or favoring by the United States Government or any agency thereof, or the Regents of the University of California. The views and opinions of authors expressed herein do not necessarily state or reflect those of the United States Government or any agency thereof or the Regents of the University of California.

Research and Development

UCRL-10865
UC-4 Chemistry
TID-4500 (19th Ed.)

UNIVERSITY OF CALIFORNIA
Lawrence Radiation Laboratory
Berkeley, California

Contract No. W-7405-eng-48

I. TENSOR-FORCE EFFECTS IN THE NUCLEAR SHELL THEORY
II. NUCLEAR SPECTROSCOPIC STUDIES OF ISOMERIC STATES IN ODD-ODD YTTRIUM NUCLEI

Yeong E. Kim

(Ph.D. Thesis)

June 12, 1963

Printed in USA. Price $2.75. Available from the
Office of Technical Services
U. S. Department of Commerce
Washington 25, D.C.

I. TENSOR-FORCE EFFECTS IN THE NUCLEAR SHELL THEORY
II. NUCLEAR SPECTROSCOPIC STUDIES OF ISOMERIC STATES IN ODD-ODD YTTRIUM NUCLEI

Contents

Abstract v

I. Tensor-Force Effects in the Nuclear Shell Theory

A. Introduction 1

B. Theory

1. j-j-Coupling Shell Model 3

2. Particle-Hole Interaction 4

3. Two-Body Residual Interaction 16

C. Particle-Particle Interaction

1. Yttrium-90 31

2. Bismuth-210 and Polonium-210 46

D. Particle-Hole Interaction 83

1. Thallium-208 83

2. Bismuth-208 86

E. Conclusion 100

II. Nuclear Spectroscopic Studies of Isomeric States in Odd-Odd Yttrium Nuclei

A. Introduction 101

B. Experimental Techniques

1. Instruments 102

2. Source Production and Chemistry 102

C. Decay-Scheme Studies 105

1. Yttrium-86m 105

2. Yttrium-90m 119

D. Conclusion 121

Acknowledgments 122

Appendices

A. Central-Force Matrix Element 123
B. Tensor-Force Matrix Element 129
C. Fortran Programs 133
D. Fortran Listing (1a) 142
E. Fortran Listing (1b) 156
F. Fortran Listing (2) 159
G. Fortran Listing (3) 171
References 175

I. TENSOR-FORCE EFFECTS IN THE NUCLEAR SHELL THEORY
II. NUCLEAR SPECTROSCOPIC STUDIES OF ISOMERIC STATES IN ODD-ODD YTTRIUM NUCLEI

Yeong E. Kim

(Ph.D. Thesis)

Lawrence Radiation Laboratory
University of California
Berkeley, California

June 12, 1963

ABSTRACT

The low-lying energy levels of odd-odd nuclei near the doubly closed shell (Y^{90}, Bi^{208}, Bi^{210}, and Tl^{208}) are calculated with finite-range central and tensor forces to the first order by means of the j-j coupled odd-group model. The two-body matrix elements for the central and tensor forces are expressed in the j-j representation, from which a generalization to off-diagonal matrix elements is obtained in the limit of zero range. A nucleon-nucleon Gaussian potential without a hard core based on the free two-nucleon potentials of Blatt-Jackson and Brueckner-Gammel-Thaler is used for the residual interaction. Eigenvalues and eigenvectors are presented and compared with experimental spectra.

The tensor-force effects are examined in detail as a function of the force range for the nuclei Y^{90} and Bi^{210}. A tensor force with reasonable range and strength accounts for the 1- state of the $h_{9/2}g_{9/2}$ multiplet being the ground state of Bi^{210}, instead of the 0- predicted by central forces. The low-lying energy levels of Po^{210} are also calculated with the same residual force used for Bi^{210} in order to obtain the RaE beta-decay matrix-element ratio $i\langle \underset{\sim}{r}\rangle/\langle \underset{\sim}{\sigma}\times\underset{\sim}{r}\rangle$. It is shown that the ground-state wave functions for Bi^{210} and Po^{210} are consistent with the experimentally determined RaE beta-decay matrix-element ratio and the measured magnetic dipole moment of Bi^{210}. The ground-state wave function

for Y^{90} is also consistent with the measured magnetic dipole moment of Y^{90}. A high-spin (J=11) isomeric state in Po^{210} is predicted with an estimated gamma partial lifetime of the order of microseconds.

A 48±1 min isomeric level in Y^{86} was produced by irradiations of rubidium (natural and enriched in Rb^{85}) with alpha particles and of strontium (natural and enriched in Sr^{86}) with deuterons. Two transitions with energies 10.15±0.1 keV and 208.0±0.3 keV were observed in the decay of Y^{86m}. From the L sub-shell ratios the multipolarity of the 10-keV transition was determined to be E3. The K-conversion coefficient of the 208-keV transition is $\epsilon_K = 0.04 \pm 0.01$. A possible decay scheme of Y^{86m} is suggested. The energy of the isomeric transition in Y^{90m} was measured to be 202.4±0.3 keV by use of a permanent-magnet 180 deg spectrograph.

I. TENSOR-FORCE EFFECTS IN THE NUCLEAR SHELL THEORY

A. INTRODUCTION

Within the past several years detailed information on nuclear spectra of the nuclei near the doubly-closed shell has become available from nuclear spectroscopy and from high-resolution nuclear reaction studies. This new information called for a refined theoretical analysis of these nuclear spectra. Since experimental information is rapidly increasing, it is worthwhile to perform a theoretical calculation of these spectra, with the hope that it might provide useful information on the effective interaction between protons and neutrons in the finite nuclei. In particular, theoretical studies of the odd-odd nuclei are very important because the Pauli principle permits all possible components of the residual force to be operative for the nonidentical nucleons.

We shall adopt the odd-group model with j-j coupling in which the nuclear properties of the nucleus are assumed to be determined by the propœrties of the odd-group particles. In our treatment of odd-odd nuclei, we assume that the residual interaction between proton and neutron is sufficiently weak so that we can neglect excited configurations of the "nuclear core", and further that the wave function is a vector-coupled product of the wave functions of two odd-group particles. Of course, it is well-known that nuclear moments and electric transition probabilities generally are sensitive to certain core polarization phenomena, but the energy-level spacings at energies below that of core-excited states may generally not be seriously affected by neglect of core excitations.

In order to justify the theoretical basis of the well-known Nordheim's coupling rule,[1] de-Shalit investigated the case of nuclei with one proton and neutron outside closed shells by using the zero-range force between them, and obtained expressions for the diagonal matrix elements.[2] Calculations for specific odd-odd nuclei have been made by several workers for the finite-range force in which central exchange forces are included.[3,4]

We shall use the central and tensor parts of the nuclear force, neglecting the spin-orbit force entirely. This practice is probably

reasonable, because it appears that the existence of the spin-orbit force in the nuclear force is still questionable. The residual interaction of nucleons outside closed shells is not well known, and there seem to be no a priori reasons for retaining the same strength parameters of the free two-nucleon problem for the residual interaction. However, because of our ignorance of the exact form of the residual interaction, we shall rely upon the free two-nucleon force parameters in estimating the strengths of our forces, which we hope simulates the residual interaction.

B. THEORY

1. j-j-Coupling Shell Model

Before discussing the tensor-force effects in detail, we describe the basic assumptions that enter into our calculation.

a. Wave function and Hamiltonian. In our odd-group model, we assume that the doubly closed shell can be treated as an inert core giving rise to the central field in which nucleons outside the doubly closed shell move. This assumption simplifies the calculation, since we treat only two nucleons outside the doubly closed shell. The wave function is then the j-j-coupled new basis vector, which is a simple vector product of the wave functions of nucleons 1 and 2 coupled to a total angular momentum J

$$|a\rangle = R_1(r_1)R_2(r_2)\,|j_1 j_2 JM\rangle,$$

where $R_1(r_1)R_2(r_2)$ is the radial part of the wave function, and $|j_1 j_2 JM\rangle$ is the angular part. Here it is understood that the wave function must be antisymmetrized for two identical nucleons. In our j-j-coupled odd-group model, the Hamiltonian describing these nuclei at low energy is assumed to be written as

$$H = H_1 + H_2 + V_{12} ,$$

where H_1 and H_2 are the single-particle Hamiltonians, and V_{12} is the residual interaction between particles 1 and 2. It is assumed that H_i acting on our wave function yields

$$H_i\,|a\rangle = \epsilon_0^i\,|a\rangle ,$$

where ϵ_0^i denotes single-particle energies for the particle i.

b. Zero- and first-order approximations. In the zero-order approximation, the sum of the single-particle energies ϵ_1^1 and ϵ_2^2 are the zero-order energies. Single-particle energies have been estimated in several works,[5,6]

but one cannot avoid arbitrariness in choosing the parameters involved. Instead we rely on the experimental single-particle levels of neighboring nuclei to eliminate the ambiguity. We treat V_{12} as a perturbation of the central field of the shell-model core, and evaluate the first-order perturbation term. The total energy for the state of a given J is then approximately

$$E \approx \sum \epsilon_0^i + \epsilon_1 \quad ;$$

for i = 1 or 2, where the higher terms are neglected. It is clear that V_{12} removes the degeneracy of the state with various J values arising from a given configuration. The value of ϵ_1, and consequently E, is obtained from the eigenvalue equation

$$\sum_{a'} [\langle a|V_{12}|a'\rangle - (E-\epsilon_{0_{a'}})\delta_{a,a'}] \langle a'|aJM\rangle = 0$$

The summation is restricted to the configurations obtained from the experimental single-particle levels of neighboring nuclei for the numerical calculations.

2. Particle-Hole Representation

In order to extend our calculations to the case of nuclei with the doubly closed-shell core plus one particle and hole (Tl^{208} and Bi^{208}), it is convenient to use the method of the second quantization. Brink and Satchler[7] showed that the occupation-number representation of Dirac[8] leads to a simpler procedure than the conventional one for the calculation of the matrix elements of operators in the shell model. The concept of particles and holes in the shell model in this representation was discussed thoroughly by Brink and Satchler, and some applications were made by Carter et al.[9] for calculations of the core-excited states in Pb^{208}. In the following, only the basic concepts leading to the

final expression for the matrix elements of the particle-hole interaction are presented. The more detailed description of the operator formalism of the second quantization many be found elsewhere.[10]

a. Occupation-number representation. As a basis for a system of n fermions, we may take the set of all antisymmetrized products of orthonormal single-particle states $|\alpha\rangle$ with eigenvalues α:

$$
\begin{aligned}
& A|\alpha^a\alpha^b\alpha^c \text{----} \alpha^g\rangle \\
&= (n!)^{-1/2} \sum P|\alpha_1^a\rangle\alpha_2^b\rangle\,|\alpha_3^c\rangle \text{----} |\alpha_n^g\rangle \\
&= (n!)^{-1/2} \begin{vmatrix} |\alpha_1^a\rangle & |\alpha_2^a\rangle & \text{-----} & |\alpha_n^a\rangle \\ |\alpha_1^b\rangle & |\alpha_2^b\rangle & \text{-----} & |\alpha_n^b\rangle \\ \vdots & \vdots & & \vdots \\ |\alpha_1^g\rangle & |\alpha_2^g\rangle & \text{-----} & |\alpha_n^g\rangle \end{vmatrix} \\
&= (n!)^{-1/2} \det\,[a\ b\ c \text{----} g]\ .
\end{aligned}
$$

Here A is an antisymmetrization operator defined as

$$A = (n!)^{-1/2} \sum P\ ,$$

where P is the permutation operator which takes either positive or negative sign according to whether P is an even or odd permutation, respectively. The superscripts refer to a set of quantum numbers (ℓ, j, m, etc.) which is necessary to specify a single-particle state, and the subscripts label n particles in an arbitrary arrangement.

Another way of obtaining a basis function is to state the probability amplitudes for finding n_1 particles in an eigenstate $|1\rangle$ and n_2 particles in an eigenstate $|2\rangle$, etc. Suppose n_1, n_2, n_3,... are the

numbers of fermions in the states $|\alpha^{(1)}\rangle$, $|\alpha^{(2)}\rangle$, $|\alpha^{(3)}\rangle$ ---, respectively. Then obviously, by definition, we have

$$n_1 + n_2 + n_3 + \dots = n ,$$

and eigenvalues are related to these occupation numbers by a linear equation

$$\alpha^a + \alpha^b + \alpha^c + \dots = n_1 \alpha^{(1)} + n_2 \alpha^{(2)} + n_3 \alpha^{(3)} + \dots \quad .$$

We treat the occupation numbers n_1 , n_2 , $\cdots$ etc. as dynamical variables or observables. Each of these variables has the eigenvalue 0 or 1 because only the fermions are considered here. The numbers n_1, n_2 $\cdots$ form a complete set of commuting variables for the fermion assembly. The set of states diagonal in the n's forms a basis for the occupation-number representation. A state in this set is determined by specifying the values of the occupation numbers of the single-particle states.

The basis for the n-fermion system in the occupation-number representation can be conveniently described if we define a set of creation operators η_a^+ and a vacuum state $|0\rangle$ (representing the closed-shell configuration) by the equation

$$\eta_a^+ \eta_b^+ \eta_c^+ \cdots \eta_g^+ |0\rangle = (n!)^{-1/2} \det [a\ b\ c \cdots g]$$

Suppose we interchange a pair of indices. Then we obtain

$$(n!)^{-1/2} \det [a\ b\ c \cdots g] = - (n!)^{-1/2} \det [b\ a\ c \cdots g]$$

$$= - \eta_b^+ \eta_a^+ \eta_c^+ \cdots \eta_g^+ |0\rangle$$

This suggests that these creation operators must have the property

$$\eta_a^+ \eta_b^+ + \eta_b^+ \eta_a^+ \equiv [\eta_a^+ , \eta_b^+]_+ = 0$$

in order to maintain the proper symmetry requirement for the state. Similarly, we define the conjugate imaginary state $\langle 0|$ of a vacuum state and the annihilation operator η_a (which is the adjoint of η_a^+) by

$$\langle 0|\eta \cdots \eta_c \eta_b \eta_a \equiv (n!)^{-1/2} \det{}^* [a\, b\, c \cdots g]$$

so that

$$\eta_a \eta_b + \eta_b \eta_a \equiv [\eta_a , \eta_b]_+ = 0.$$

Furthermore, the symmetry and normalization relations require that

$$\langle 0| \eta_{g'} \cdots \eta_{c'} \eta_{b'} \eta_{a'} \eta_a^+ \eta_b^+ \eta_c^+ \cdots \eta_g |0\rangle$$

$$= \frac{1}{n!} \int \det{}^*[a'b' \cdots g'] \det [a\, b \cdots g]\, d\tau_1 \cdots d\tau_n$$

$= +1$, if the sets $(a\, b\, c \cdots g)$ and $(a'\, b'\, c' \cdots g')$ are the same sets and differ by an even permutation,

$= -1$, if they are the same and differ by an odd permutation,

$= 0$, if they are not the same set.

These requirements can be incorporated into our formalism if we assume that

$$\eta_{a'} | 0\rangle = 0 ,$$

$$\langle 0| \eta_a^+ = 0 ,$$

$$\langle 0| 0\rangle = 1 ,$$

and

$$\eta_{a'} \eta_a^+ + \eta_a^+ \eta_{a'} \equiv [\eta_{a'} , \eta_a^+] = \delta_{a,a'} .$$

Conversely, we may state that the basic states in the occupation-number representation can be built up from the vacuum states by introducing the creation operator η_a^+ and its adjoint, the annihilation operator η_a, for each single-particle state $|\alpha^a\rangle$, and imposing the simple anti-commutation relation between them as described above.

Now let us consider a single-particle operator, T, which is a symmetric sum of single-particle operators t_i,

$$T = \sum_i t_i ,$$

where t_i acts only on the ith particle. It can be shown[8] that in occupation-number representation this operator has the form

$$T = \sum_{a,b} \eta_a^+ \eta_b \langle \alpha^a | t | \alpha^b \rangle ,$$

where $\langle \alpha^a | t | \alpha^b \rangle$ is the matrix element of t between single-particle states $|\alpha^a\rangle$ and $|\alpha^b\rangle$. The two-body operator,

$$V = \sum_{ij} v_{ij} ,$$

can be expressed as

$$V = \sum_{abcd} \eta_a^+ \eta_b^+ \eta_d \eta_c \langle \alpha^a \alpha^b | v | \alpha^c \alpha^d \rangle .$$

For a mixed system, such as in nuclei, of two different fermions, two formalisms may be used. The first is to regard neutrons and protons as different states of the same fundamental particle by adopting the isobaric spin formalism, and require complete antisymmetry of the wave

function with respect to exchange of isobaric spin as well as space and ordinary spin variables. Then the subscript of the operator η includes the quantum number specifying the isobaric spin for the state in addition to the space and spin quantum numbers. In this way the complete antisymmetry for the mixed system of two different nucleons is ensured. The second method is the conventional one in which protons and neutrons are regarded as distinct particles, and no symmetry requirement is imposed on the interchange of one kind with the other. This implies that we must define two different sets of creation operators, η and ξ, one for each kind of particle, and impose the commutation relation between one kind and the other, while still keeping the anticommutation relation among themselves.

It should be noted here that the use of the isobaric formalism for the nucleon system does not introduce physical consequence any different from the result of the treatment of protons and neutrons as distinct particles. One has to be cautious, however, when dealing with a mixed system of fermions that has more than two isobaric spin states, such as the sigma particles (Σ^+, Σ^-, and Σ^0), because the isobaric formalism does not necessarily yield the same physical results as the conventional one.

b. Vector-coupled states. In most shell-model calculations, we are interested in states that are eigenfunctions of the angular momenta. For this purpose, we specify the angular-momentum quantum numbers (j,m) for the one-particle state and write the state vector as

$$|jm\rangle = \eta^+_{jm} \; |0\rangle ,$$

where all other quantum numbers that may be required to specify the state completely are not written explicitly. Because η^+_{jm} has the same transformation properties as the corresponding state $|jm\rangle$, η^+_{jm} transforms under rotations of the coordinate system as the mth row of the matrix element of finite rotation $D^j(\alpha, \beta, \gamma)$.[11] Vector-coupled states of two particles may then be constructed in the usual way

$$|j_1 j_2\ JM\rangle = N \sum_{m_1} \eta^+_{j_1 m_1}\ \eta^+_{j_2\ M-m_1}\ |0\rangle\ (j_1 m_1 j_2 M-m_1\ |JM)\ ,$$

where $(j_1 m_1 j_2 M-m_1 |JM)$ is the usual vector-coupling coefficient. The factor N is necessary to account for the normalization, and in most cases takes unity, except that it is $(2)^{-1/2}$ when two particles are in the same orbit $(j_1 = j_2)$.

This procedure may be extended to construct states for n-particle systems. This can be done by operating with a creation operator on the vectors for (n-1) particles, and taking proper linear combinations. We consider n particles in the same orbit j in some symmetric order $\beta(n)$ with total angular momentum J. Since the occupation number of the state $|\alpha^a\rangle$ is the eigenvalue of

$$\eta^+_a\ \eta_a\ |\ \alpha^a\ \rangle = n_a\ |\ \alpha^a\ \rangle\ ,$$

the total number in the orbit j is given by

$$n = \sum_m n_m = \sum_m \eta^+_{jm}\ \eta_{jm}\ .$$

We may expand into intermediate states of (n-1) particles in the arrangement γ (n-1) to obtain

$$n|\ \beta(n)JM\rangle = \sum_m \eta^+_{jm}\ \eta_{jm}\ |\ \beta\ (n)\ JM\rangle$$

$$= \sum_{m,\beta,p} \eta^+_{jm}\ |\gamma\ (n-1)_p JM_p\rangle\ \langle\gamma\ (n-1)J_p|\ \eta_{jm}|\beta(n)JM\rangle$$

$$= \sum_{m,\beta,p} \eta^+_{jm}\ |\gamma\ J_p M_p\rangle\ \langle\gamma\ J_p\ \|\ \eta_j\ \|\ \beta J\rangle\ (J_p M_p\ jm\ |JM)\ .$$

The last expression is obtained by the use of the Wigner-Eckart theorem.[11] This method is very similar to the ordinary seniority scheme, and in fact the reduced matrix element appearing in the last expression is related to the coefficient of fractional parentage by[12]

$$n^{-1/2}\langle\gamma(n-1)J_p\|\eta_j\|\beta(n)J\rangle = \langle\gamma(n-1)J_p j\,|\}\beta(n)J\rangle .$$

c. Particle-hole concept. When all $2j + 1$ single-particle magnetic substates $j > m > -j$ are occupied, a shell or orbit is said to be closed. We represent this closed shell by a single vector $|n_{jm}=1, \text{ all } m\rangle$ or $|C\rangle$, which is a spherically symmetric state with total angular momentum $J = 0$. One extra particle in the single-particle state $|j'm'\rangle$ outside the closed shell is represented by the resultant vector

$$|(C + 1)j'm'\rangle = \eta^{+}_{j'm'}|C\rangle .$$

Similarily, a shell filled by $2j$ particles with a resultant angular momentum j or the absence of a particle from the state $|j-m\rangle$ may be represented by the vector

$$|(C - 1)jm\rangle = (-1)^{j + m}\,\eta_{j-m}|C\rangle .$$

The phase factor $(-1)^{j + m}$ and the reversal of sign for m are necessary because our basic single-particle states are spherically symmetric and hence we require that η^{+}_{jm} and η_{jm} transform under finite rotation in the same way. The annihilation operator η_{jm} transforms as the complex conjugate $(D^{j}_{m',m}(\alpha,\beta,\gamma))^{*}$ which is equal to $(-1)^{m'-m}D^{j}_{-m',-m}(\alpha,\beta,\gamma)$, so that if we choose $(-1)^{j + m}\,\eta_{j-m}$ instead of η_{jm} , it will transform under rotation as the $\underline{m}$th row of $D^{j}_{m',m}(\alpha,\beta,\gamma)$ in the same way as η^{+}_{jm} . Generalizing this to a system with some closed shells (denoted by C) plus n particles in some arrangement $\beta(n)$, we may represent this state in the occupation-number representation as the product vector

$$|C + \beta(n)\rangle = |C\rangle\,|\beta(n)\rangle \quad ,$$

where $|\beta(n)\rangle$ is to be built up from single-particle vectors.

For the system of closed shells C plus n vacancies or holes, we may regard $(-1)^{j+m}\,\eta_{j-m}$ as the hole-creation operator with angular momentum j, and η^{+}_{j-m} as the hole-annihilation operator, because any occupation-number vector can be equally well regarded as describing the number of holes in each state so that the superposition of such vectors describing the arrangement $|\delta\rangle$ of (C-n) particles can also be understood as describing the conjugate state $|\delta\rangle$ of n holes. Furthermore, we do not need to know the exact relation between such conjugate states, since the hole states form a complete set themselves and may be used throughout. The basic single-hole states are

$$|jm\rangle = (-1)^{j+m}\,\eta_{j-m}|C\rangle \; .$$

With the above conventions, we may write for (C - n) particles

$$|\overline{C} + \overline{\beta}(n)\rangle = |\overline{C}\rangle\,|\overline{\beta}(n)\rangle \; ,$$

where $\overline{C}$ refers now to all completely unoccupied shells, and $\overline{\beta}(n)$ is built up from single-hole states.

d. <u>Matrix elements of the particle-hole interaction</u>. So far, we have discussed the basic concept of the particle and hole in the shell model in terms of the second quantization method. We now apply this formalism to evaluate the matrix elements of the two-body operator $V = \frac{1}{2}\sum_{i \neq j} v_{ij}$ for a system of C particles in which there is one vacancy or hole in the closed shells, and one particle in an orbit outside the closed shells $|C\rangle$. The particle-plus-hole state is given by operating the operators η and η^{+} on the closed-shell vector $|C\rangle$,

$$|\overline{j}_1 j_2 JM\rangle = \sum_m (-1)^{j_1-m}\,\eta_{j_1 m}\,\eta^{+}_{j_2 M+m}|C\rangle(j_1 -m j_2 M+m|JM\rangle \; ,$$

where the hole quantum numbers are distinguished by a bar. We are interested here in evaluating the matrix element

$$\langle \bar{j}_1 j_2 JM | V | \bar{j}_1' j_2' JM \rangle = \sum_{m,m'} (-1)^{j_1 - m + j_1' - m'} (j_1 - m j_2 M+m | JM)$$

$$\times \quad (j_1' - m' j_2' M+m' | JM) \sum_{abcd} \langle ab | v_{12} | cd \rangle$$

$$\times \quad \langle C | \eta_{j_2 M+m} \, \eta^+_{j_1 m} \, \eta^+_a \eta^+_b \eta_d \eta_c \eta_{j_1' m'} \eta^+_{j_2' M+m'} | C \rangle \; .$$

The sum over a, b, c, and d may be divided into three sets of terms: (a) a set in which all indices refer to states in C, so that we have either a=c, b=d, or a=d, b=c ($j_1=j_1'$ and $j_2=j_2'$); (b) one in which only one pair refers to states in C, so that we have $j_1=j_1'$ or $j_2=j_2'$, and (c) one in which none refers to C, so that we have $j_1 \neq j_1'$ and $j_2 \neq j_2'$. After some manipulation of the creation and annihilation operators by using the anticommutation relation already mentioned, these three sets of terms reduce to

$$\langle \bar{j}_1 j_2 JM | V | \bar{j}_1' j_2' JM \rangle = \sum_{j_c, j_c'} \frac{1}{2} \; \langle j_c j_c' JM | V | j_c j_c' JM \rangle_a$$

$$+ \sum_{j_c} \left[- \langle j_c j_1 JM | V | j_c j_1 JM \rangle_a + \langle j_c j_2 JM | V | j_c j_2 JM \rangle_a \right]$$

$$+ \; \langle \bar{j}_1 j_2 JM | i_{12} | \bar{j}_1' j_2' JM \rangle_a$$

where the subscript a refers to only like particles with the following antisymmetrization:

$$\langle j_1 j_2 JM|V|j_1' j_2' JM\rangle_a = \langle j_1 j_2 JM|V|j_1' j_2' JM\rangle - (-1)^{j_1'+j_2'-J}\langle j_1 j_2 JM|V|j_2' j_1' JM\rangle .$$

The first term of these three sets of terms represents the total core energy, and we may consider this term as our zero point of energy. The second term represents the interaction of the core with one hole, and the third term is the interaction of the core with the one extra particle outside the closed shells. The minus sign of the second term can be physically understood if one remembers that the total core energy already included the interaction of the particle that is missing from the core with all the other particles in the core. The second and third terms are considered to be the single-hole or -particle energies of the hole or particle, respectively, and are estimated from the single-hole or -particle levels of neighboring nuclei as discussed in the Section B1.

The last term $\langle \bar{j}_1 j_2 JM|i_{12}|\bar{j}_1' j_2' JM\rangle$ represents the particle-hole interaction and may be expressed as (for simplicity, the subscript a is omitted in the following)

$$\langle \bar{j}_1 j_2 JM|i_{12}|\bar{j}_1' j_2' JM\rangle = -\sum_{m,m} (-1)^{j_1-m+j_1'-m'} (j_1 -m j_2 M+m|JM)(j_1' -m' j_2' M+m'|JM)$$

$$\times \langle j_1' m' j_2 M+m|v_{12}|j_1 m j_2' M+m'\rangle .$$

Note the minus sign in front of the summation. It indicates that the particle-hole interaction may be regarded as repulsive for an attractive force. Since $\langle \bar{j}_1 j_2 JM|i_{12}|\bar{j}_1' j_2' JM\rangle$ is independent of M, we can write

$$\langle \bar{j}_1 j_2 JM'|i_{12}|\bar{j}_1' j_2' JM'\rangle = [J]^{-1}\sum_M \langle \bar{j}_1 j_2 JM|i_{12}|\bar{j}_1' j_2' JM\rangle ,$$

where M' is one value of the M's, and $[J] = (2J + 1)$. Using the relation[13]

$$(j_1 - m j_2 M+m | JM)\ (JM j_1' m' | j_2' M+m') = \sum_k [k]^{1/2} [J]^{1/2} W(j_1 j_2 j_2' j_1' ;\ Jk)$$

$$\times\ (j_2 M+m j_1' m' | kq)(j_1 - mkq | j_2' M+m')\ ,$$

we obtain

$$\langle j_1 j_2 JM' | i_{12} | j_1' j_2' JM' \rangle = -\ [J]^{-1} \sum_M \sum_{m,m'} (-1)^{j_1 - m + j_1' - m'} (j_1 - m j_2 M+m | JM)$$

$$\times\ (j_1' - m' j_2' M+m | JM)\ \langle j_1' m' j_2 M+m | v_{12} | j_1 m j_2' M+m' \rangle$$

$$= -[J]^{-1} \sum_{k,q,m,m'} [J](-1)^{j_1 + j_2 + j_1' + j_2'}\ W(j_2' j_1 j_1' j_2\ ;kJ)$$

$$\times\ (j_1' m' j_2 M+m | kq)(j_1 m j_2' M+m' | kq) \langle j_1' m' j_2 M+m | v_{12} | j_1 m j_2' M+m' \rangle$$

$$= -\sum_k (-1)^{j_1 + j_2 + j_1' + j_2'}\ W(j_2' j_1 j_1' j_2 ;kJ) \sum_q \langle j_1' j_2 kq | v_{12} | j_1 j_2' kq \rangle\ .$$

The final expression is

$$\langle \bar{j}_1 j_2 JM | i_{12} | \bar{j}_1' j_2' JM \rangle = -\sum_k (-1)^{j_1 + j_2 + j_1' + j_2'} [k] W(j_2' j_1 j_1' j_2 ;kJ)$$

$$\times\ \langle j_1' j_2 kq | v_{12} | j_1 j_2' kq \rangle\ .$$

The matrix elements of the particle-particle interaction v_{12} are discussed in the next section.

3. Two-Body Residual Interaction

a. Explicit form of the residual interaction. Now we assume an explicit form of the proton-neutron residual interaction, and proceed to evaluate the matrix element. The residual interaction V_{12} is chosen as

$$V_{12} = V^C(\underline{r}_{12}) + V^T(\underline{r}_{12})S_{12} ,$$

where the first term is the central force, and the second term is the tensor force. The explicit forms of these forces are

$$V^C(\underline{r}_{12}) = [V_{TE}{}^C P_{TE} \exp(-\beta_{TE}{}^C \underline{r}_{12}^2) + V_{SE}{}^C P_{SE} \exp(-\beta_{SE}{}^C \underline{r}_{12}^2)$$

$$+ V_{TO}{}^C P_{TO} \exp(-\beta_{TO}{}^C \underline{r}_{12}^2) + V_{SO}{}^C P_{SO} \exp(-\beta_{SO}{}^C \underline{r}_{12}^2)]$$

and

$$V^T(\underline{r}_{12}) = V_{TE}{}^T P_{TE} \exp(-\beta_{TE}{}^T \underline{r}_{12}^2) + V_{TO}{}^T P_{TO} \exp(-\beta_{TO}{}^T \underline{r}_{12}^2)] ,$$

where P_{TE} , P_{SE} , P_{TO} , and P_{SO} are the projection operators for the triplet-even, singlet-even, triplet-odd, and singlet-odd states, respectively, and the V's are the corresponding strength parameters. The operator S_{12} is the tensor-force operator defined as

$$S_{12} = \frac{3(\underline{\sigma}_1 \cdot \underline{r}_{12})(\underline{\sigma}_2 \cdot \underline{r}_{12})}{\underline{r}_{12}^2} - \underline{\sigma}_1 \cdot \underline{\sigma}_2 .$$

b. Matrix elements of residual interaction. The matrix element for the central force may be expressed as

$$\langle a|V^C(\underline{r}_{12})|a'\rangle = \frac{1}{2}\Big[(V_{TE}{}^C + V_{TO}{}^C)$$

$$+ (V_{TE}{}^C - V_{TO}{}^C)\,(-1)^{j_1'+j_2'+J}\,P_{12}'\Big]\langle a|U^C(\underline{r}_{12})|a'\rangle$$

$$- \frac{1}{2}\Big[(V_{TE}{}^C - V_{SE}{}^C + V_{TO}{}^C - V_{SO}{}^C)$$

$$+ (V_{TE}{}^C + V_{SE}{}^C - V_{TO}{}^C\, V_{SO}{}^C)(-1)^{j_1'+j_2'+J}\,P_{12}\Big]\langle a|U^C(\underline{r}_{12})P_S|a'\rangle\ ,$$

where P_S is the singlet projection operator, and P_{12}' is an exchange operator which interchanges $\ell_1' \longleftrightarrow \ell_2'$ and $j_1' \longleftrightarrow j_2'$ in the primed initial states. The matrix element $\langle a|U^C(\underline{r}_{12})|a'\rangle$ and $\langle a|U^C(\underline{r}_{12})P_S|a'\rangle$ are given by (see Appendix A)

$$\langle a|U^C(\underline{r}_{12})|a'\rangle = (-1)^{j_2'+j_2+J}\,([j_1][j_2][j_1'][j_2'])^{1/2}$$

$$\times \sum_k F_k(j_1'\,\tfrac{1}{2}\,j_1\,-\tfrac{1}{2}\,|k0)(j_2'\,\tfrac{1}{2}\,j_2\,-\tfrac{1}{2}\,|k0)$$

$$\times\ W\,(j_1 j_1' j_2 j_2';\ kJ)\ ,$$

$$\langle a|U^C(\underline{r}_{12})P_S|a'\rangle = (-1)^{j_2'+j_2+J+1}([j_1][j_2][j_1'][j_2'])^{1/2}([\ell_1][\ell_2][\ell_1'][\ell_2'])^{1/2}$$

$$\times W(\ell_1 j_1 \ell_2 j_2 \; ; \tfrac{1}{2} J)\; W(\ell_1' j_1' \ell_2' j_2' \; ; \tfrac{1}{2} J)$$

$$\times \sum_k F_k(\ell_1\; 0\ell_1'\; 0|k0)(\ell_2 0 \ell_2' 0|k0)\; W(\ell_1 \ell_1' \ell_2 \ell_2' \; ; kJ) \; ,$$

and with the restriction that $k + \ell_1 + \ell_1'$ and $k + \ell_2 + \ell_2'$ are both even. The symbol $[a]$ stands for $[2a + 1]$ and $(\;|\;)$ and W are the usual Clebsch-Gordan and Racah coefficients. The Slater integral F_k is defined as

$$F_k = \int_0^\infty dr_1\; r_1^2\; R_1 R_1' \int_0^\infty dr_2\; r_2^2\; R_2 R_2'$$

$$\times \int_{-1}^{1} d\left(\frac{\cos\theta_{12}}{2}\right) P_k(\cos\theta_{12})\; U^C(r_{12}) \; ,$$

where $U^C(\underline{r}_{12})$ takes the Gaussian form $\exp(-\beta \underline{r}_{12}^2)$ with different values of β for the corresponding states.

The tensor force has been evaluated in terms of spherical tensors by Talmi.[14] The tensor-force matrix element can be conveniently expressed in either the L-S representation or the j-j representation.[15,16] In the j-j representation, the matrix element for the tensor force is (see Appendix B)

$$\langle \alpha j_1 j_2 JM|V^T(\underline{r}_{12})S_{12}|\alpha' j_1' j_2' J'M'\rangle$$

$$= \frac{1}{2} V_{TE}^{\;T} \Big[\langle \alpha j_1 j_2 JM|U_{TE}^{\;T}(\underline{r}_{12})S_{12}|\alpha' j_1' j_2' J'M'\rangle$$

$$+ (-1)^{j_1'+j_2'+J} \langle \alpha j_1 j_2 JM | U_{TE}{}^{T}(\underline{r}_{12}) S_{12} | \alpha' j_2' j_1' J'M' \rangle \Big]$$

$$+ \frac{1}{2} V_{TO}{}^{T} \Big[\langle \alpha j_1 j_2 JM | U_{TO}{}^{T}(\underline{r}_{12}) S_{12} | \alpha' j_1' j_2' J'M' \rangle$$

$$+ (-1)^{j_1'+j_2'+J} \langle \alpha j_1 j_2 JM | U_{TO}{}^{T}(\underline{r}_{12}) S_{12} | \alpha' j_2' j_1' J'M' \rangle \Big] \quad ,$$

and

$$\langle \alpha j_1 j_2 JM | U_T(\underline{r}_{12}) S_{12} | \alpha' j_1' j_2' J'M' \rangle = \sum_{K,x,y} \langle \alpha | F_{xy} | \alpha' \rangle \; W(1x\; 1y;\; K2)$$

$$\times \langle j_1 j_2 JM | \underset{\sim}{T}_1{}^{(1x)K} \cdot \underset{\sim}{T}_2{}^{(1y)K} | j_1' j_2' J'M' \rangle .$$

Here we define

$$\langle \alpha | F_{xy} | \alpha' \rangle = -5 \sum_{k,i,j} \langle \alpha | r_i r_j | \alpha' \rangle \; X_{ij} \; , \quad \text{for} \quad i,\, j = 1,\, 2$$

$$X_{11} = \left(\frac{2}{15} [x] \right)^{1/2} (20k0 | x0) \; ,$$

$$X_{22} = \left(\frac{2}{15} [y] \right)^{1/2} (20k0 | y0) \; ,$$

$$X_{12} = ([x][y])^{1/2} (10k0 | x0)(10k0 | y0) W(1xy;2k) \; ,$$

and

$$\langle\alpha|r_1 r_j|\alpha'\rangle = (2k+1)\int_0^\infty dr_1 r_1^2 R_1 R_1' \int_0^\infty dr_2 r_2 R_2 R_2' r_i r_j$$

$$\times \int_{-1}^{1} d\left(\frac{\cos\omega_{12}}{2}\right) P_k(\cos\omega_{12}) \frac{U^T(r_{12})}{r_{12}^2} ,$$

where $U^T(r_{12})$ take the Gaussian form

$$U_{TE}^{\ T}(r_{12}) = \exp\left(-\beta_{TE}^{\ C} r_{12}^2\right)$$

for the triplet-even, and

$$U_{TO}^{\ T}(r_{12}) = \exp\left(-\beta_{TO}^{\ C} r_{12}^2\right)$$

for the triplet-odd. The angular part in terms of the 3-, 6-, and 9-j symbols is

$$\langle j_1 j_2 JM|\underset{\sim}{T}_1^{(1x)K} \cdot \underset{\sim}{T}_2^{(1y)K}|j_1' j_2' J'M'\rangle = (-1)^{j_1'+j_2+\ell_1+\ell_2+J}$$

$$\times\ 6\delta_{JJ'}\delta_{MM'} \begin{Bmatrix} J & j_2 & j_1 \\ K & j_1' & j_2' \end{Bmatrix} ([j_1][j_2][j_1'][j_2'])^{1/2}([\ell_1][\ell_2][\ell_1'][\ell_2'])^{1/2}$$

$$\begin{pmatrix} \ell_1 & x & \ell_1' \\ 0 & 0 & 0 \end{pmatrix}\begin{pmatrix} \ell_2 & y & \ell_2' \\ 0 & 0 & 0 \end{pmatrix}\begin{Bmatrix} \frac{1}{2} & \frac{1}{2} & \frac{1}{2} \\ \ell_1' & \ell_1 & x \\ j_1' & j_1 & K \end{Bmatrix}\begin{Bmatrix} \frac{1}{2} & \frac{1}{2} & 1 \\ \ell_2' & \ell_2 & y \\ j_2' & j_2 & K \end{Bmatrix}$$

The above expression for the tensor-force matrix element is still sufficiently complicated so that it is very difficult to draw any conclusions before doing the actual numerical work. The detailed numerical work is presented in the next chapter (C 1 and 2).

In the zero range, the tensor force vanishes, and the central force matrix element reduces to

$$\langle a|V^C(\underline{r}_{12})|a'\rangle \to (4\pi)^{-1}\left(\frac{\pi}{\beta}\right)^{3/2}\left[(3V_{TE}^C + V_{SE}^C)\,\langle a|\delta(\underline{r}_1 - \underline{r}_2)|a'\rangle\right.$$

$$\left. + (V_{TE}^C - V_{SE}^C)\,\langle a|\delta(\underline{r}_1 - \underline{r}_2)\,\underset{\sim}{\sigma}_1\cdot\underset{\sim}{\sigma}_2|a'\rangle\right] ,$$

where (see Appendix A)

$$\langle a|\delta(\underline{r}_1 - \underline{r}_2)|a'\rangle = \frac{1}{2[J]}\,F_0([j_1][j_2][j_1'][j_2'])^{1/2}$$

$$\times\,(j_1\,\tfrac{1}{2}\,j_2 - \tfrac{1}{2}\,|J0)(j_1'\,\tfrac{1}{2}\,j_2' - \tfrac{1}{2}|J0)$$

$$\times\,[(-1)^{j_1+j_1'+\ell_1+\ell_1'+1} + (-1)^{j_1'+j_1'+j_2+j_2'}\,\frac{AA'}{4J(J+1)}],$$

and

$$\langle a|\delta(\underline{r}_1 - \underline{r}_2)\,\underset{\sim}{\sigma}_1\cdot\underset{\sim}{\sigma}_2|a'\rangle = \frac{1}{2[J]}\,F_0([j_1][j_2][j_1'][j_2'])^{1/2}$$

$$\times\,(j_1\,\tfrac{1}{2}\,j_2 - \tfrac{1}{2}\,|J0)(j_1'\,\tfrac{1}{2}\,j_2' - \tfrac{1}{2}\,|J0)$$

$$\times\left\{(-1)^{j_1+j_1'+\ell_1+\ell_1'}\,[1 + 2(-1)^{\ell_1+\ell_2+J}]\right.$$

$$\left. + (-1)^{j_1+j_1'+j_2+j_2'}\,\frac{AA'}{4J(J+1)}\right\},$$

with

$$A = [(2j_1 + 1) + (-1)^{j_1+j_2+J} (2j_2 + 1)] .$$

The matrix element $\langle a|V^0(r_{12})\underset{\sim}{\sigma}_1 \cdot \underset{\sim}{\sigma}_2|a'\rangle$ vanishes unless both $\ell_1 + \ell_2 + J$ and $\ell_1' + \ell_2' + J$ are even. Similarily, $\langle a|V^0(r_{12})|a'\rangle$ vanishes unless $\ell_1 + \ell_1' + \ell_2 + \ell_2'$ is even. The Slater integral F_0 is given by

$$F_0 = \int_0^\infty R_1(r)R_2(r)R_1'(r)R_2'(r)r^2dr .$$

c. Choice of radial wave function. For the radial part of the wave function, we choose the harmonic-oscillator wave function. It is generally believed that the harmonic-oscillator wave function is a fairly good approximation for light and medium nuclei, whereas the square-well potential is a closer approximation for heavy nuclei. The radial wave function has the explicit form[17]

$$R_{n\ell}(r) = N_{n\ell}\, e^{-(\nu/2)r^2}\, r^\ell\, v_{n\ell}(r)$$

where $N_{n\ell}$ is a normalization constant chosen so that

$$\int R^*_{n\ell}(r)R_{n\ell}(r)r^2dr = 1 .$$

The function $v_{n\ell}(r)$ is the associated Laguerre polynomial defined as

$$v_{n\ell}(r) = L^{\ell+1/2}_{n+\ell 1/2}(\nu r^2) = \sum_{k=0}^{n} (-1)^k 2^k \binom{n}{k} \frac{(2\ell+1)!!}{(2\ell+k+1)!!} (\nu r^2)^k$$

The nuclear size parameter $\nu^{-1/2}$ appearing in the wave function has to be evaluated for the numerical calculation. The harmonic-oscillator spacing is known to be roughly

$$\hbar\omega = \frac{\hbar^2\nu}{m} \cong 41A^{-1/3} \text{ MeV} ,$$

from which ν may be evaluated. The evaluation of the central-force radial integral has been simplified analytically by Ford and Konopinski.[18] The tensor-force radial integral $\langle\alpha|r_i r_j|\alpha'\rangle$ can not be evaluated directly, since the integral has singularities due to the r_{12}^2 term appearing in the denominator. This difficulty is eliminated by expanding the integral into a linear combination of the Talmi integral.[17,18] (See Appendix B). For the delta-function force, the radial integral can be easily evaluated analytically, and the numerical values of the integral have been given by several workers for the diagonal case.[6,19]

d. Shell-model residual force and two-nucleon force. In most of the past shell-model calculations, the central force alone has been used, neglecting the tensor force. The main motivation for neglecting the tensor force has probably been the computational complexity involved in using it, but the success of shell-model calculations without the tensor force does not necessarily imply the absence of the tensor force in the residual interaction. In fact, Visscher and Ferrell have shown that the tensor force is essential in explaining the ft values of C^{14} and O^{14} (both 0+ states decay to the 1+ ground state of N^{14}).[20]

The shell-model residual interaction is not expected to be the same as the free two-nucleon force because the presence of other nucleons might modify the basic meson-exchange forces. However, the work on the properties of nuclear matter by Brueckner and Gammel,[21] Bethe and Goldstone,[22] and others have indicated that the free two-nucleon interaction may give rise to very satisfactory results for many-body problem if an approximate solution to the many-body Schrordinger equation can be found. Furthermore, the shell-model calculations of True and Ford,[23] and of Dawson, Talmi, and Welecka[24] have indicated that the appropriate shell-model residual force may not be very different from the free two-nucleon force.

Inclusion of the tensor with the central force in the free two-nucleon force has the theoretical support that the one-pion-exchange potential (OPEP), which is the meson theoretic potential of the lowest order, explicitly includes the four components of the central force and two components of the tensor force. Yukawa's original hypothesis was that the nuclear force is caused by transmitting a particle, now called the pion, between two nucleons.[25] For the exchange of n pions, the force range is expected to be of the order of $(n\mu_\pi)^{-1}$, so that the tail end of the two-nucleon potential has its main contribution from one-pion exchange (OPE). In the OPEP, it is assumed that the nucleons are point particles moving with nonrelativistic velocities. This assumption makes it possible to solve the field equations in the first approximation in which only one-meson exchange is considered between two nucleons. The solution of the resulting Schroedinger equation leads to an interaction potential between two nucleons of the form

$$V(\mathrm{OPE}) = \mu\, c^2 f^2 (\underset{\sim}{\tau}_1 \cdot \underset{\sim}{\tau}_2)\ \frac{e^{-\mu r}}{\mu r}\ \frac{1}{3}\left\{[\underset{\sim}{\sigma}_1 \cdot \underset{\sim}{\sigma}_2 - 4\pi\delta(r)] + S_{12}\left[1 + \frac{3}{\mu r} + \frac{3}{(\mu r)^2}\right]\right\},$$

where $(\mu)^{-1} = \lambda\!\!\!^{-} = 1.41$ F is the pion Compton wavelength, and S_{12} is the tensor-force operator. The coupling constant f^2 is the only adjustable constant in this expression. Cziffra and Moravcsik have attempted to determine the coupling constant f^2 from an analysis of neutron- proton scattering data.[26] However, the more accurate value of $f^2 = 0.08$ was determined from an analysis of pion-nucleon scattering data. Since the rest energy of the pion, μc^2, is 140 MeV, the overall strength of the OPEP, $\mu c^2 f^2$, is 11.2 MeV.[27]

MacGregor, Moravcsik and Stapp have done some interesting work on analysis of proton-proton scattering at 310 MeV.[28] At this high energy, nucleon-nucleon scattering is sensitive only to the tail of the nuclear potential for high-ℓ partial waves. Assuming that the OPE is the only significant contribution at large distances, they analyzed the phase shifts for $\ell \geqslant 5$ by using the relativistic OPE amplitudes instead of nonrelativistic OPEP. The phase shifts for $\ell \leqslant 4$ are determined

phenomenologically by analyzing the data. Their value of $f^2 = 0.06$ agrees fairly well with the value determined from the pion-nucleon scattering data.

The presence of the delta-function term, $\delta(r)$, supports the introduction of a hard core in the nuclear potential, which is necessary for S states to be repulsive at the shorter distance. However, OPEP is only valid at a large distance, i.e., at the tail of the two-nucleon static potential, so that the delta-function term is usually omitted from OPEP.

To serve the purpose of comparison of OPEP with other phenomenological two-nucleon potentials, we write OPEP in terms of the projection operators, neglecting the delta-function term, as

$$V(\mathrm{OPE}) = \mu c^2 f^2 \frac{e^{-\mu r}}{\mu r} \left\{ \left[- P_{TE} - P_{SE} + P_{TO} + 3P_{SO} \right] + S_{12}\left(1 + \frac{3}{\mu r} + \frac{3}{(\mu r)^2}\right) \left[- P_{TE} + P_{TO} \right] \right\} .$$

Here the projection operators are given by

$$P_{TE} = \left(\frac{1 + P_\sigma}{2}\right)\left(\frac{1 - P_\tau}{2}\right) ,$$

$$P_{SE} = \left(\frac{1 - P_\sigma}{2}\right)\left(\frac{1 + P_\tau}{2}\right) ,$$

$$P_{TO} = \left(\frac{1 + P_\sigma}{2}\right)\left(\frac{1 + P_\tau}{2}\right) ,$$

and

$$P_{SO} = \left(\frac{1 - P_\sigma}{2}\right)\left(\frac{1 - P_\tau}{2}\right) ;$$

where,

$$P_\sigma = \frac{1 + \underset{\sim}{\sigma}_1 \cdot \underset{\sim}{\sigma}_2}{2} ,$$

and

$$P_\tau = \frac{1 + \underset{\sim}{\tau}_1 \cdot \underset{\sim}{\tau}_2}{2} .$$

The tensor force was known to be essential to account for the deuteron quadrupole moment even before the pion was discovered. The tensor force in OPEP shown above was shown to give a good account of the quadrupole moment of the deuteron.[29]

We may regard OPEP as a constraint to the nuclear force in addition to the experimental data of nucleon-nucleon scattering and the deuteron properties, since all meson-theoretic derivations of nuclear potentials agree with the result that the nuclear potential must behave like the OPEP at large distance. The inner region of the potential remains extremely controversial, including even the two-pion-exchange potential. Many different forms based on meson theory have been derived.[30] However, there are very few works that calculate the corresponding properties of the two-nucleon system.[31]

Most of the n-p data has been analyzed in terms of phenomenological potentials such as those by Signell and Marshak,[32] Gammel and Thaler,[33] Hamada,[34] and recently Glendenning and Kramer.[35] The Signell-Marshak potential, while satisfying the OPEP, does not fit the deuteron data. The Gammel-Thaler potential does not fit the deuteron data nor satisfy the OPEP. (This potential has now been corrected to fit all the low-energy parameters, and several sets of the parameters for the potential have been presented in the review article by Gammel and Thaler.[36]) On the other hand, Hamada has been fairly successful in reproducing the deuteron properties and n-p scattering data with potentials that have OPEP tails. A more detailed analysis similar to Hamada's has been recently done by Glendenning and Kramer to construct triplet-even potentials that are asymptotic to the OPEP and are modified in the inner region with ranges corresponding to the exchange of more than one pion in such a way as to obtain agreement with the deuteron properties and the n-p scattering data.

e. Choice of Force Parameters. Because we set out to make shell-model calculations with a residual force more general than usually used, we usually faced the problem of essentially more parameters than data. With each of four central-force and two tensor-force components are two parameters, depth and range of the Gaussian function, or twelve parameters in all. We adopted the approach that we would begin calculations with residual forces close to those satisfying the free-space two-nucleon scattering data and deuteron properties. If necessary, we would then make a minimum of adjustments to the force to give a general fit to the experimental-level spectra.

It has often been pointed out that the free-space nucleon-nucleon force may be subject to modification for shell-model calculations, but as yet there seems to be no strong evidence that large modifications necessarily occur. In fact, there are successful shell-model calculations of Dawson, Talmi, and Walecka[24] on the O^{18} spectrum using the Brueckner-Gammel-Thaler (BGT) potentials[21] including the tensor force and hard cores. Their results lend encouragement to our approach.

Apart from the success of O^{18} calculations by Walecka et al., there are two additional desirable reasons for choosing the Brueckner-Gammel-Thaler potential in the shell-model calculations, although we do not necessarily believe that the BGT potential is the best two-nucleon potential. The first reason is that it satisfies most of the constraints imposed upon the two-nucleon potential, such as the two-nucleon scattering data and the deuteron properties, although the tail end of this potential does not satisfy the OPEP constraint. The second reason is that it is successfully used in the nuclear-matter calculation by Brueckner and Gammel. The force parameters of the BGT potential are listed in Table I.

Introduction of a hard core along with Yukawa radial dependence would have made our computational work extremely complex. This is especially true for a heavy nucleus which involves higher angular momenta. For this reason we start with a phenomenological Gaussian potential without a hard core, based on the free two-nucleon potentials

Table I. Values of the force parameters for the BGT potential. The radial shape of the potential is Yukawa form with a hord core of radius 0.4F.

Force components	Strength (MeV)	Range (fm)
Central triplet-even	-877.39	0.478
Central singlet-even	-434.0	0.690
Central triplet-odd	- 14.0	1.00
Central singlet-odd	130.0	1.00
Tensor triplet-even	-159.40	0.953
Tensor triplet-odd	22.0	1.25
Spin-orbit triplet-even	-5000	0.270
Spin-orbit triplet-odd	-7315	0.270

of Brueckner, Gammel, and Thaler (BGT) and of Blatt and Jackson.[37] We use the well-depth parameter and intrinsic range defined by Blatt and Jackson in the shape-independent approximation of the effective-range theory to replace the Yukawa radial dependence with a hard core (the BGT potential) by a Gaussian form without a hard core. If one considers a nuclear potential of $V(r) = sV'(r)$ so that $V'(r)$ is the potential that gives rise to zero binding energy for the ground state of the proton-neutron system, then $V(r)$ for $s > 1$ allows bound states, whereas $V(r)$ for $s < 1$ gives rise to virtual states. The intrinsic range b of $V(r)$ is then defined as the effective range of $V'(r)$, and s is called the well-depth parameter. The Yukawa and Gaussian potentials in the shape-independent approximation are expressed by Jackson and Blatt in terms of s and b as

$$- V(r) = s(147.585 \text{ MeV})b^{-2}(b/r)\exp[-2.1196(r/b)]$$

for the Yukawa potential, and

$$- V(r) = s(229.208 \text{ MeV})b^{-2} \exp[-2.0604(r/b)^2]$$

for the Gaussian potential, where b is in units of 10^{-13} cm. To reduce the number of adjustable parameters, we arbitrarily take the intrinsic ranges of our potential to be same as the BGT potential. From shape-independent effective-range theory, the force range $\beta^{-1/2}$ of a Gaussian potential is larger by a factor of 1.477 than the force range of a Yukawa potential, such as the BGT potential. The well-depth parameters of our potential are expected to be smaller than those of the BGT potential, since the introduction of a repulsive hard core always requires the attractive Yukawa potential to be deeper than for no core.

We adjust the well-depth parameters so as to be consistent with the low-energy properties of the deuteron. If we choose s = 1 in the Gaussian formula above, the central triplet-even potential thus obtained will itself cause the deuteron to have zero binding energy. Because of the repulsive cores, the Yukawa tail of the BGT force needs s = 2.88. The reduction factor 2.88 is then applied to reduce all well-depth parameters for other components of the force to go from BGT to Gaussian without hard core. Values of the force parameters thus obtained are listed in Table II, and hereafter this potential is called Potential I.

Kalos et al. have calculated deuteron properties and scattering properties with Gaussian forces and showed that several combinations of central and tensor strengths and ranges could fit the data.[38] The triplet components of our Potential I are fairly close to an interpolation of two of their satisfactory potentials, so we feel that our Potential I is consistent with free-space properties of the n-p system, although we have not verified this supposition by actual scattering phase-shift calculations.

Table II. Values of the intrinsic range and well-depth parameters, s and b, for the BGT and simulated BGT potentials. The intrinsic ranges for the simulated BGT potential are assumed to be same as the BGT potential and are not shown. The corresponding strength and force range parameters for the simulated BGT are also shown.

States	BGT		Potential I		
	s	b(F)	s	Strength (MeV)	Force range (F)
Central triplet-even	2.882	1.013	1.0	-223.02	0.706
Central singlet-even	2.964	1.461	1.028	-110.03	1.018
Central triplet-odd	0.201	2.119	0.070	-3.57	1.476
Central singlet-odd	-1.867	2.119	-0.648	+33.06	1.476
Tensor triplet-even	2.078	2.019	0.721	-40.50	1.407
Tensor triplet-odd	-0.493	2.649	-0.171	+5.58	1.845

C. PARTICLE-PARTICLE INTERACTION

1. Yttrium-90

a. Zero-order energies. Recently an isomer state in the odd-odd nucleus Y^{90} has been found.[39] It is interesting to see if this isomeric state can be explained in terms of the j-j coupling shell model. Several other low-energy states were reported previously.[40] It is assumed that 38 protons and 50 neutrons form closed-shell cores. The assumption that 50 neutrons form a closed shell has been established because Zr^{90} exhibits typical properties of a closed-shell nucleus.[41] The 38-proton closed sub-shell has been assumed by several workers,[42] and we make the same assumption. These assumptions simplify the calculation, since there will be only one proton and one neutron outside the doubly closed-shell core in Y^{90}. For the proton single-particle levels, we choose the average values between Y^{89} and Y^{91}, and for the neutron single-particle levels the average between Sr^{89} and Zr^{91}. The experimental single-particle levels are presented in Tables III and IV, and the resulting zeroth-order energy levels are listed in Table V. The assignment for the lowest state of the fifty-first neutron as the $d_{5/2}$ configuration is evident from the fact that the observed ground-state spins and parities of Sr^{89} and Zr^{91} are 5/2+.[43] The lowest state of the thirty-ninth proton is assumed to be $p_{1/2}$, since both Y^{89} and Y^{91} are known to have ground-state spin 1/2.[43] Recently the atomic-beam measurement of the ground-state spin has been made for Y^{91}, confirming the $p_{1/2}$ configuration.[44] The observed low-energy levels in Y^{90} are shown in Fig. 1. The ground-state spin of Y^{90} has been determined recently by the atomic-beam method to be two.[45]

b. Energy spectrum. Before introducing the tensor force, the numerical calculations are carried out extensively with various central force mixtures including Serber, Ferrell-Visscher, and Rosenfeld forces and with various ranges. Although the delta-function force may give the correct sequence of the observed levels in Y^{90} as shown by Pollak et al.,[46] the calculations with realistic finite-range forces indicate

Table III. Single-particle levels of the thirty-nith proton.

Configuration	Energy (keV)		
	Y^{89} [a]	Y^{91} [a]	Y^{90} [b]
$p_{1/2}$	0	0	0
$g_{9/2}$	913	551	732

[a] Experimental data from reference.[43]

[b] Average between Y^{89} and Y^{91}.

Table IV. Single-particle levels of the fifty-first neutron.

Configuration	Energy (keV)		
	Sr^{89} [a]	Zr^{91} [b]	Y^{90} [c]
$d_{5/2}$	0	0	0
$s_{1/2}$	1050	1225	1138
$d_{3/2}$	2020	2070	2045
$g_{7/2}$	----	2205	2205

[a] Experimental data from B. L. Cohen, Phys. Rev. 125, 1358 (1962).

[b] Experimental data from Cohen (cit. supra) and reference 48.

[c] Average between Sr^{89} and Zr^{91}.

Table V. The zeroth-order levels in Y^{90}

Configuration (proton-neutron)	Energy (keV)
$p_{1/2}d_{5/2}$	0
$g_{9/2}d_{5/2}$	732
$p_{1/2}s_{1/2}$	1138
$g_{9/2}s_{1/2}$	1870
$p_{1/2}d_{3/2}$	2045
$p_{1/2}g_{7/2}$	2205
$g_{9/2}d_{3/2}$	2777
$g_{9/2}g_{7/2}$	2937

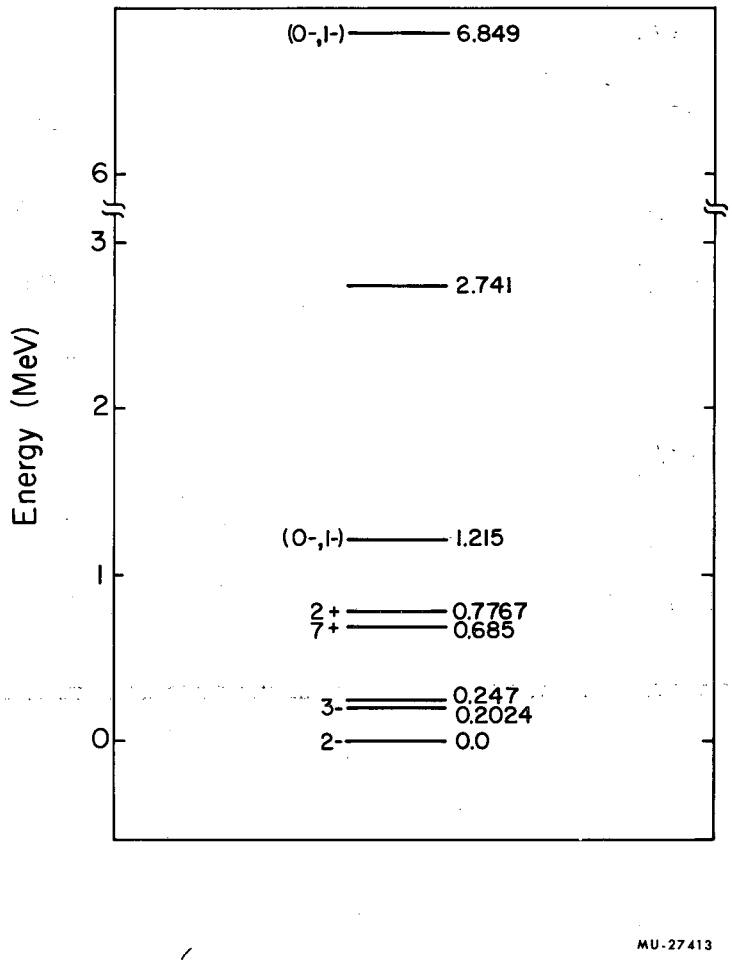

Fig. 1. Experimentally observed low energy levels in Y^{90}.

that we must introduce a fairly strong attractive odd force to fit the experimental data if we were to retain the singlet-even to triplet-even ratio (~ 0.5) of the free two-nucleon potential. A calculation with one set of central force parameters with rather strong attractive odd forces, which is chosen so as to fit both the doublet spacings of $J = 2, 3-$ and $J = 2+, 7+$, is shown in Fig. 2. Although the fit with the experiment is good, there is no justification for assuming the central force mixture of strong attractive odd force. Furthermore, this is not the only set of parameters which gives rise to a good fit with the experiment, since there are other sets of the parameters which yield equally good fits. From the free two nucleon potential, it is known that the triplet-odd force is weak, and the singlet-odd is even repulsive.

The diagonal tensor-force matrix elements $(1/3)\langle a|P_{TE}U^T(r_{12})S_{12}|a\rangle$ and $(1/3)\langle a|P_{TO}U^T(r_{12})S_{12}|a\rangle$ are plotted as a function of the range in Figs. 3 through 5. As we can see from these figures, the tensor-force matrix elements are not always a monotonically increasing function of the range, and may be either positive or negative. This is to be contrasted with the fact that the central force matrix elements are positive and monotonically increasing functions with increasing range and constant depth. The results of the calculation with Potential I of Table II are compared with the experiment in Fig. 6. In diagonalizing the matrix, the off-diagonal tensor-force matrix elements are neglected, since they are small compared to the diagonal tensor-force matrix elements. The numerical results are also presented in Table V, and are shown schematically in Fig. 7. In Fig. 7, notice that the lowest and highest J states (2+ and 7+) are separated from the other J states arising from the same configuration, $g_{9/2}\ d_{5/2}$. This is consistent with the revised "weak" coupling rule of Brennan and Bernstein.[47]

The results of other configurations presented in Fig. 7 and Table VI are also consistent with coupling rules of Nordheim,[1] and de-Shalit and Walecka.[15] The eigenfunctions are also computed, and the results are shown in Tables VII and VIII. As we can see from these

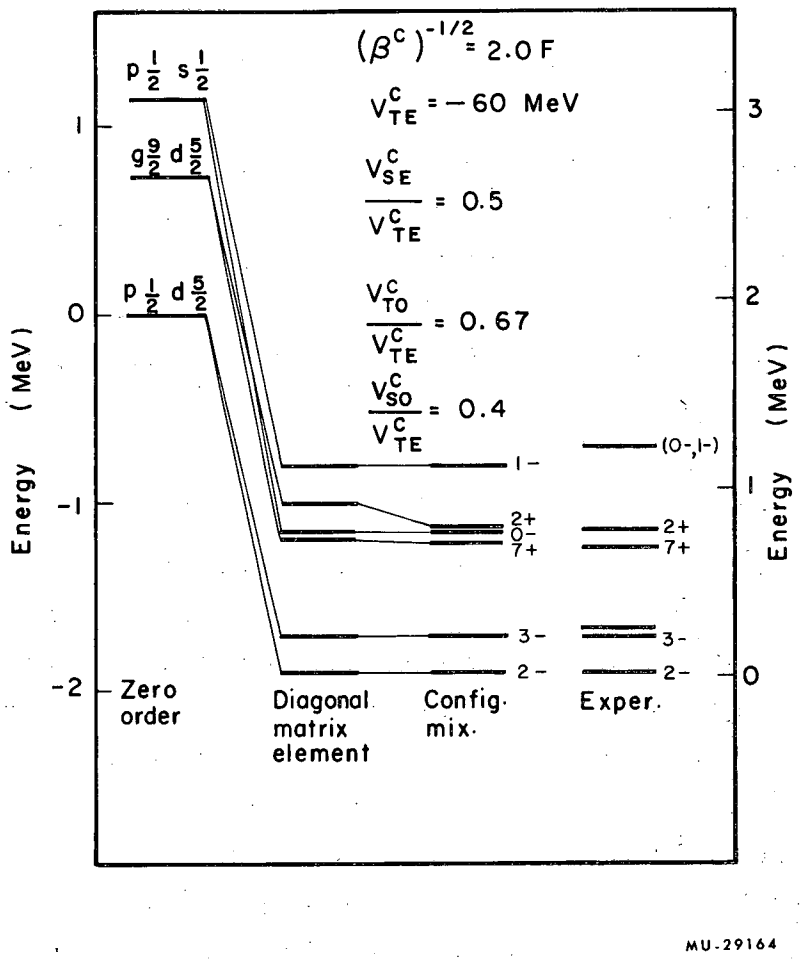

Fig. 2. Calculated Y^{90} spectrum with the central force alone. The central-force parameters are adjusted to fit both the doublet spacings of J = 2-, 3- and J = 2+, 7+.

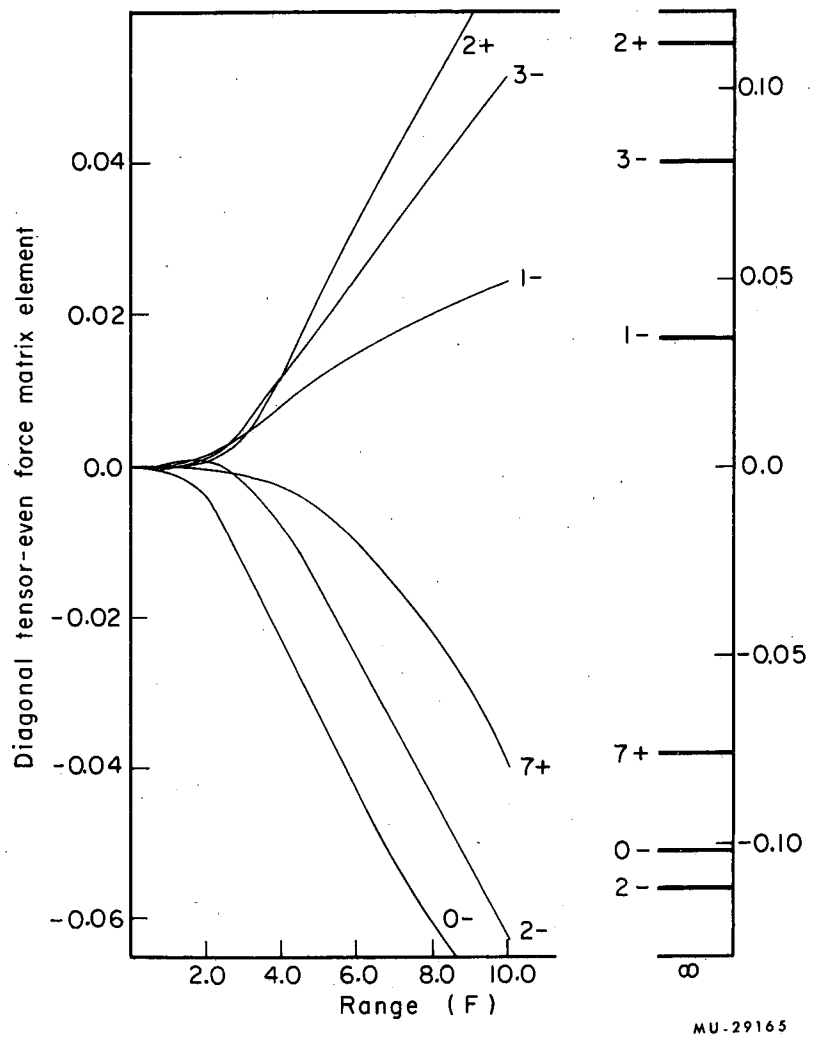

Fig. 3. Diagonal tensor-even-force matrix elements for several observed states in Y^{90} as a function of the range parameter.

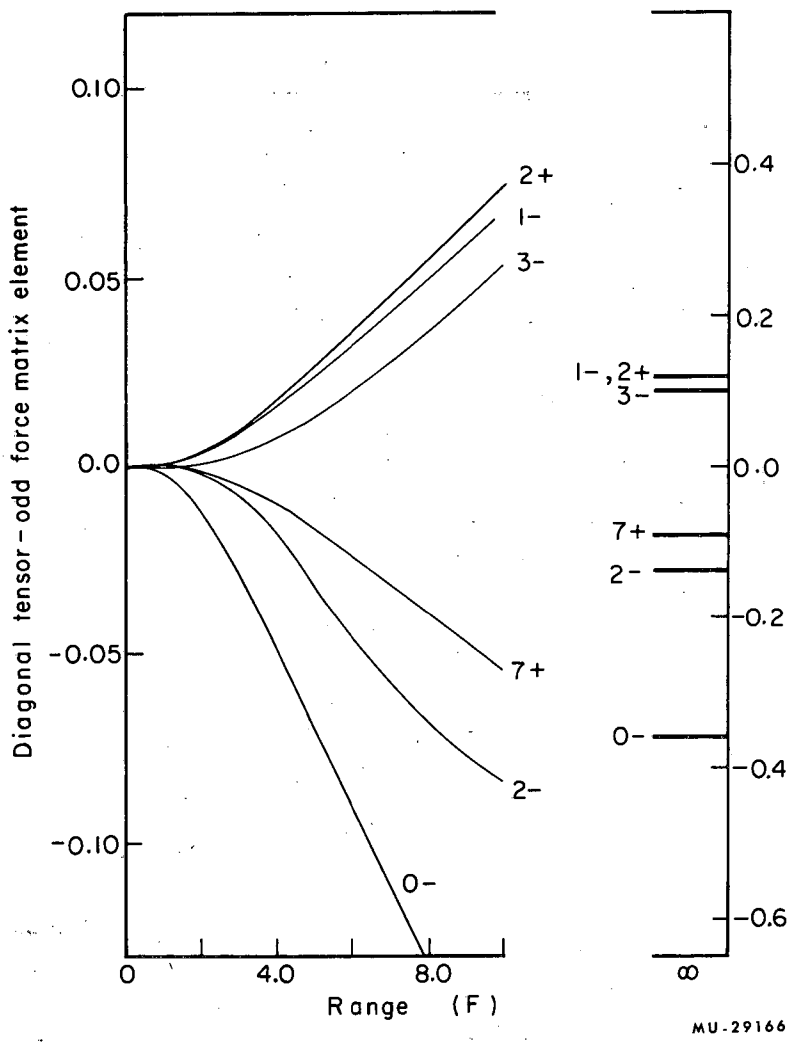

Fig. 4. Diagonal tensor-odd-force matrix elements for several observed states in Y^{90} as a function of the range parameter.

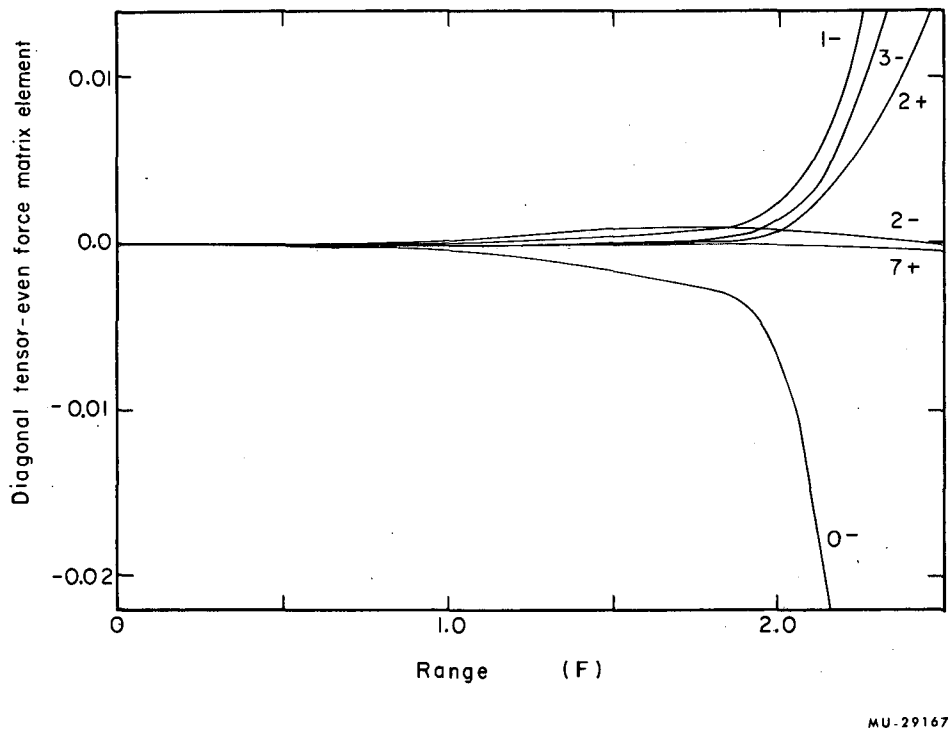

Fig. 5. Diagonal tensor-even-force matrix elements for the observed states in Y^{90} as a function of the range at the shorter ranges.

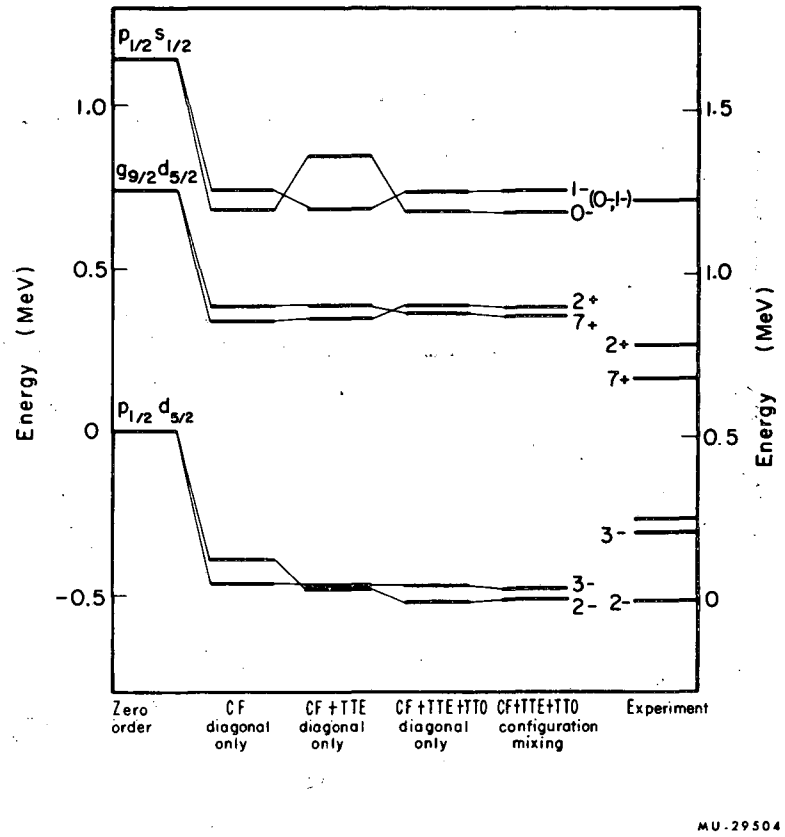

Fig. 6. Comparison of experimental and calculated spectra of Y^{90} with Potential I. The symbols CF, TTE, and TTO stand for the central, tensor-even, and tensor-odd forces, respectively. In diagonalizing the matrix, the off-diagonal matrix elements for the tensor force are neglected.

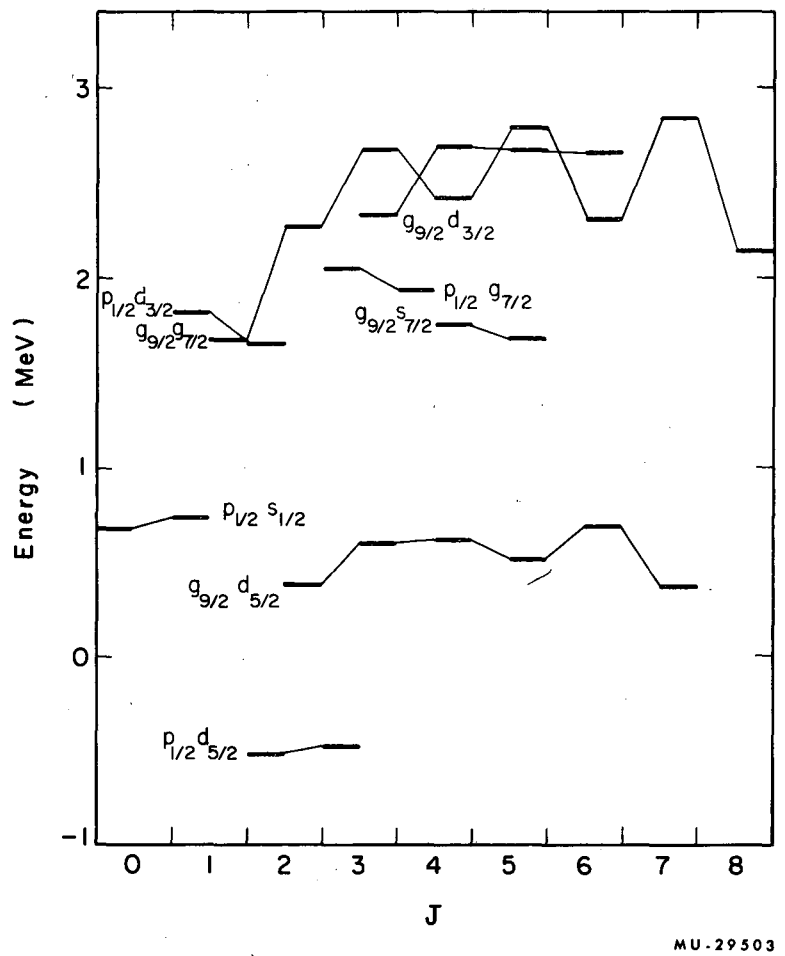

Fig. 7. Calculated energy levels in Y^{90}. For each spin, the left-hand column gives the odd-parity states, and the right-hand column the even-parity states Various J states arising from the same configuration are connected by thin lines.

Table VI. Calculated energy levels in Y^{90}. The results before and after diagonalization are shown in columns A and B, respectively. In column C, the energy scale is shifted so that the ground state lies at zero energy. In diagonalizing, the matrix the tensor-force off-diagonal matrix elements are neglected.

Proton-neutron configurations	Jπ	Energy (MeV)		
		A	B	C
$p_{1/2}d_{5/2}$	2-	-0.515	-0.516	0.0
	3-	-0.480	-0.487	0.029
$g_{9/2}d_{5/2}$	2+	0.382	0.377	0.893
	3+	0.622	0.600	1.116
	4+	0.624	0.610	1.126
	5+	0.583	0.551	1.067
	6+	0.679	0.679	1.195
	7+	0.359	0.357	0.873
$p_{1/2}s_{1/2}$	0-	0.672	0.672	1.188
	1-	0.734	0.734	1.250
$g_{9/2}s_{1/2}$	4+	1.736	1.745	2.261
	5+	1.655	1.671	2.187
$p_{1/2}d_{3/2}$	1-	1.815	1.816	2.332
	2-	1.650	1.650	2.166
$p_{1/2}g_{7/2}$	3-	2.047	2.054	2.570
	4-	1.927	1.927	2.443
$g_{9/2}d_{3/2}$	3+	2.372	2.326	2.842
	4+	2.609	2.686	3.202
	5+	2.677	2.671	3.187
	6+	2.487	2.663	3.179
$g_{9/2}g_{7/2}$	1+	1.669	1.669	2.185
	2+	2.269	2.274	1.758
	3+	2.615	2.683	3.199
	4+	2.491	2.420	2.936
	5+	2.769	2.790	3.306
	6+	2.470	2.295	2.811
	7+	2.841	2.842	3.358
	8+	2.129	2.129	2.645

Table VII. Calculated eigenfunctions for odd-parity states in Y^{90}.

	Eigenvalues	Eigenfunctions			
$J\pi$	(MeV)	$p_{1/2}d_{5/2}$	$p_{1/2}s_{1/2}$	$p_{1/2}d_{3/2}$	$p_{1/2}g_{7/2}$
1-	0.734		0.9997	0.0246	
	1.816		0.0246	-0.9997	
2-	-0.516	-0.9998		0.0158	
	1.650	-0.0158		-0.9998	
3-	-0.487	0.9987			0.0500
	2.054	0.0500			-0.9987

Table VIII. Calculated eigenfunctions for even-parity states in Y^{90}.

Jπ	Eigenvalues (MeV)	Eigenfunctions			
		$g_{9/2}d_{5/2}$	$g_{9/2}s_{1/2}$	$g_{9/2}d_{3/2}$	$g_{9/2}g_{7/2}$
2+	0.377	0.9987			0.0491
	2.274	0.0491			-0.9987
3+	0.600	-0.9937		0.1070	0.0332
	2.326	-0.1108		-0.8962	-0.4294
	2.683	-0.0161		-0.4304	0.9024
4+	0.610	0.9938	0.1100	0.0079	-0.0040
	1.745	0.1101	-0.9906	-0.0736	-0.0314
	2.420	0.0064	-0.0648	0.5174	0.8532
	2.686	0.0037	0.0472	-0.8524	0.5206
5+	0.551	0.9860	0.1578	-0.0466	-0.0248
	1.671	0.1623	-0.9871	0.0949	0.0295
	2.671	0.0361	0.1060	0.9105	0.3980
	2.790	0.0058	-0.0100	-0.3997	0.9165
6+	0.679	0.9997		-0.0115	-0.0174
	2.295	0.0206		0.6906	0.7229
	2.663	0.0037		-0.7231	0.6907
7+	0.357	-0.9996			0.0263
	2.842	-0.0263			-0.9996

tables, the configuration mixing is not very important for most of the observed states. The almost pure configuration of the ground state $(p_{1/2}d_{5/2})^{J=2-}$ is consistent with the measured magnetic moment. The measured magnetic moment of the ground state of Y^{90} is -1.629 nm, whereas the calculated magnetic moment with the empirical g factors evaluated from neighboring nuclei is -1.609 nm if we assume that the configuration is pure.[45] A level at 0.247 MeV has been suggested by Bartholomew et al.[40] to be the J=3- state arising from the $p_{1/2}g_{7/2}$ configuration. They have indicated that this assignment is consistent with their data and with the observed beta decay of Sr^{90}(total disintegration energy of 0.535 MeV) only to the ground state, thus eliminating the possibility of this state being J = ± 0, 1±, or 2-. However, the $g_{7/2}$ neutron single-particle level has been found[48] to be 2.2 MeV above the ground state $d_{5/2}$ in Zr^{91}, and it is very difficult to understand the $(p_{1/2}g_{7/2})^{J=3}$ state being near the ground state. This would require an extremely large matrix element to overcome this initial neutron single-particle spacing of 2.2 MeV. The low energy of 0.247 MeV suggests that this level is probably not attributable to the configuration $(p_{1/2}g_{9/2})$ nor other configurations caused by the core excitation of the 38-proton core. It remains to be seen if the experiment can definitely assign the spin and parity to this state.

The spin and parity of the state of 2.7 MeV have not been determined experimentally, and there are several calculated levels around 2.7 MeV. The probable states within the energy limit of 2.7±0.2 MeV are $(p_{1/2}g_{7/2})^{J=3,4}$, $(g_{9/2}d_{3/2})^{J=3}$, and $(g_{9/2}g_{7/2})^{J=2,6,8}$.

c. Discussion. Although the experimental spectrum is not sufficiently resolved to test all components of our choice of the residual force, there is a remarkable agreement between the calculated spectrum and experiment if one notes that several shell-model approximations have been made and the force parameters are not all adjusted arbitrarily. A slight increase of the triplet-even part of the central and tensor forces is sufficient to increase the doublet spacings of J = 2-, 3-, and J = 2+, 7+ so as to improve agreement with experiment. Furthermore, by introducing the tensor force, we can eliminate the need for unrealistic strong attractive odd central forces, required for a shell-

model force with central components only. Potential I was also applied to Bi^{210},[49] (see Section C2) where most levels of the ground state-state multiplet (a total of nine levels out of a possible ten) are resolved by the high resolution (d,p) reaction on Bi^{209} at Massachusetts Institute of Technology.[50] The analysis of those multiplets in Bi^{210} along with Po^{210} also indicates that the triplet-even part of Potential I is slightly too weak to account for the overall spacings of the Bi^{210} ground-state multiplet. A slight increase of the triplet-even part of Potential I improves the spacing of $J = 2-, 3$-states. It would be very interesting to see if one can resolve the $g_{9/2}d_{5/2}$ and $p_{1/2}s_{1/2}$ multiplets by high-resolution studies of $Y^{89}(d,p)\ Y^{90}$, $Zr^{91}(\alpha,5)\ Nb^{92}$, or $Zr^{90}(\alpha,d)\ Nb^{92}$ reactions.

2. Bismuth-210 and Polonium-210

a. Introduction. The low-lying energy-level spectrum of Bi^{210} has been the object of several shell-model theoretical studies.[51] The nucleus has one proton and one neutron beyond the doubly closed-shell nucleus Pb^{208}. The lowest proton orbital is $h_{9/2}$, and the lowest neutron orbital, $g_{9/2}$. One thus expects a low-lying multiplet of ten levels with spins from zero to nine for Bi^{210}. With the experimental determination eight years ago a ground-state spin of one, a difficult problem was posed for shell-model theory, for almost any reasonable attractive central-force mixture acting between the neutron and proton bring spin 0 lower than spin 1, whereas experimentally spin 0 lies 47 keV higher.

The inversion of 0- and 1- states of the $h_{9/2}g_{9/2}$ configuration in Bi^{210} is a striking exception to Nordheim's "strong"-coupling rule for odd-odd nuclei. To explain this inversion, Newby and Konopinski[51] and Kharitonov, Sliv, and Sogomonova[52] attribute the 1- state to the configuration $h_{9/2}i_{11/2}$. More recently the study by de-Shalit and Walecka of the angular ordering function suggested that the inversion of 0- and 1- states of $h_{9/2}g_{9/2}$ may be explained with a proper choice of the central-force range.[15] Newby and Konopinski gave qualitative

arguments that an attractive tensor force would be repulsive for the 0- state and help force it up.

The low-energy, high-resolution (d,p) reaction studies of Erskine et al. on Bi^{209} present a wealth of new information on the $h_{9/2}g_{9/2}$ multiplet[50] and necessitate a thorough reexamination of the shell-model theory. They resolve nine of the expected ten levels of the $h_{9/2}g_{9/2}$ multiplet and make tentative spin assignments on the basis that the reaction cross sections are proportional to 2J+1. Furthermore, they see higher multiplets attributable to capture of the neutrons into $d_{5/2}$ and $s_{1/2}$ excited orbitals. The multiplets arising from capture into $i_{11/2}$ or $j_{15/2}$ orbitals are weak and not resolved completely, presumably because the high orbital-angular-momentum transfers are strongly discriminated against in the (d,p) reaction.

Figure 8 shows Erskine's spectrum with indicated level numbers. The spins are assigned in sequence of J = 1, 0, 9, 2, 3, 5 and 8 (or 5 and 7), 4, 6, and 7 (or 8) with corresponding level numbers 0, 1, 2, 3, 5, 6, 7, and 8. These results strongly indicate that the ground state involves mainly the $g_{9/2}$ neutron orbital and not the $i_{11/2}$. Erskine made shell-model calculations with a finite Gaussian Serber force (central-even components only) as a function of range.[53] He took a ratio of 0.66 for singlet-to-triplet strength, which free-space two-body scattering and other shell-model work indicate is reasonable. At a force range of 2.7 fm he found a fairly good fit for all except the spin-0 and -1 levels, which are inverted from their experimental order.

The spectrum of Po^{210} was theoretically calculated by Hoff and Hollander[54] with a delta-function force, and by Newby and Konopinski with a central singlet-even force, which is reasonable from the free two-nucleon potential. We also shall treat the Po^{210} spectrum to see the effects of a tensor force and to determine if one can explain the spectra of both Bi^{210} and Po^{210} with the same residual force. The experimentally observed low-lying energy levels in Bi^{210} and Po^{210} are presented in Fig. 9. We assume that Pb^{208} can be treated as an inert

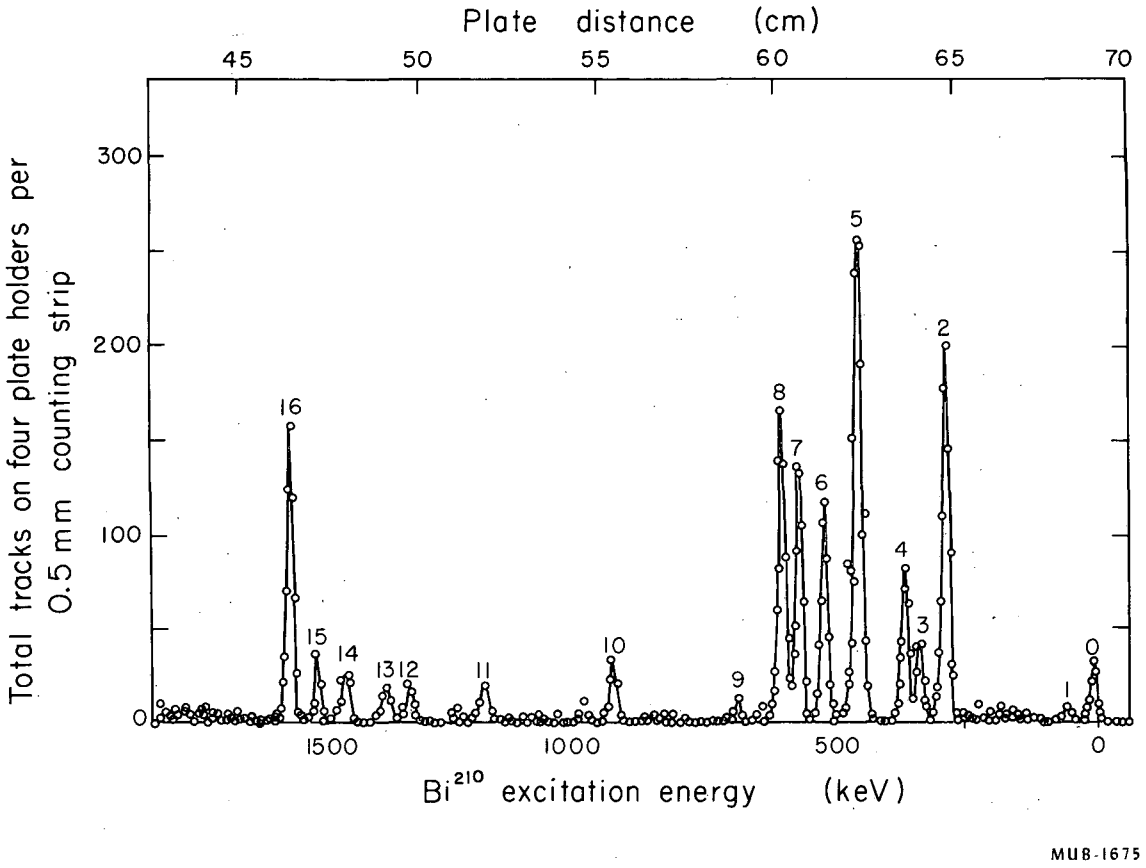

Fig. 8. Spectrum of protons from the (d,p) reaction on Bi^{209} as observed by Erskine et al. (Ref. 50).

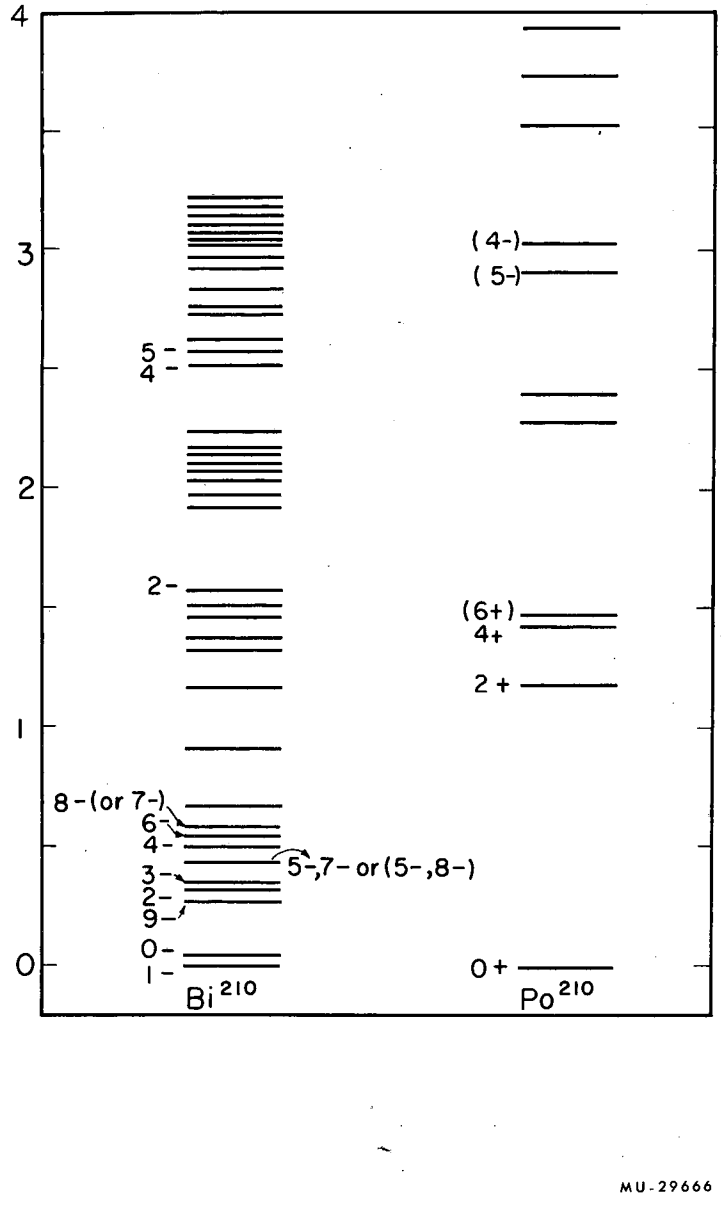

Fig. 9. The experimentally observed low-lying energy levels in Bi^{210} and Po^{210}.

core providing a harmonic-oscillator potential well for the extra nucleons, (i.e., harmonic-oscillator radial eigenfunctions are used, although eigenvalues for single-nucleon states are taken from data on nuclei with Pb^{208} plus one nucleon. There are two nucleons outside this doubly closed shell in Bi^{210} and Po^{210}. Sliv et al. have included the effects of Pb^{208} core excitation of a quadrupole surface-oscillation type. It generally appears from their work that such a refinement brings an important enhancement of E2 transition probabilities and a general lowering of levels, but that the relative level spacings for low-lying levels are not greatly altered.

The independent-particle energies are taken from the neighboring nuclei Pb^{209} and Bi^{209}, and the resulting zero-order energies are listed in Table IX. Recently seven single-particle levels for the neutron in Pb^{209} have been reported by Cohen et al.[55]

If one investigates the effects of the four central-force components separately, one finds that a central-force mixture cannot explain the inversion without losing the agreement on positions of other levels. The triplet-even central force which should be attractive and strongest of the components always brings the 0- state below the 1- state in energy. Although the triplet-odd part yields significantly large matrix elements similar to those for the triplet-even, we expect the triplet-odd matrix elements to be very small compared to the triplet-even contribution since the triplet-odd strength is known to be very weak from the free-space two-nucleon potential. The above arguments are seen by examination of Figs. 10 and 11, which are plots of the magnitude of diagonal matrix elements for $h_{9/2}g_{9/2}$ multiplet states. From Fig. 10 and 11 it is clear that a reasonable central force, predominantly attractive triplet-even, can explain most of the levels of the $h_{9/2}g_{9/2}$ multiplet except the inversion of the 0- and 1- states and that it is very difficult to adjust the force parameters so as to invert the 0- and 1- states without disturbing the sequence of other spin states in the $h_{9/2}g_{9/2}$ configuration. At this point we feel it most important to quantitatively evaluate the tensor-force matrix elements with a realistic radial dependence.

Table IX. Independent-particle energies[a] for Bi^{210} and Po^{210}.

Bi^{210}		Po^{210}	
Configuration (proton-neutron)	Energy (MeV)	Configuration (proton-proton)	Energy (MeV)
$h_{9/2}g_{9/2}$	0.0	$h_{9/2}h_{9/2}$	0.0
$h_{9/2}i_{11/2}$	0.77	$h_{9/2}f_{7/2}$	0.90
$f_{7/2}g_{9/2}$	0.90	$h_{9/2}i_{13/2}$	1.62
$h_{9/2}j_{15/2}$	1.41	$f_{7/2}f_{7/2}$	1.80
$h_{9/2}d_{5/2}$	1.56	$f_{7/2}i_{13/2}$	2.52
$f_{7/2}i_{11/2}$	1.67	$i_{13/2}i_{13/2}$	3.24
$h_{9/2}s_{1/2}$	2.03		
$f_{7/2}j_{15/2}$	2.31		
$f_{7/2}d_{5/2}$	2.46		
$h_{9/2}g_{7/2}$	2.47		
$h_{9/2}d_{3/2}$	2.52		
$f_{7/2}s_{1/2}$	2.93		
$f_{7/2}g_{7/2}$	3.37		
$f_{7/2}d_{3/2}$	3.42		

[a]The single-particle energies are taken from references 54 and 55.

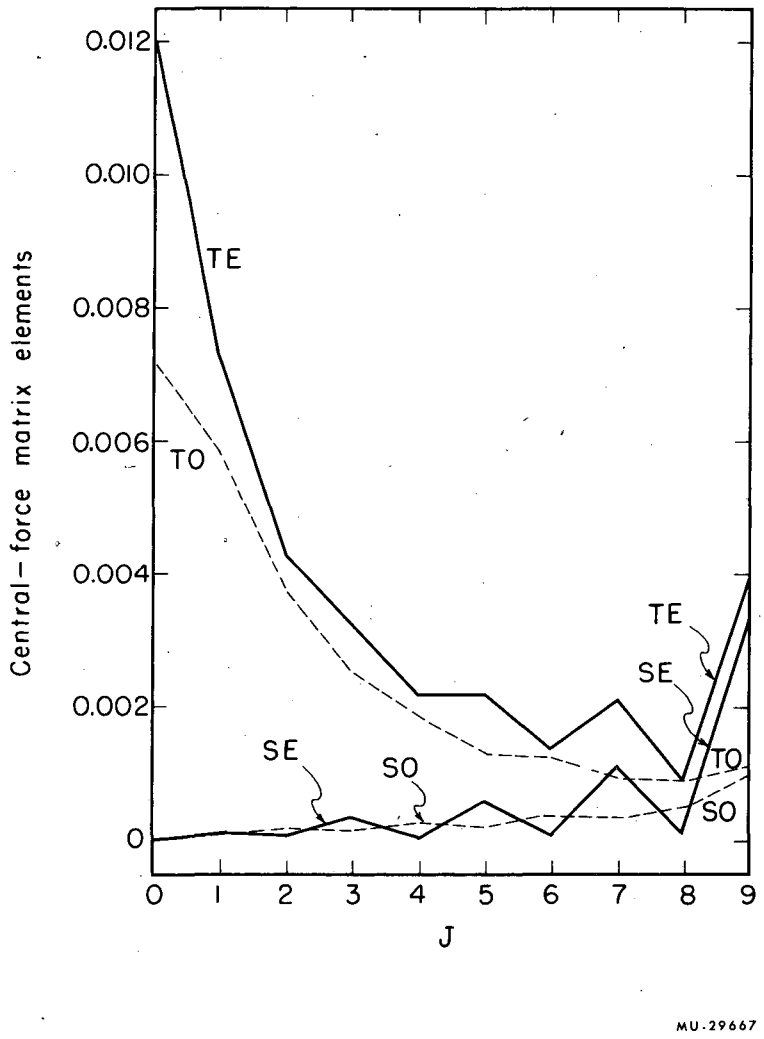

Fig. 10. The matrix elements of the four central-force components for the configuration $h_{9/2}\ g_{9/2}$ in Bi^{210}. The same range, 1.5 fm, is taken for all cases. The symbols TE, SE, TO, and SO stand for triplet-even, singlet-even, triplet-odd, and singlet-odd, respectively.

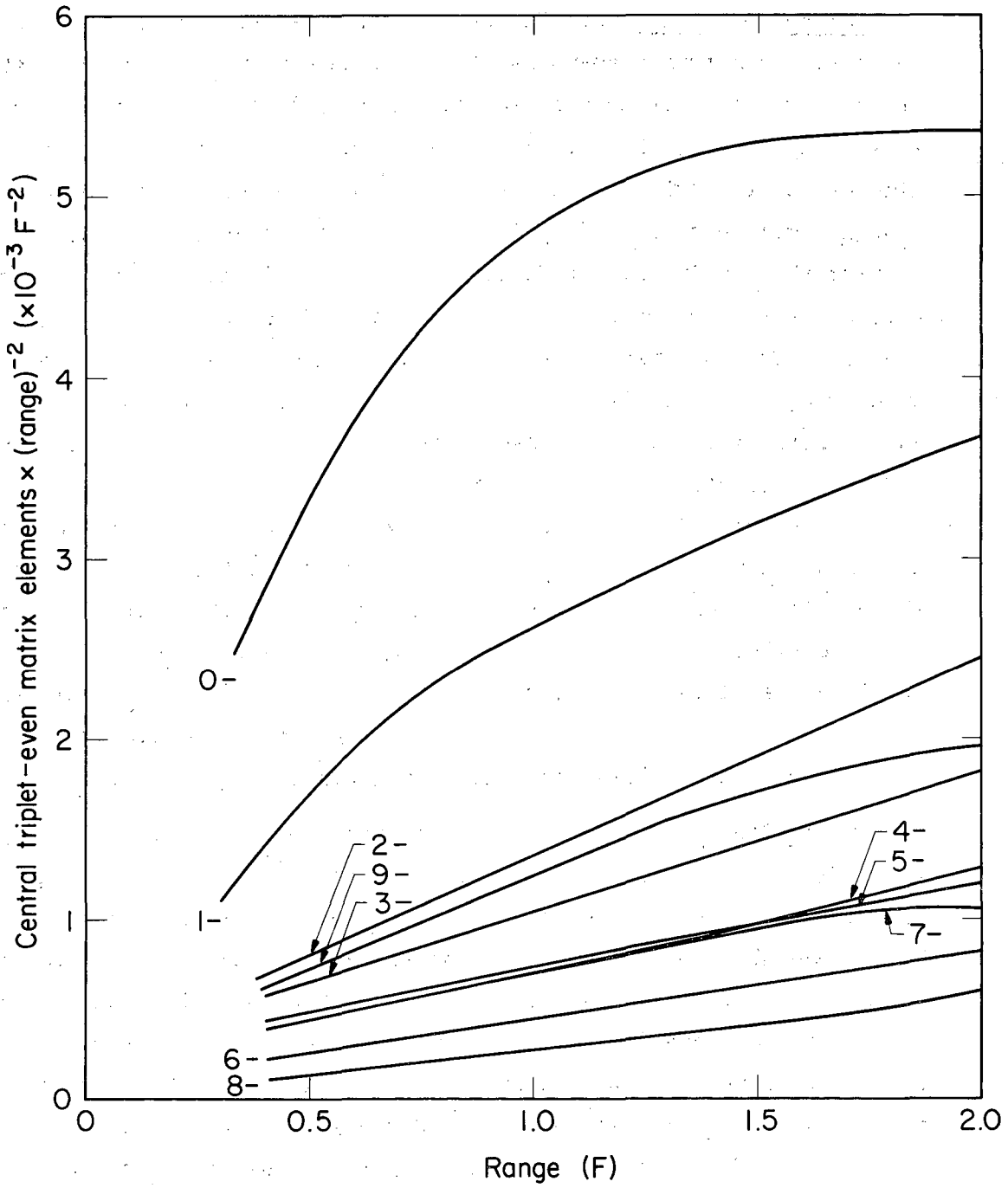

MUB-1935

Fig. 11. Diagonal matrix elements of the central triplet-even force $P_{TE}U^{C}_{TE}(r_{12})$ for the multiplet $h_{9/2}g_{9/2}$ in Bi^{210} as a function of the range parameter $(\beta^{C}_{TE})^{-1/2}$.

b. Tensor-Force Effects. The previously given expression for the tensor-force matrix element is still sufficiently complicated so that it is very difficult to draw any conclusions before doing the numerical work. Figures 11, 12, 13, 14, 15, 16, and 17 present the results for the diagonal contribution of the tensor-even and tensor-odd forces on the $h_{9/2}g_{9/2}$ multiplet as a function of the range parameter. These results confirm the qualitative predictions of Newby and Konopinski; for an attractive tensor force in that both even and odd components are quite repulsive for the spin-0 state. At the ranges comparable to the free-space ranges of Gammel-Thaler, the tensor force affects the spin-1 in an opposite sense to the spin-0 state, and it has only a rather small effect on the states of spin 2 or higher.

As shown in the figures, the tensor-force matrix elements are not always a monotonically increasing function of the range, and they may be either positive or negative in contrast to the central-force matrix elements. Thus the shorter-range tensor-force matrix elements are in quite different ratios to one another than in the infinite-range limit. This implies that the infinite-range approximation for the tensor force is not very realistic for shell-model calculations.

c. Energy Spectra. As the first approximation, Potential I listed in Table II was used for our calculation. The Po^{210} calculations gave somewhat too close spacing of the lowest 2+, 4+, 6+ level grouping. Their spacing seemed relatively insensitive to details of configuration mixing and to the tensor-force strength. Therefore, the central singlet-even force component seemed somewhat too weak and was strengthened by about 20% in the adjusted Potential II (see Table X). It should be noted that the singlet-even part of Potential I gives zero binding energy for a free-space, two-nucleon system. The calculations with Potential I on Bi^{210} showed that the central triplet-even part of Potential I is somewhat too weak to account for the overall spacings of the multiplet $h_{9/2}g_{9/2}$. Hence, the central triplet-even strength was increased by about 60% in Potential II. The central triplet-odd part was neglected entirely in Potential II, because it was very small

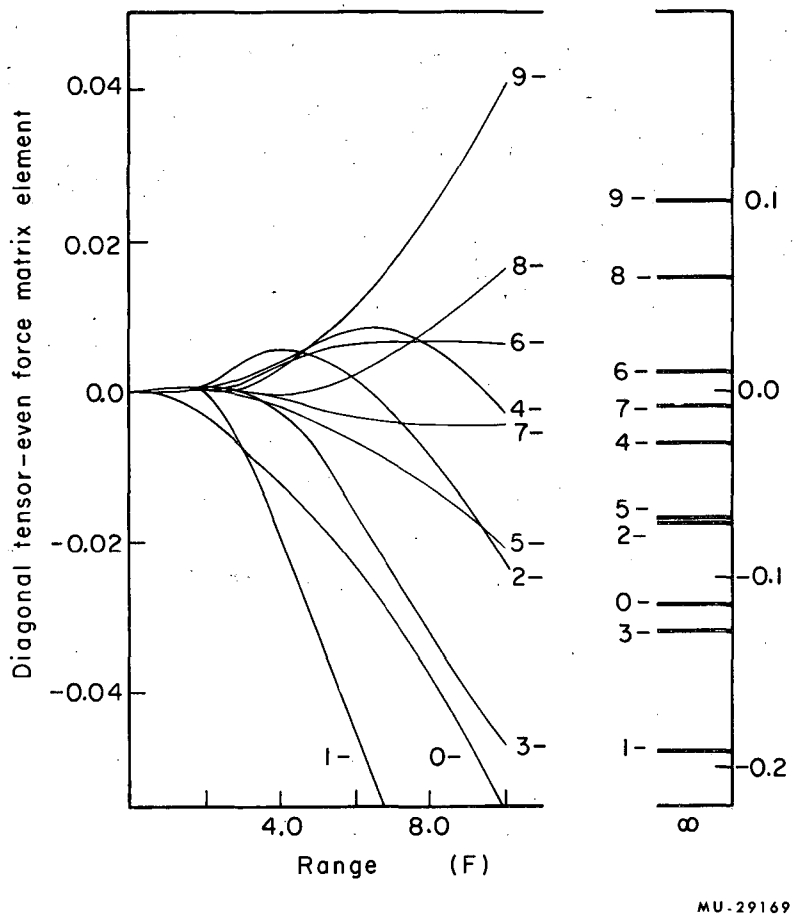

Fig. 12. Diagonal matrix elements of the tensor-even force $(1/3)\,P_{TE}U^{T}_{TE}(r_{12})S_{12}$ for the multiplet $h_{9/2}\,g_{9/2}$ in Bi^{210} as a function of the range parameters $(\beta^{T}_{TE})^{-1/2}$.

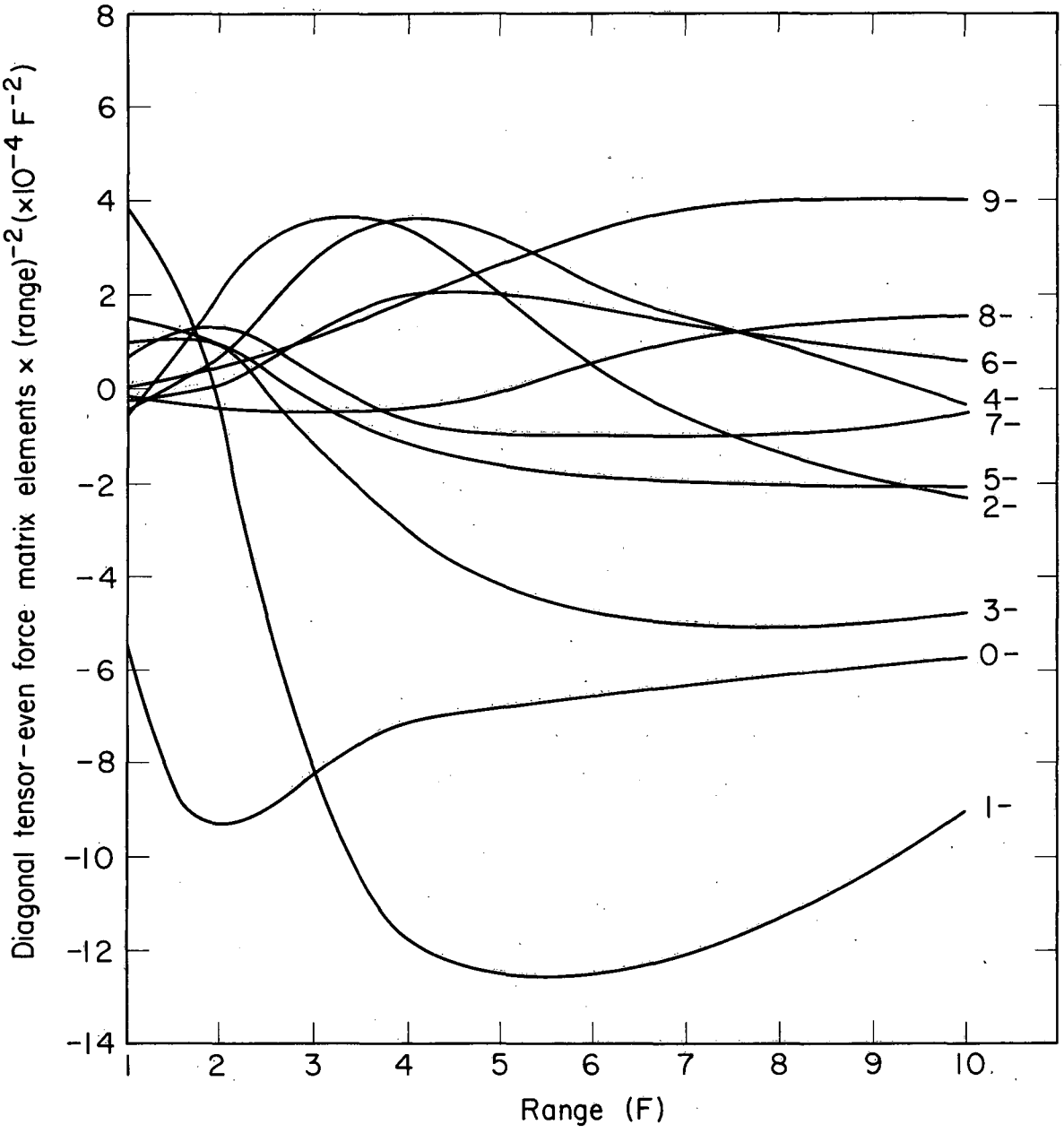

MUB-1936

Fig. 13. Diagonal matrix elements of the tensor-even force $\left[(1/3)P_{TE}U^{T}_{TE}(r_{12})S_{12} \right] (\beta^{T}_{TE})$ for the multiplet $h_{9/2}\, g_{9/2}$ in Bi^{210} as a function of the range parameter $(\beta^{T}_{TE})^{-1/2}$.

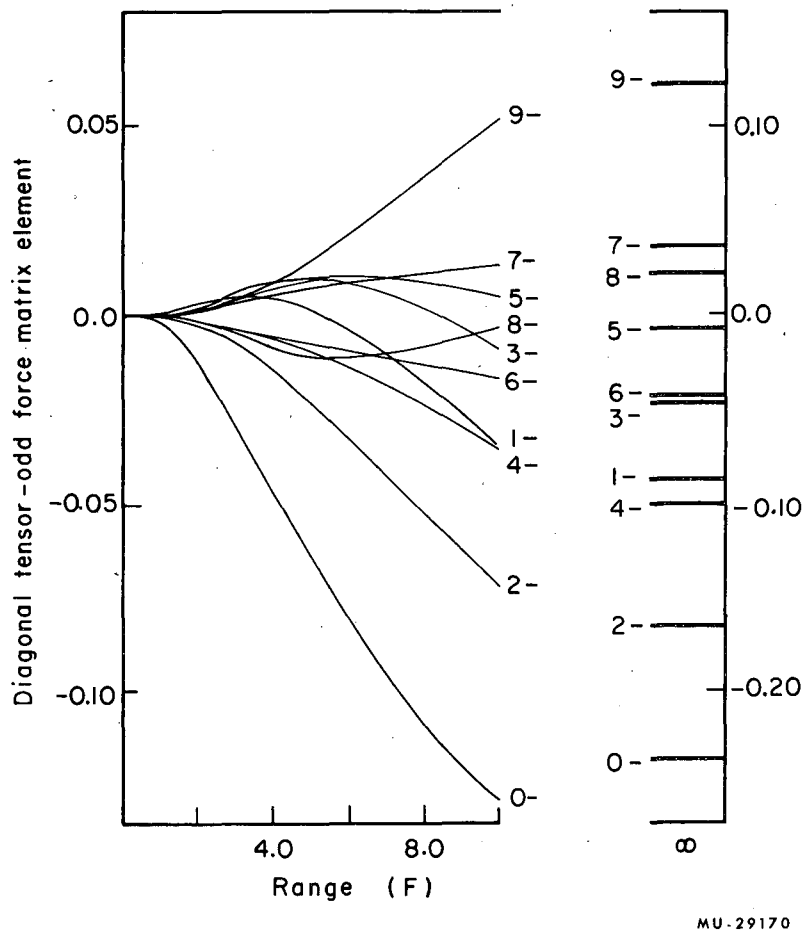

Fig. 14. Diagonal matrix elements of the tensor-odd force $(1/3)P_{TO}\ U^{T}_{TO}(r_{12})S_{12}$ for the multiplet $h_{9/2}\ g_{9/2}$ in Bi^{210} as a function of the range parameter $(\beta^{T}_{TO})^{-1/2}$.

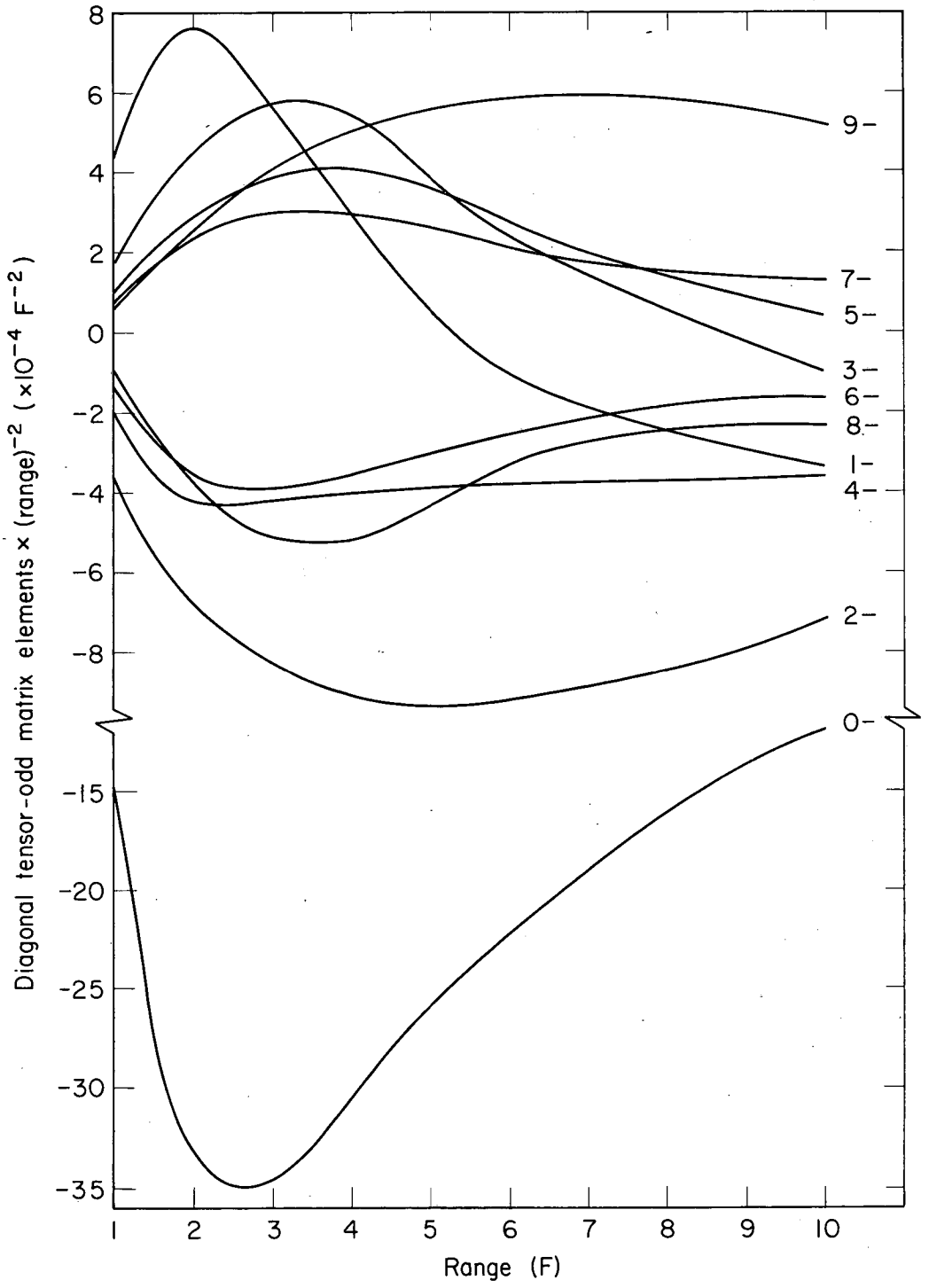

Fig. 15. Diagonal matrix elements of the tensor-odd force $\left[(1/3)P_{TO}U^{T}_{TO}(r_{12})S_{12} \right](\beta^{T}_{TO})$ for the multiplet $h_{9/2}\ g_{9/2}$ in Bi^{210} as a function of the range parameter $(\beta^{T}_{TO})^{-1/2}$.

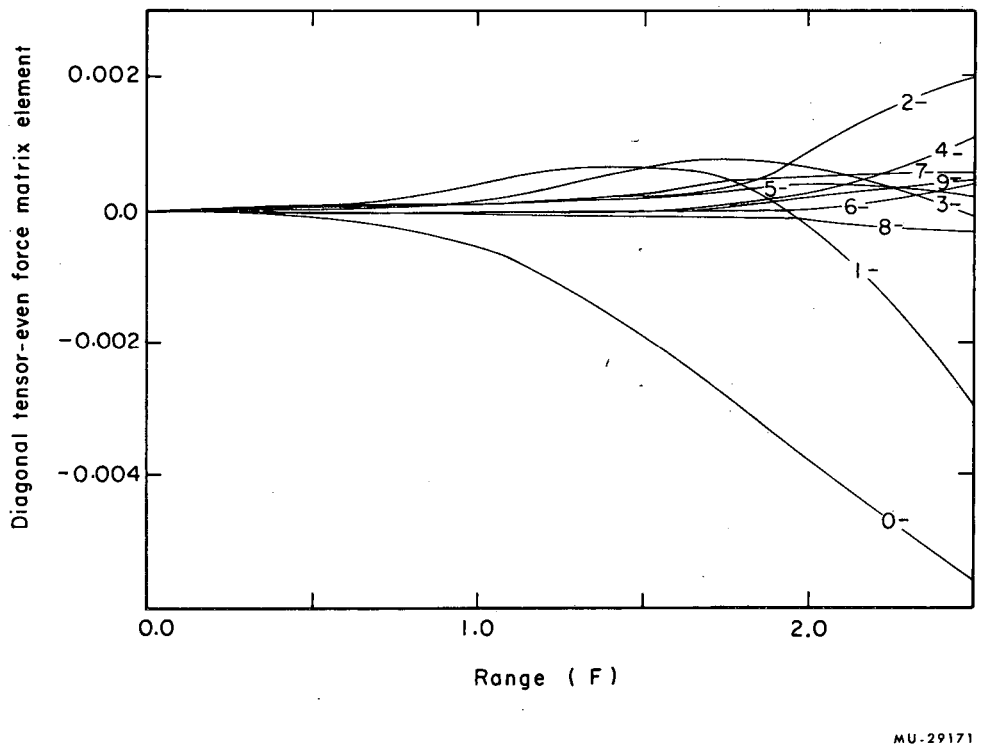

Fig. 16. Diagonal matrix elements of the tensor-even force for the multiplet $h_{9/2}\ g_{9/2}$ in Bi^{210} as a function of the range at the shorter ranges.

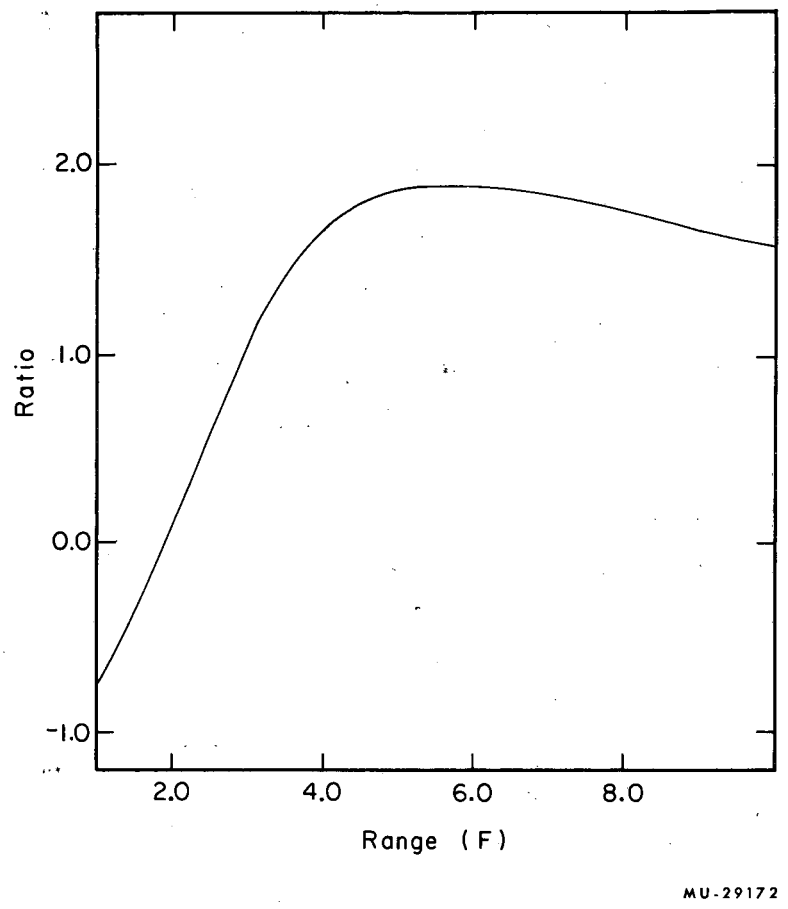

Fig. 17. Ratio of the diagonal tensor-even-force matrix element for the spin-1 state to the spin-0 state of the configuration $h_{9/2}\ g_{9/2}$ as a function of the range.

compared to the other components and did not affect the results very much. The singlet-odd force is repulsive, and it affects mostly the higher J states, particularly the J = 9 state, as can be seen from Fig. 10. The central singlet-odd force of Potential I was found to have an effect too strong for the J = 9 level, thus bringing the latter level above the J = 2 and 3 states in the energy spectrum, and we arbitrarily reduced the strength of the central singlet-odd force by a factor of about three to bring the J = 9 level down near the J = 2 level. In the next calculation, with the above modifications to the central force, and somewhat strengthened tensor force, it was found that the positions of the 0- and 1- level were incorrect. Therefore, tensor forces were further strengthened to give Potential II, listed in Table X.

In Figs. 18 and 19, we plot the effects on the ground-state multiplets of Bi^{210} and Po^{210} of adding successive components of our residual force. The $h_{9/2}d_{5/2}$ and $h_{9/2}s_{1/2}$ multiplets of Bi^{210} seen in the (d,p) reaction are also plotted in Fig. 18, and the $h_{9/2}i_{13/2}$(J = 4-, 5-) multiplet of Po^{210} is plotted in Fig. 19. All diagonal matrix elements include central and tensor forces. In diagonalizing the matrix, only central-force contributions to the off-diagonal matrix elements were used in Po^{210}. For Bi^{210} the off-diagonal tensor-force matrix elements of the lowest three configurations $h_{9/2}g_{9/2}$, $h_{9/2}i_{11/2}$, and $f_{7/2}g_{9/2}$ were calculated and included, but only central-force off-diagonal elements apply to other configurations. A complete list of the eigenvalues for our calculations is presented in Tables XI and XII. The eigenfunctions are also calculated both for Bi^{210} and Po^{210} and are presented in Tables XIII and XIV, respectively. For Bi^{210}, the eigenfunctions are listed for the eigenvalues that correspond to the states arising from the lowest six odd-parity configurations, and for Po^{210} the eigenfunctions only for the even parity states are listed.

Table X. Values of the force parameters for Potential II used in Bi^{210} and Po^{210} calculations.

Components	Strength (MeV)	Range (F)
Central triplet-even	-355.24	0.706
Central singlet-even	-133.20	1.018
Central triplet-odd	0.0	-----
Central singlet-odd	11.01	1.476
Tensor triplet-even	- 99.28	1.407
Tensor triplet-odd	9.50	1.845

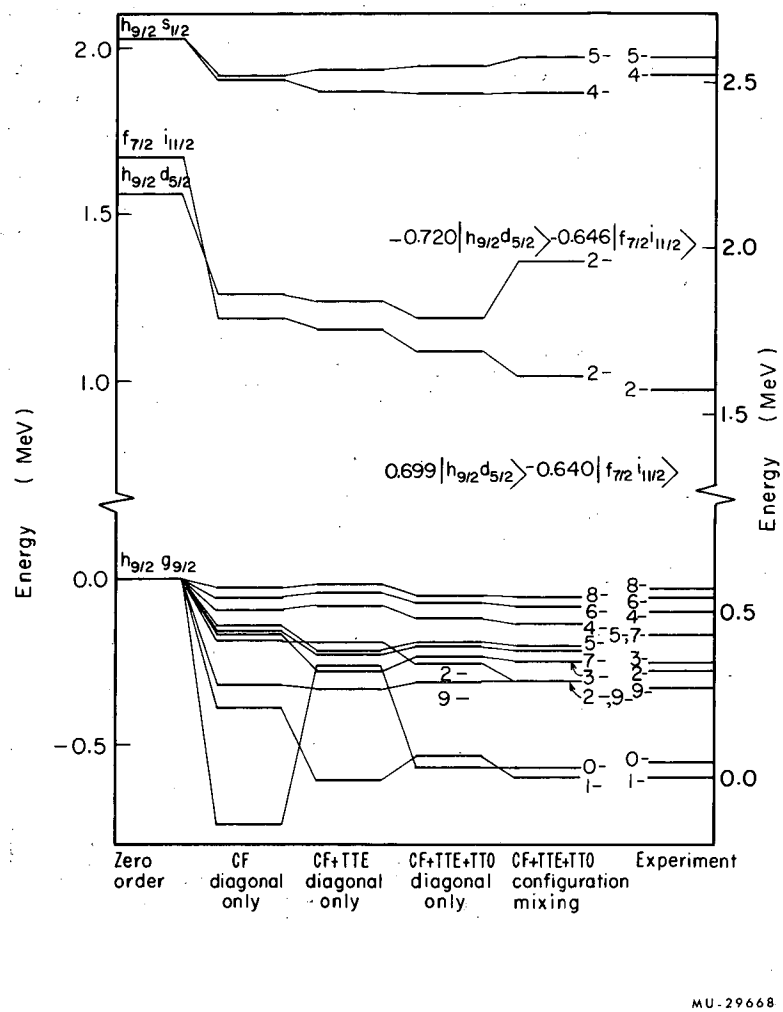

Fig. 18. Comparison of the experimental and calculated spectra of Bi^{210} with the slightly modified residual force. The symbols CF, TTE, and TTO refer to the central, tensor-even, and tensor-odd forces, respectively.

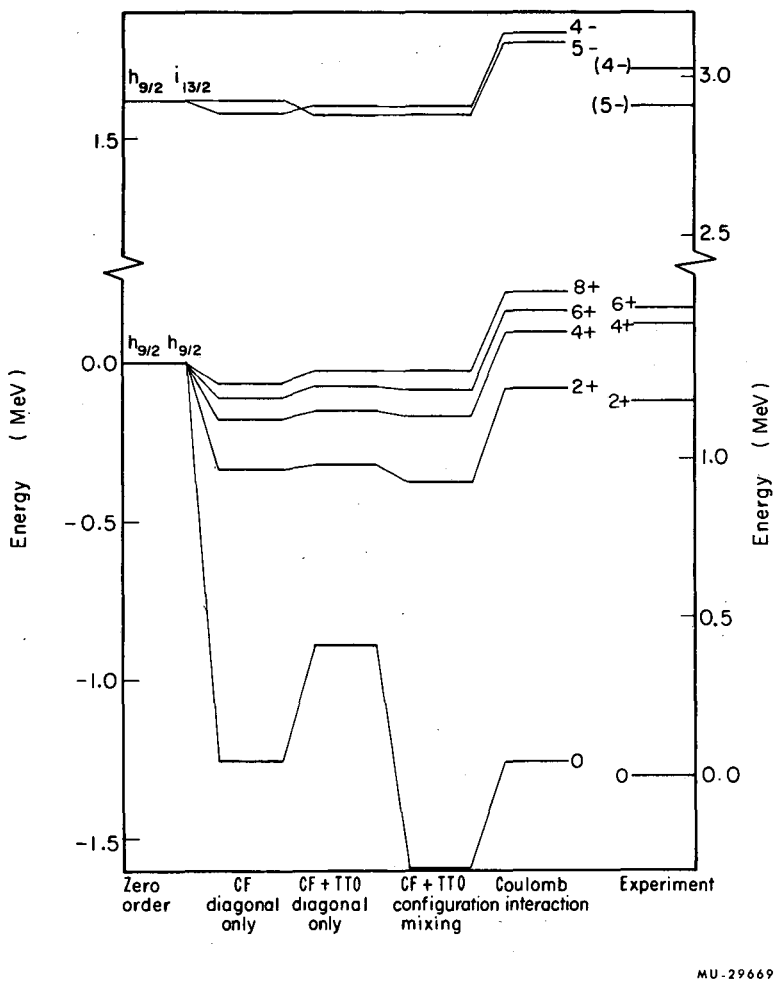

Fig. 19. Comparison of the experimental and calculated spectra of Po^{210}. The abbreviations CF and TTO refer to the central and tensor-odd forces, respectively.

Table XI. Calculated eigenvalues and energy levels in Bi^{210}. In the last column, eigenvalues are expressed in a new energy scale in which the ground state lies at zero energy. The indicated configuration is taken to be the dominant one.

Configuration (proton-neutron)	$J\pi$	Eigenvalues (MeV)	Energy (MeV)
$h_{9/2}\ g_{9/2}$	0-	-0.572	0.022
	1-	-0.594	0.0
	2-	-0.311	0.283
	3-	-0.251	0.343
	4-	-0.135	0.459
	5-	-0.202	0.392
	6-	-0.084	0.510
	7-	-0.218	0.376
	8-	-0.062	0.532
	9-	-0.310	0.284
$h_{9/2}\ i_{11/2}$	1-	0.076	0.670
	2-	0.534	1.128
	3-	0.573	1.167
	4-	0.688	1.282
	5-	0.655	1.249
	6-	0.646	1.240
	7-	0.708	1.302
	8-	0.345	0.939
	9-	0.753	1.347
	10-	0.212	0.806
$f_{7/2}\ g_{9/2}$	1-	0.529	1.123
	2-	0.701	1.295
	3-	0.796	1.390
	4-	0.776	1.370
	5-	0.818	1.412

Table XI. (Continued)

Configuration (proton-neutron)	Jπ	Eigenvalues (MeV)	Energy (MeV)
$f_{7/2}\ g_{9/2}$	6-	0.761	1.355
	7-	0.854	1.448
	8-	0.671	1.265
$h_{9/2}\ d_{5/2}$	2-	1.015	1.609
	3-	1.390	1.984
	4-	1.390	1.984
	5-	1.421	2.015
	6-	1.483	2.077
	7-	1.402	1.996
$f_{7/2}\ i_{11/2}$	2-	1.358	1.952
	3-	1.469	2.063
	4-	1.529	2.123
	5-	1.498	2.092
	6-	1.573	2.167
	7-	1.490	2.084
	8-	1.600	2.194
	9-	1.324	1.918
$h_{9/2}\ s_{1/2}$	4-	1.869	2.463
	5-	1.970	2.564
$f_{7/2}\ d_{5/2}$	1-	2.066	2.660
	2-	2.256	2.850
	3-	2.283	2.877
	4-	2.263	2.857
	5-	2.393	2.987
	6-	2.126	2.720

Table XI. (Continued)

Configuration (proton-neutron)	Jπ	Eigenvalues (MeV)	Energy (MeV)
$h_{9/2}\ g_{7/2}$	1-	2.176	2.770
	2-	2.444	3.038
	3-	2.354	2.948
	4-	2.390	2.984
	5-	2.417	3.011
	6-	2.235	2.829
	7-	2.449	3.043
	8-	2.180	2.774
$h_{9/2}\ d_{3/2}$	3-	2.485	3.079
	4-	2.521	3.115
	5-	2.505	3.099
	6-	2.476	3.070
$f_{7/2}\ s_{1/2}$	3-	2.800	3.394
	4-	2.778	3.372
$f_{7/2}\ g_{7/2}$	0-	2.530	3.124
	1-	2.698	3.292
	2-	3.034	3.628
	3-	3.035	3.629
	4-	3.220	3.814
	5-	3.056	3.650
	6-	3.268	3.862
	7-	2.942	3.536

Table XI. (Continued)

Configuration (proton-neutron)	Jπ	Eigenvalues (MeV)	Energy (MeV)
$f_{7/2}\ d_{3/2}$	2-	3.094	3.688
	3-	3.247	3.841
	4-	3.327	3.921
	5-	3.156	3.750
$h_{9/2}\ j_{15/2}$	3+	0.496	1.090
	4+	1.083	1.677
	5+	1.140	1.734
	6+	1.131	1.725
	7+	1.249	1.846
	8+	1.133	1.727
	9+	1.290	1.884
	10+	1.090	1.684
	11+	1.311	1.905
	12+	0.880	1.474
$f_{9/2}\ j_{15/2}$	4+	2.051	2.645
	5+	2.243	2.837
	6+	2.230	2.824
	7+	2.221	2.815
	8+	2.269	2.863
	9+	2.177	2.771
	10+	2.291	2.885
	11+	1.969	2.563

Table XII. Calculated eigenvalues and energy levels in Po^{210}. In the last column, eigenvalues are expressed in a new nergy scale in which the ground state lies at zero energy. The indicated configuration is taken to be the dominant one.

Configuration (proton-proton)	J^{π}	Eigenvalues (MeV)	Energy (MeV)
$h_{9/2}\ h_{9/2}$	0+	-1.597	0.0
	2+	-0.373	1.224
	4+	-0.166	1.431
	6+	-0.084	1.513
	8+	-0.027	1.570
$h_{9/2}\ f_{7/2}$	1+	0.303	1.900
	2+	0.582	2.179
	3+	0.792	2.389
	4+	0.928	2.525
	5+	0.855	2.452
	6+	0.896	2.493
	7+	0.864	2.461
	8+	0.863	2.460
$f_{7/2}\ f_{7/2}$	0+	0.868	2.465
	2+	0.764	2.361
	4+	1.664	3.261
	6+	1.741	3.338
$i_{13/2}\ i_{13/2}$	0+	2.718	4.315
	2+	2.903	4.500
	4+	3.050	4.647
	6+	3.118	4.715
	8+	3.158	4.755
	10+	3.187	4.784
	12+	3.222	4.819

Table XII. (Continued)

Configuration (proton-proton)	Jπ	Eigenvalues (MeV)	Energy (MeV)
$h_{9/2}\ i_{13/2}$	2-	1.526	3.123
	3-	1.645	3.242
	4-	1.575	3.172
	5-	1.602	3.199
	6-	1.582	3.179
	7-	1.567	3.164
	8-	1.583	3.180
	9-	1.510	3.107
	10-	1.583	3.180
	11-	1.315	2.912
$f_{7/2}\ i_{13/2}$	3-	2.315	3.912
	4-	2.497	4.094
	5-	2.438	4.035
	6-	2.510	4.107
	7-	2.474	4.071
	8-	2.512	4.109
	9-	2.499	4.096
	10-	2.506	4.103

Table XIII. Calculated eigenfunctions for Bi^{210}.

Eigenvalues	Eigenfunctions											
(MeV)	$h_{9/2}\ g_{9/2}$	$h_{9/2}\ i_{11/2}$	$f_{7/2}\ g_{9/2}$	$h_{9/2}\ d_{5/2}$	$f_{7/2}\ i_{11/2}$	$h_{9/2}\ s_{1/2}$	$f_{7/2}\ d_{5/2}$	$h_{9/2}\ g_{7/2}$	$h_{9/2}\ d_{3/2}$	$f_{7/2}\ s_{1/2}$	$f_{7/2}\ g_{7/2}$	$f_{7/2}\ d_{3/2}$
J = 0												
-0.572	-0.9999										0.0099	
J = 1												
-0.594	0.9767	-0.1883	0.0578				0.0130	-0.0819			-0.0130	
0.076	0.0893	0.6836	0.7167				0.0753	0.0232			-0.0686	
0.529	0.1735	0.6925	-0.6708				0.0680	-0.0154			0.1878	
J = 2												
-0.311	-0.9727	-0.1114	0.0175	-0.1049	0.1696		-0.0010	-0.0305			0.0073	0.0139
0.534	-0.1694	0.9000	-0.1774	0.0038	-0.3500		-0.0480	0.0638			-0.0131	0.0233
0.701	-0.0094	-0.2073	-0.9711	0.1073	-0.0300		-0.0272	0.0017			0.0114	0.0211
1.015	-0.1564	-0.2632	0.1510	0.6690	-0.6403		-0.0089	0.1526			-0.0458	-0.0153
1.358	-0.0065	-0.2511	-0.0063	-0.7205	-0.6459		0.0030	0.0141			0.0015	-0.0123
J = 3												
-0.251	-0.9951	0.0212	-0.0151	-0.0593	-0.0660		-0.0053	0.0041	0.0272	-0.0136	-0.0006	-0.0088
0.573	-0.0145	-0.8796	-0.4721	0.0186	0.0230		-0.0277	-0.0193	-0.0125	-0.0116	0.0286	0.0057
0.796	-0.0187	-0.4734	0.8758	0.0121	-0.0586		0.0021	-0.0002	0.0447	-0.0058	-0.0520	-0.0058
1.390	-0.0909	0.0140	0.0441	0.7650	0.6245		0.0031	-0.0543	-0.0957	0.0138	0.0368	0.0213
1.469	-0.0132	-0.0181	0.0514	-0.6366	0.7657		-0.0187	-0.0641	-0.0158	-0.0048	0.0092	0.0173
J = 4												
-0.135	0.9944	0.0643	0.0168	0.0407	-0.0606	0.0227	0.0100	0.0160	0.0124	0.0122	-0.0071	-0.0078
0.688	-0.0691	0.9414	0.3117	-0.0259	-0.0858	-0.0493	-0.0129	0.0196	-0.0221	-0.0092	-0.0106	-0.0007
0.776	-0.0040	0.3112	-0.9492	-0.0003	-0.0311	0.0026	-0.0265	0.0073	0.0101	0.0025	0.0120	0.0110
1.390	-0.0702	-0.0154	0.0116	0.8492	-0.4537	0.2189	0.0040	0.0981	0.0953	0.0064	-0.0259	-0.0090
1.529	-0.0266	-0.0963	-0.0027	-0.4679	-0.8762	-0.0371	0.0085	0.0396	0.0035	0.0101	-0.0064	-0.0088
0.869	-0.0153	0.0446	0.0173	-0.2299	0.0829	0.9519	-0.0240	0.1039	0.1395	-0.0120	-0.0225	-0.0008

Table XIII. (Continued)

Eigenvalues	Eigenfunctions											
(MeV)	$h_{9/2}\ g_{9/2}$	$h_{9/2}\ i_{11/2}$	$f_{7/2}\ g_{9/2}$	$h_{9/2}\ d_{5/2}$	$f_{7/2}\ i_{11/2}$	$h_{9/2}\ s_{1/2}$	$f_{7/2}\ d_{5/2}$	$h_{9/2}\ g_{7/2}$	$h_{9/2}\ d_{3/2}$	$f_{7/2}\ s_{1/2}$	$f_{7/2}\ g_{7/2}$	$f_{7/2}\ d_{3/2}$
J = 5												
-0.202	-0.9967	-0.0005	-0.0107	-0.0565	-0.0410	-0.0326	-0.0049	-0.0081	-0.0030		-0.0136	-0.0103
0.655	-0.0020	0.9564	0.2849	-0.0212	-0.0444	-0.0200	0.0134	0.0119	0.0001		-0.0258	-0.0107
0.818	-0.0106	-0.2857	0.9554	0.0353	-0.0291	0.0343	0.0041	0.0005	0.0175		-0.0419	-0.0022
1.421	-0.0715	0.0433	-0.0199	0.9421	0.2651	0.1841	0.0067	0.0027	-0.0156		0.0204	0.0103
1.498	-0.0198	0.0249	0.0498	-0.2624	0.9575	-0.0499	-0.0205	-0.0686	-0.0335		0.0248	0.0365
1.970	-0.0222	0.0219	-0.0213	-0.1952	0.0006	0.9788	0.0324	0.0339	0.0022		0.0111	-0.0027
J = 6												
-0.084	-0.9953	-0.0739	-0.0334	-0.0210	0.0348		-0.0091	-0.0197	-0.0229		0.0018	
0.646	-0.0809	0.8091	0.5785	-0.0069	-0.0516		0.0018	0.0149	-0.0272		-0.0164	
0.761	-0.0157	0.5786	-0.8142	-0.0139	-0.0251		-0.0277	0.0110	-0.0092		0.0118	
1.483	-0.0346	-0.0062	-0.0108	0.9381	-0.3194		0.0154	0.0743	0.1032		-0.0106	
1.573	-0.0226	-0.0594	-0.0079	-0.3297	-0.9392		0.0309	0.0546	0.0330		-0.0058	
J = 7												
-0.218	-0.9960	-0.0166	-0.0087	-0.0829	-0.0207			-0.0106			0.0012	
0.708	-0.0142	0.9827	0.1686	-0.0313	-0.0591			0.0072			-0.0331	
0.854	-0.0090	-0.1708	0.9819	0.0488	-0.0301			0.0004			-0.0569	
1.402	-0.0846	0.0416	-0.0404	0.9919	0.0707			0.0215			0.0045	
1.490	-0.0151	0.0513	0.0452	-0.0713	0.9924			-0.0572			0.0423	
J = 8												
-0.062	0.9884	0.1138	0.0928		-0.0204			0.0316				
0.345	0.1333	-0.4186	-0.8979		0.0249			-0.0075				
0.671	0.0648	-0.8991	0.4301		0.0383			-0.0280				
1.600	0.0176	0.0507	0.0074		0.9917			-0.1158				
J = 9												
-0.310	0.9993	0.0363			-0.0026							
0.753	0.0364	-0.9946			0.0962							
1.324	0.0008	-0.0963			-0.9953							

Table XIV. Calculated eigenfunctions for the even-parity states in Po^{210}.

Eigenvalue (MeV)	Eigenfunctions			
	$h_{9/2}\ h_{9/2}$	$h_{9/2}\ f_{7/2}$	$f_{7/2}\ f_{7/2}$	$i_{13/2}\ i_{13/2}$
J = 0				
-1.597	-0.8845		-0.3032	0.3544
1.016	-0.3697		0.9190	-0.1364
2.718	-0.2844		-0.2517	-0.9250
J = 2				
-0.372	-0.9895	-0.0305	-0.0873	0.1109
0.928	-0.0350	0.9989	0.0216	-0.0208
1.518	-0.0979	-0.0269	0.9896	-0.1013
2.904	-0.1003	-0.0217	-0.1116	-0.9884
J = 4				
-0.166	-0.9965	-0.0369	-0.0446	0.0589
0.896	-0.0390	0.9988	0.0152	-0.0224
1.664	-0.0474	-0.0183	0.9969	-0.0586
3.051	-0.0553	-0.0236	-0.0616	-0.9962
J = 6				
-0.084	-0.9980	-0.0433	-0.0254	-0.0383
0.0863	-0.0446	0.9986	0.0113	-0.0251
1.741	-0.0263	-0.0134	0.9989	-0.0363
3.118	-0.0362	-0.0263	-0.0376	-0.9982
J = 8				
-0.027	-0.9977	-0.0622		0.0260
0.764	-0.0630	0.9974		-0.0336
3.158	-0.0239	-0.0352		-0.9900

d. Discussion. From the analysis of various shell-model calculations and the study of the properties of nuclear matter, there are indications that the nuclear force inside the nucleus is not very different from the free two-nucleon force. We have relied upon the free two-nucleon potential in estimating the parameters of the central and tensor forces. Our analysis of the tensor-force effect indicates that the tensor force behaves quite differently from the central force and, indeed, seems to correct the order and spacing of the troublesome spin-0 and 1 levels in Bi^{210}. The analysis of Bi^{210} leads to the conclusion that the range of the tensor force in the residual interaction is about 2 fm or less. As shown clearly in Figs 12 and 14, the infinite-range approximation for the tensor force is very dangerous. At the short ranges employed, the tensor force acts so specifically on the two levels of spin 0 and 1 that it can not be simulated by a linear combination of the four central-force components. Our choice of the residual force (Potential II) which is slightly modified from the simulated BGT potential (Potential I) seems to give a rather good agreement with the experimental spectra. Since our residual force explains the ground-state multiplet of Bi^{210} very well, it is interesting to see if we can explain the other observed multiplets from our theoretical calculation. Levels from 0 to 0.581 MeV are clearly from the configuration $(h_{9/2}g_{9/2})$, and the spin assignments shown in Fig. 9 are probably correct. Also the assignments of $(h_{9/2}d_{5/2})^{J=2}$ and $(h_{9/2}s_{1/2})^{J=4,5}$ for levels at 1.577, 2.517, and 2.572 MeV seem reasonable. Erskine suggested from the central-force calculation that levels at 0.672 and 0.912 are $(g_{9/2}i_{11/2})^{J=10}$ and $(f_{7/2}g_{9/2})^{J=8}$, respectively.[53] The relative cross sections also appear to support these assignments. Erskine et al. found that the level at 0.672 MeV is very weak, suggesting $(h_{9/2}i_{11/2})^{J=10}$. If this is true, the other J states from $(h_{9/2}i_{11/2})$ are not expected to appear. Six levels ranging from 0.912 to 1.517 MeV are probably from the admixture of $(f_{7/2}g_{9/2})$ and $(h_{9/2}i_{11/2})$, the dominant part being $(f_{7/2}g_{9/2})$. Because of the configuration mixing, the relative cross sections are not very useful for assigning the spins of these levels.

At higher energies, the various other factors such as core excitation and core vibration must be considered, and it is very difficult to conclude any assignments of spin and parity. However, six levels at 1.577, 1.916, 2.075, 2.138, 2.173, and 2.235 MeV have comparatively smaller relative cross sections than four levels at 1.972 (doublet), 2.027, and 2.102 MeV, and this suggests these six levels are probably from the admixture of $(h_{9/2}d_{5/2})$ and $(f_{7/2}i_{11/2})$, with $(h_{9/2}d_{5/2})$ being the dominant configuration. Four other levels at 1.972 (doublet), 2.027, and 2.102 MeV seem to come from the configuration $(p_{3/2}g_{9/2})$ arising from the core-excitation. It appears to be very difficult to assign configurations to the levels above 2.5 MeV, because the core vibration and core excitation surely become more important. The suggested spin and parity assignments for the levels below 2.6 MeV are summarized in Table XV.

The β-decay properties of Bi^{210} have played an important role in the developement of β-decay theory, because it is one of the few known cases of a first-forbidden transition $\Delta I = 1$(yes) showing striking deviations from the allowed shape. The so called ξ approximation can explain the spectrum shape if certain beta-decay matrix elements bear certain ratios to each other. As an independent check from the shell-model theory on the value of ξ, which is the ratio $i\langle r\rangle/(\underset{\sim}{\sigma}\times\underset{\sim}{r})$, we use the ground-state wave functions of Bi^{210} and Po^{210} presented in Tables XIII and XIV and find $\xi \approx -0.63$. (Only the lowest three configurations are used for Bi^{210}, since these three configurations are dominant. We used the results of Newby and Konopinski to evaluate the β-decay matrix elements.[51]) For the pure configuration $h_{9/2}i_{11/2}$, the value of ξ is +1.0, whereas it is -0.1 for the pure $h_{9/2}g_{9/2}$ configuration.[55a] The recent paper by Fujita[56] on the beta-decay of RaE based upon the conserved-current hypothesis of Feynman and Gell-Mann[57] indicated that the value of ξ should be $-1.2 \leqslant \xi \leqslant -0.48$ in order to fit both the beta-spectrum shape and the beta-polarization data, whereas we have $-1.2 \leqslant \xi \leqslant 0.12$ if we consider only the spectrum shape. Our value of $\xi = -0.63$ is consistent with the limit set by Fujita.

Table XV. Suggested spin and parity assignments for levels below 2.6 MeV in Bi^{210}. Level energies and relative differential cross sections are taken from Erskine et al. (reference 50). The spins for $(h_{9/2}\ g_{9/2})^{J=0,\ldots,9}$, $(h_{9/2}\ d_{5/2})^{J=2}$, and $(h_{9/2}\ s_{1/2})^{J=4,5}$ have been suggested by Erskine et al.

Energy (MeV)	Relative differential cross section	Suggested $J\pi$	Suggested configuration
0.0	1.4	1-	$(h_{9/2}\ g_{9/2})$
0.047	0.4	0-	
0.268	9.6	9-	
0.320	2.3	2-	
0.347	3.8	3-	
0.433	14.9	5- and 7-	
0.501	5.3	4-	
0.547	7.0	6-	
0.581	8.0	8-	
0.672	0.4	(10-)	$(h_{9/2}\ i_{11/2})$
0.912	1.9	(8-)	$\alpha(f_{7/2}\ g_{9/2})+\beta(h_{9/2}\ i_{11/2})$
1.172	1.2	(3- or 5-)	
1.325	0.9	(5- or 3-)	
1.372	1.0	(4-)	
1.460	1.6	(6- or 7-)	
1.517	1.4	(7- or 6-)	
1.577	6.9	2-	$\gamma(h_{9/2}d_{5/2})+\delta(f_{7/2}i_{11/2})$
1.916	21.6	(4-)	
2.075	26.3	(7-)	
2.138	9.3	(3-)	
2.173	24.9	(6-)	
2.235	23.5	(5-)	

Table XV. (Continued)

Energy (MeV)	Relative differential cross section	Suggested $J\pi$	Suggested configuration
1.972 (doublet)	123	(3- and 6-)	$(p_{3/2}\ g_{9/2})$
2.027	58.9	(5-)	
2.102	51.4	(4-)	
2.517	125	4-	$(h_{9/2}\ s_{1/2})$
2.572	181	5-	

The reason we obtain the value of $\xi(-0.63)$ outside the limit of the two pure configurations ($\xi = -0.1$ for $h_{9/2}g_{9/2}$ and $\xi = 1.0$ for $h_{9/2}i_{11/2}$) is the large positive value of the off-diagonal tensor-force matrix element $\langle h_{9/2}g_{9/2}|V^T(\underline{r}_{12})S_{12}|h_{9/2}i_{11/2}\rangle$, which in turn yields a negative component of the eigenvector $|h_{9/2}i_{11/2}\rangle$. To show that the off-diagonal tensor-force matrix element $\langle h_{9/2}g_{9/2}|V^T(\underline{r}_{12})S_{12}|h_{9/2}i_{11/2}\rangle$ is positive and rather large for the range we are using, we plot $(1/3)\langle h_{9/2}g_{9/2}|P_{TE}U_{TE}{}^T(\underline{r}_{12})S_{12}|h_{9/2}i_{11/2}\rangle$ and $(1/3)\langle h_{9/2}g_{9/2}|P_{TO}U_{TO}{}^T(\underline{r}_{12})S_{12}|h_{9/2}i_{11/2}\rangle$ as a function of the force range in Fig. 20. The central-force off-diagonal matrix element is smaller and of the opposite sign compared to the tensor, so we see the essential role of the tensor force in inducing configuration mixtures of the proper phase to explain the beta-decay phenomena.

Most recently, a reanalysis by Spector[58] of RaE beta decay has established the limits $-1.6 < \xi < -0.8$, which aregely overlap Fujita's limits. From a shell-model analysis (without tensor force) in which the mixing of the core-excited states is taken into account through a delta-function force, Spector obtains $\xi \approx -1$ for $\Delta E = \hbar\omega \approx 4$ MeV. The strength of the delta-function force is chose by Spector so as to preserve the volume energy of the delta-function potential when compared to the finite-range force used by Newby and Konopinski.[51] Therefore, we feel that Spector's calculation may overestimate the amplitudes of mixing of the core-excited states, because it is known[59,60] that this choice of the strength of the delta-function force yields larger matrix elements (by a factor of 3 to 4) than the finite-range force used by Newby and Konopinski. We feel that the dominant consideration leading to satisfactory ξ values for the shell model is the reversed sign of the configuration mixture of the principal two configurations, as caused by the tensor force. The additional smaller contribution due to the core-excited states may well bring our value of ξ (= -0.63) within the limit ($-1.6 < \xi < -0.8$) set by Spector. More refined analysis is necessary to obtain quantitative results with inclusion of both the core excitation and the tensor force.

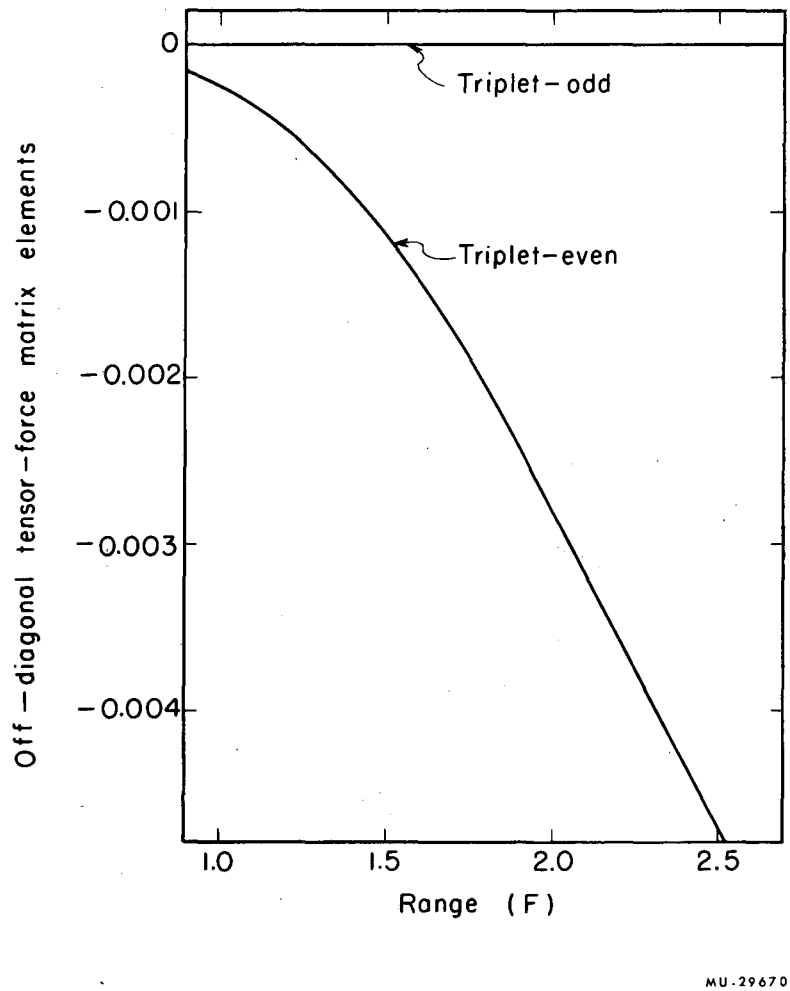

Fig. 20. Off-diagonal tensor-force matrix elements $(1/3)\langle h_{9/2}\, g_{9/2} | P_{TE}\, S_{12} | h_{9/2}\, i_{11/2}\rangle$ and $(1/3)\langle h_{9/2}\, g_{9/2} | P_{TO}\, S_{12} | h_{9/2}\, i_{11/2}\rangle$ for Bi^{210} as a function of the force range.

Another interesting quantity is the magnetic dipole moment of Bi^{210}. Using the atomic-beam technique, Alpert et al. have measured this moment to be 0.0442±0.0001 nm.[61] If one assumes pure configurations, the magnetic moment in the Schmidt limit is +0.08 nm for $h_{9/2}g_{9/2}$, -0.36 nm for $h_{9/2}i_{11/2}$, and -4.07 nm for $f_{7/2}g_{9/2}$. On the other hand, if one uses the empirical g factor for the $h_{9/2}$ proton from Bi^{209} (unfortunately the empirical g factor for the $g_{9/2}$ neutron is not known yet), the magnetic moment of Bi^{210} is 0.24 nm and -1.08 nm for the pure configuration of $h_{9/2}g_{9/2}$ and $h_{9/2}i_{11/2}$, respectively.

Using our wave function for the 1- state of Bi^{210},

$$\psi_{Bi^{210}}(J=1) = 0.9767\,|h_{9/2}g_{9/2}\rangle - 0.1883\,|h_{9/2}i_{11/2}\rangle + 0.0578\,|f_{7/2}g_{9/2}\rangle ,$$

we find the magnetic dipole moment of Bi^{210} to be 0.050 nm in the Schmidt limit, whereas it is 0.177 nm if we take the empirical g factor for the $h_{9/2}$ proton. Because the measured magnetic moment is small and the sign of the moment is not determined by the experiment, the above calculated results seem to be consistent with the experiment. It should be noted that the wave function of the Bi^{210} ground state obtained by Newby and Konopinski and predominantly $h_{9/2}i_{11/2}$ yields the magnetic moment of -0.75 nm. The same problem applies to the Bi^{210} eigenfunction of Kharitanov et al.[52] and of Lee-Whiting.[55a]

For Po^{210}, we note at 2.91 MeV a predicted state $(h_{9/2}i_{13/2})^{J=11-}$ which could be an E3 isomeric state of detectable half life. It cannot decay by dipole or quadrupole transitions but may decay into the state $(h_{9/2}h_{9/2})^{J=8+}$ (1.57 MeV) or $(h_{9/2}f_{7/2})^{J=8+}$ (2.46 MeV) by E3 transitions, which then may cascade to the ground state by several E2 transitions. This is schematically shown in Fig. 21. Calculations with our eigenfunctions predict considerable retardation below single-particle strength for the higher energy E3. For the E3 transitions the product of the partial gamma half life and transition energy to the seventh power should be $t_{1/2}E^7 = 2.3\times10^{-5}$ sec MeV^7 for the 1.34-MeV E3 and $t^{1/2}E^7 = 7.5\times10^{-6}$ sec MeV^7 for the 0.45-MeV transition. The half life of the 11-state should

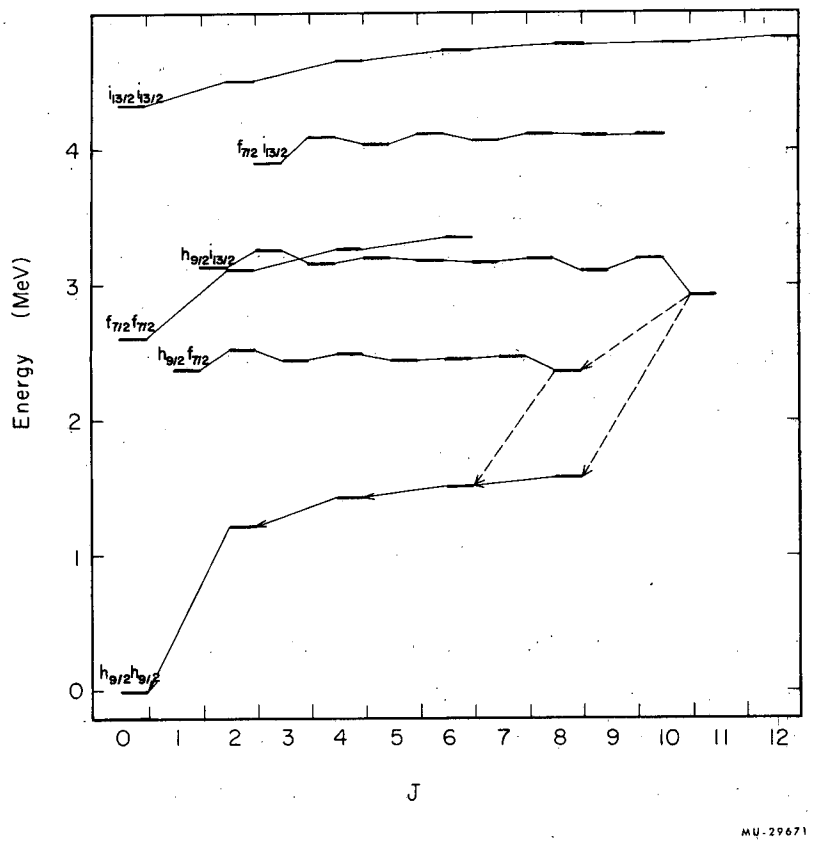

Fig. 21. Calculated energy levels of Po^{210}. For each spin, the left column lists the odd-parity states and the right column the even-parity states. The various spin-J states arising from the same configuration are connected by lines, and the possible E3 and E2 transitions from the predicted isomeric state $(h_{9/2}\ i_{13/2})^{J=11-}$ are shown by arrows and dashed lines.

thus be a few microseconds. (Here we have used the harmonic-oscillator radial wave functions, and an effective charge of 1.0e is assumed.)

Funk et al.[62] have recently measured the γ- transition probabilities of 46.7 keV($6+ \longrightarrow 4+$) and 246 keV($4+ \longrightarrow 2+$) in Po^{210}. They obtained 5.3×10^{4} sec^{-1} and 3.1×10^{8} sec^{-1}, respectively. Our eigenfunctions for the lowest 2+, 4+, and 6+ states show so little configuration mixing that it is appropriate to calculate the shell-model lifetimes between pure $(h_{9/2})^2_J$ states and estimate an effective charge for the protons. We have computed these E2 transition probabilities, using our wave functions presented previously with the harmonic radial wave functions. The effect of configuration mixing was found to be negligible, and the ratio of the observed to calculated transition probabilities is $T(E2)_{obs}/T(E2)_{calc} \approx 8$ for both 46.7-keV and 246-keV transitions. One may attempt to explain this discrepancy by assuming the effective charge of $(8e^2)^{1/2} (\cong 2.9e)$ for the proton. The presence of the extra protons outside the core tends to polarize the core, thus giving rise to the effective increase of the proton charge. The effective proton charge due to the polarized core is expected to be

$$e_{eff.} = e(1 + \frac{Z}{A} \gamma) ,$$

where γ is 1 for the harmonic-oscillator potential[63] and γ is 3 to 5 for the square-well potential.[64] Our value of $\gamma \approx 2.2$ seems reasonable if one notes that various effects such as the core excitation and vibration have not been taken into account in our calculation.

D. PARTICLE-HOLE INTERACTION

In the preceding chapter, it was shown that the tensor force must be included in the residual interaction to explain the low-energy phenomena of Y^{90}, Bi^{210}, and Po^{210}. Since Potential II appears to give rather good semi-quantitative agreement between theory and experiment in Bi^{210} and Po^{210}, it is interesting to see if one can use the same force for nuclei with a particle and a hole plus the doubly closed shell. We will consider two odd-odd nuclei, Tl^{208} and Bi^{208}. The theoretical aspects of these calculations already have been discussed in Chapter B, Section 2. Detailed assumptions and results of calculations are presented in the following.

1. Thallium-208

a. Introduction. Six levels in Tl^{208} were observed from the alpha-decay of Bi^{212}. The alpha-gamma angular-correlation measurements of Horton and Sherr[65] and of Weale[66] suggest that the angular momenta of the ground state and the first excited state are 5 and 4, respectively, which is also consistent with the beta-decay of the Tl^{208} ground state to the excited states in Pb^{208}. The Tl^{208} ground state decays predominantly into the 5- and 4- states of Pb^{208} with log ft ~ 5.7, but very weakly to the 3- state of Pb^{208}.[67,68] The 40-keV gamma transition in the ground-state doublet has been established by Graham and Bell[69] to be predominantly M1 from both the L-subshell conversion-electron intensity ratio ($L_I/L_{II}/L_{III}$) and lifetime. Spin and parity assignments for the observed levels in Tl^{208} are presented in Fig. 22, and are consistent with the internal-conversion-coefficient measurements by Nielson,[70] and more recent work by Emery and Kane.[71] The most recent work of alpha-gamma angular-correlation measurements by Cobb confirms these assignments shown in Fig. 22.[72]

From the shell-model calculation with a delta-function force, Pryce has interpreted the two lowest levesl to be a doublet resulting from the splitting of the $(s_{1/2}g_{9/2})$ configuration.[51] Similarily, the four upper levels can be attributed to the various spin states arising from the configuration $[(d_{3/2})^{-1}(g_{9/2})]$. Pryce's calculation disagrees

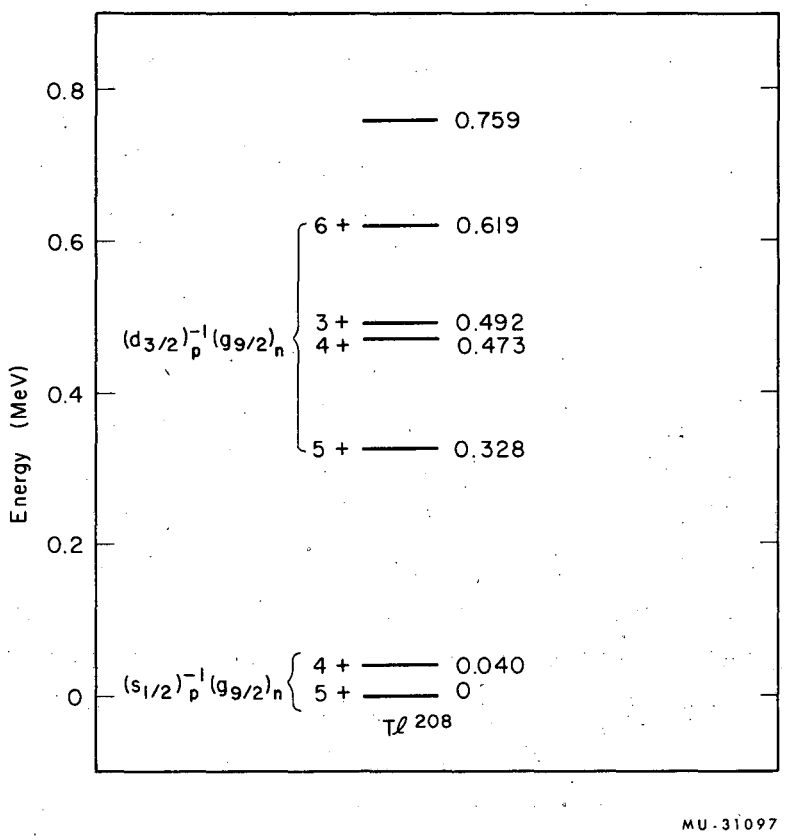

Fig. 22. Experimentally observed low-energy levels in Tl^{208}.

slightly with the experimental level sequence shown in Fig. 22. The 3+ and 6+ states are inverted in his calculated results.

b. Zeroth-order energies and calculated spectrum. The neutron single-particle energies are taken from Pb^{209} single-particle levels observed by Mukherjee and Cohen,[55] and the proton single-hole levels are taken from Tl^{207}.[73] The resulting zeroth-order energies are listed in Table XVI.

Table XVI. Zeroth-order energies for Tl^{208}.

Even-parity states		Odd-parity states	
Configuration (proton-neutron) (hole-particle)	Energy (MeV)	Configuration (proton-neutron) (hole-particle)	Energy (MeV)
$s_{1/2}g_{9/2}$	0.0	$s_{1/2}j_{15/2}$	1.41
$d_{3/2}g_{9/2}$	0.37	$d_{3/2}j_{15/2}$	1.78
$s_{1/2}i_{11/2}$	0.77		
$d_{3/2}i_{11/2}$	1.14		
$s_{1/2}d_{5/2}$	1.56		
$d_{3/2}d_{5/2}$	1.93		
$s_{1/2}s_{1/2}$	2.03		
$d_{3/2}s_{1/2}$	2.40		
$s_{1/2}g_{7/2}$	2.47		
$s_{1/2}d_{3/2}$	2.52		
$d_{3/2}g_{7/2}$	2.84		
$d_{3/2}d_{3/2}$	2.89		

The calculated results with Potential II are schematically compared in Fig. 23. The eigenvalues are presented in Table XVII, and the corresponding eigenfunctions are presented in Table XVIII for only the even-parity states of the lowest three configurations.

c. Discussion. The agreement of calculated and experimental spectra as shown in Fig. 23 is good if one considers that the same potential (Potential II) used in Bi^{210} and Po^{210} was used without any modifications. The comparison of the other calculated levels with experiment is not feasible at present since no further experimental information is available. Although the tensor-force effects are not large in Tl^{208}, the ground-state doublet states (4+ and 5+) have their tensor-force matrix elements with favorable opposite signs, so that the tensor force tends to raise the energy of the 4+ state and lower that of the 5+ state, as shown in Fig. 23. The tensor force also plays a specific role in correcting the inversion of the 3+ and 6+ states of the $[(d_{3/2})^{-1}(g_{9/2})]$ configuration; a strengthened tensor force would improve the calculation with respect to several spacings.

2. Bismuth-208

a. Experimental spectrum. Recently, Mukherjee and Cohen have studied the low-energy spectrum of Bi^{208} by the (d,t) reaction on Bi^{209}.[55] Nineteen levels were resolved as shown in Fig. 24. Their experimental data on Bi^{208} are summarized in Table XIX.

Prior to this experiment, Duffield and Vegors found an isomeric state in Bi^{208} with a lifetime of 2.7 msec from the (γ, n) reaction on Bi^{209}.[74] This isomeric state cascades to the ground state by two gamma transitions of 921 and 509 keV. Partly from the internal-conversion-coefficient measurements and partly from Wahlborn's shell-model calculation with a delta-function force,[75] they proposed the following decay scheme:

$$10- \xrightarrow[921\ \text{keV}]{E3} 7+ \xrightarrow[509\ \text{keV}]{E2} 5+ .$$

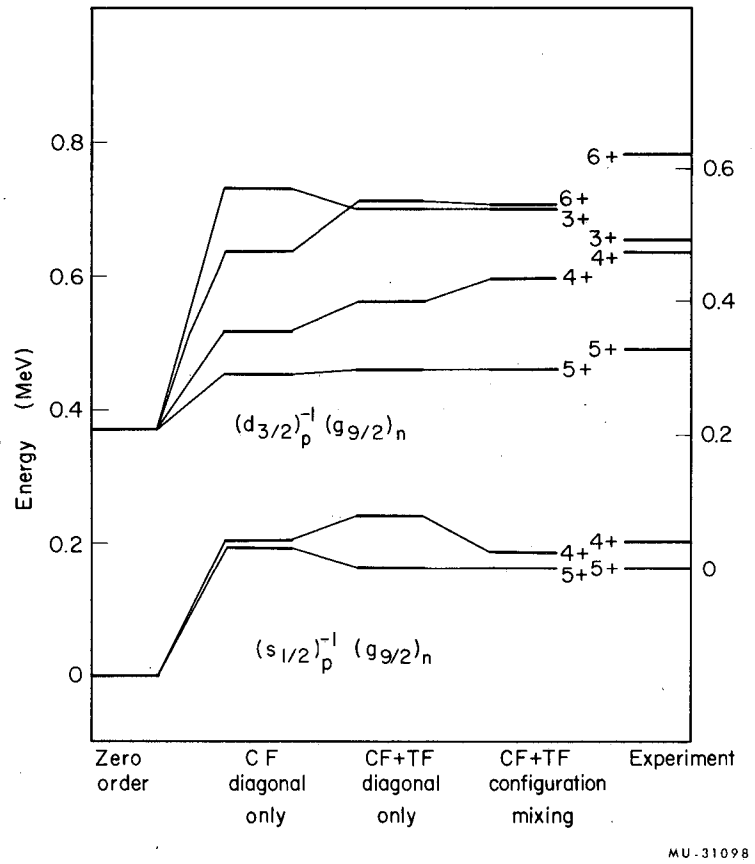

Fig. 23. Comparison of the experimental and calculated spectra of Tl^{208}. The abbreviations CF and TF refer to the central and tensor forces, respectively.

Table XVII. Calculated eigenvalues and energy levels in Tl^{208}. In the right column, eigenvalues are expressed in a new energy scale in which the ground state lies at zero energy. The indicated configuration is taken to be dominant.

Configuration (proton-neutron) (hole-particle)	J	Eigenvalues (MeV)	Energy (MeV)
$s_{1/2}\ g_{9/2}$	4+	0.185	0.024
	5+	0.161	0.0
$d_{3/2}\ g_{9/2}$	3+	0.698	0.537
	4+	0.596	0.435
	5+	0.459	0.298
	6+	0.704	0.543
$s_{1/2}\ i_{11/2}$	5+	0.878	0.717
	6+	0.940	0.779
$d_{3/2}\ i_{11/2}$	4+	1.516	1.355
	5+	1.233	1.072
	6+	1.283	1.122
	7+	1.276	1.115
$s_{1/2}\ d_{5/2}$	2+	1.718	1.557
	3+	1.791	1.630
$d_{3/2}\ d_{5/2}$	1+	2.482	2.321
	2+	2.115	1.954
	3+	2.135	1.974
	4+	2.379	2.218
$s_{1/2}\ s_{1/2}$	0+	2.878	2.717
	1+	2.597	2.436

Table XVII. (Continued)

Configuration (proton-neutron) (hole-particle)	J	Eigenvalues (MeV)	Energy (MeV)
$d_{3/2}\ s_{1/2}$	1+	2.872	2.711
	2+	2.614	2.453
$s_{1/2}\ g_{7/2}$	3+	2.601	2.440
	4+	2.662	2.501
$s_{1/2}\ d_{3/2}$	1+	2.879	2.718
	2+	2.704	2.543
$d_{3/2}\ g_{7/2}$	2+	3.064	2.903
	3+	2.965	2.804
	4+	2.990	2.829
	5+	2.992	2.831
$d_{3/2}\ d_{3/2}$	0+	3.424	3.263
	1+	3.352	3.191
	2+	3.279	3.118
	3+	3.064	2.903
$s_{1/2}\ j_{15/2}$	7-	1.580	1.419
	8-	1.525	1.364
$d_{3/2}\ j_{15/2}$	6-	2.029	1.868
	7-	1.960	1.799
	8-	1.856	1.695
	9-	2.105	1.944

Table XVIII. Calculated eigenfunctions for Tl^{208}.

Eigenvalues	Eigenfunctions								
(MeV)	$s_{1/2}\ g_{9/2}$	$d_{3/2}\ g_{9/2}$	$s_{1/2}\ i_{11/2}$	$d_{3/2}\ i_{11/2}$	$s_{1/2}\ d_{5/2}$	$d_{3/2}\ d_{5/2}$	$s_{1/2}\ g_{7/2}$	$d_{3/2}\ g_{7/2}$	$d_{3/2}\ d_{3/2}$
J = 3									
0.698		-0.9996			0.0042	-0.0214	-0.0165	-0.0051	-0.0012
J = 4									
0.185	0.9427	0.3256		0.0180		0.0153	-0.0673	-0.0047	
0.596	0.3262	-0.9421		-0.0641		-0.0133	-0.0058	-0.0407	
1.516	0.0015	0.0673		-0.9930		-0.0635	0.0663	0.0303	
J = 5									
0.161	-0.9984	0.0532	0.0007	-0.0122				-0.0064	
0.459	-0.0532	-0.9980	-0.0312	-0.0021				0.0041	
0.878	-0.0014	-0.0313	0.9983	0.0473				-0.0038	
1.233	-0.0120	-0.0001	-0.0475	0.9982				-0.0323	
J = 6									
0.704		-0.9879	0.0801	-0.1321					
0.940		-0.1266	-0.9102	0.3942					
1.283		-0.0886	0.4062	0.9094					
J = 7									
1.276				1.0000					

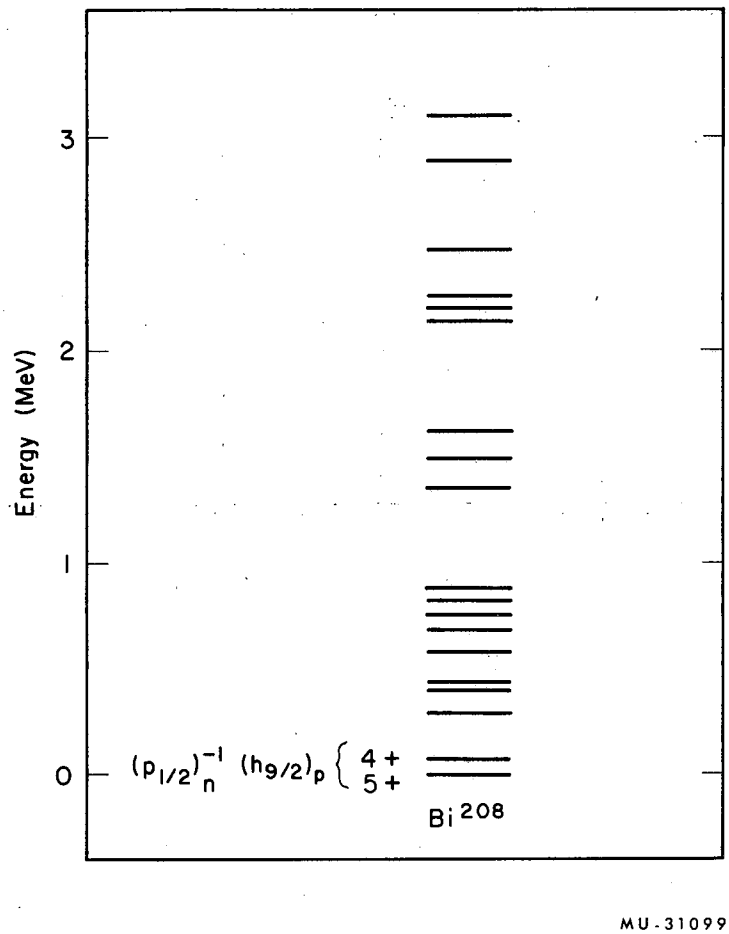

Fig. 24. Experimentally observed low-lying levels in Bi^{208}.

Table XIX. Energy levels excited in $Bi^{209}(d,t)Bi^{208}$ reaction (Ref. 55)

Excitation energy (MeV)	Relative yield at 45°	Excitation energy (MeV)	Relative yield at 45°
0	104	1.35	6
0.07	84	1.49	5
0.29	29	1.62	5
0.40	72	2.14	15
0.43	53	2.20	25
0.58	19	2.25	6
0.68	60	2.47	8
0.75	65	2.89	2
0.82	18	3.10	4
0.88	122		

As will be shown later, our calculated results indicate a possibility of such a high-spin isomeric state. The ground state is clearly 5+, and the first excited state 4+, since the ground state has a higher relative cross section.

b. Zeroth-order energies and results. The proton single-particle levels are taken from Bi^{209},[54] and the neutron single-hole states are taken from Pb^{207}.[76] The resulting zeroth-order energies are shown in Table XX.

Table XX. Zeroth order energies for Bi^{208}

Even-Parity States		Odd-Parity States	
Configuration (neutron-proton) (hole-particle)	Energy (MeV)	Configuration (neutron-proton) (hole-particle)	Energy (MeV)
$p_{1/2}h_{9/2}$	0.0	$i_{13/2}h_{9/2}$	1.63
$f_{5/2}h_{9/2}$	0.57	$i_{13/2}f_{7/2}$	2.53
$p_{3/2}h_{9/2}$	0.90		
$p_{1/2}f_{7/2}$	0.90		
$f_{5/2}f_{7/2}$	1.47		
$p_{3/2}f_{7/2}$	1.80		
$f_{7/2}h_{9/2}$	2.35		
$f_{7/2}f_{7/2}$	3.25		

The particle-hole matrix elements are calculated with Potential II by the method described in Chapter B, Section 2. The resulting matrix is diagonalized to obtain the eigenvalues and eigenfunctions. The eigenvalues are presented in Table XXI, and the eigenfunctions for the even-parity states of the lowest four configurations are presented in Table XXII.

Table XXI. Calculated eigenvalues and energy levels in Bi^{208}. In the right column, eigenvalues are expressed in a new energy scale in which the ground state lies at zero energy. The indicated configuration is taken to be dominant.

Configuration (neutron-proton) (hole-particle)	J	Eigenvalues (MeV)	Energy (MeV)
$p_{1/2}\ h_{9/2}$	4+	0.146	0.080
	5+	0.066	0.0
$f_{5/2}\ h_{9/2}$	2+	1.009	0.943
	3+	0.745	0.679
	4+	0.644	0.578
	5+	0.706	0.640
	6+	0.579	0.513
	7+	0.727	0.661
$p_{3/2}\ h_{9/2}$	3+	1.058	0.992
	4+	1.043	0.977
	5+	0.951	0.885
	6+	1.146	1.080
$p_{1/2}\ f_{7/2}$	3+	1.079	1.013
	4+	1.117	1.051
$f_{5/2}\ f_{7/2}$	1+	2.335	2.269
	2+	1.785	1.719
	3+	1.771	1.705
	4+	1.742	1.676
	5+	1.630	1.564
	6+	2.057	1.991

Table XXI. (Continued)

Configuration (neutron-proton) (hole-particle)	J	Eigenvalues (MeV)	Energy (MeV)
$p_{3/2}\ f_{7/2}$	2+	2.205	2.139
	3+	1.972	1.906
	4+	1.958	1.892
	5+	2.029	1.963
$f_{7/2}\ h_{9/2}$	1+	2.911	2.845
	2+	2.559	2.493
	3+	2.537	2.471
	4+	2.527	2.461
	5+	2.472	2.406
	6+	2.546	2.480
	7+	2.431	2.365
	8+	2.697	2.631
$f_{7/2}\ f_{7/2}$	0+	4.348	4.282
	1+	4.198	4.132
	2+	3.645	3.579
	3+	3.572	3.506
	4+	3.444	3.378
	5+	3.484	3.418
	6+	3.344	3.278
	7+	3.578	3.512
$i_{13/2}\ h_{9/2}$	2-	2.816	2.750
	3-	1.893	1.827
	4-	2.063	1.997
	5-	1.884	1.818

Table XXI. (Continued)

Configuration (neutron-proton) (hole-particle)	J	Eigenvalues (MeV)	Energy (MeV)
$i_{13/2}\ h_{9/2}$	6-	1.913	1.847
	7-	1.898	1.832
	8-	1.828	1.762
	9-	1.963	1.897
	10-	1.751	1.685
	11-	2.300	2.234
$i_{13/2}\ f_{7/2}$	3-	3.086	3.020
	4-	2.696	2.630
	5-	2.685	2.619
	6-	2.650	2.584
	7-	2.609	2.543
	8-	2.649	2.583
	9-	2.570	2.504
	10-	2.735	2.669

Table XXII. Calculated eigenfunctions for Bi^{208}.

Eigenvalues	Eigenfunctions							
(MeV)	$p_{1/2}\ h_{9/2}$	$f_{5/2}\ h_{9/2}$	$p_{3/2} h_{9/2}$	$p_{1/2} f_{7/2}$	$f_{5/2}\ f_{7/2}$	$p_{3/2}\ f_{7/2}$	$f_{7/2}\ h_{9/2}$	$f_{7/2}\ f_{7/2}$
J = 2								
1.009		0.9958			0.0316	-0.0010	-0.0850	-0.0100
J = 3								
0.745		-0.9982	-0.0524	0.0076	-0.0046	-0.0233	0.0033	-0.0081
1.058		-0.0525	0.9931	0.0131	0.0317	-0.0006	-0.0988	-0.0018
1.079		-0.0089	0.0057	-0.9873	0.1541	0.0289	-0.0193	-0.0011
J = 4								
0.146	-0.9780	0.1814	0.0950	-0.0259	-0.0121	-0.0024	0.0259	0.0037
0.644	-0.1465	-0.9473	0.2515	-0.1234	-0.0179	-0.0077	0.0462	-0.0031
1.043	-0.1289	-0.2186	-0.9579	-0.0885	0.0233	0.0097	0.0969	0.0094
1.117	-0.0531	-0.1295	-0.0539	0.9591	-0.1631	0.1712	-0.0014	0.0386
J = 5								
0.066	0.9813	-0.1914	0.0181		-0.0009	0.0003	0.0037	0.0023
0.706	0.1899	0.9797	0.0617		0.0028	0.0111	0.0049	0.0052
0.951	0.0294	0.0569	-0.9971		-0.0175	0.0014	0.0357	0.0000
J = 6								
0.579		-0.9852	0.1659		-0.0252		0.0323	-0.0016
1.146		-0.1611	-0.9796		0.0022		0.1190	0.0153
J = 7								
0.727		0.9999					0.0119	0.0015

c. Discussion. As in Tl^{208}, we obtain rather good agreement on the ground-state doublet. There has been some speculation as to whether the ground state is 4+ or 5+. The experimental relative cross sections obtained by Mukherjee and Cohen for the ground-state doublet as shown in Table XIX clearly suggest that the ground state is 5+, since the ratio of relative cross sections for the first excited state to the ground state is 84/104 = 0.807, and this ratio is theoretically expected to be (2(4)+1)/(2(5)+1) = 0.818 if the configurations are pure. The results of our calculation are very consistent with this experimental information. The other excited states are not completely resolved, so that relative cross-section information is not yet helpful for assigning spins and parities to these states.

An explanation of the 2.7-msec isomeric state comes directly from the results of our calculation. As shown in Fig. 25, the latter state may be attributed to the 10- state of the $[(i_{13/2})^{-1}(h_{9/2})]$ configuration, which may cascade through the 7+ state of the $[(f_{5/2})^{-1}(h_{9/2})]$ configuration to the ground state.

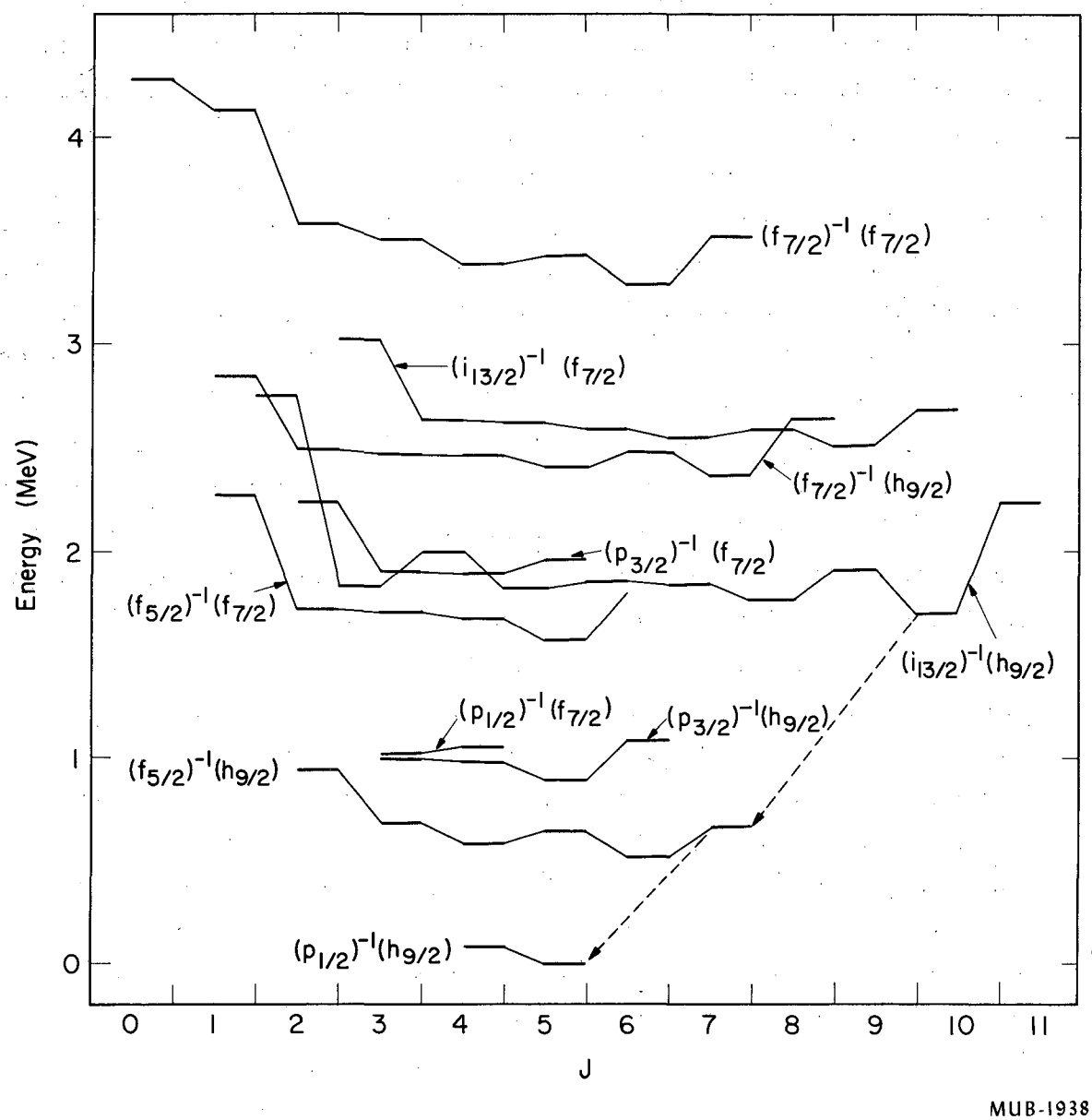

Fig. 25. Calculated energy levels of Bi^{208}. For each spin the left column lists the odd-parity states, and the right column the even-parity states. The various spin-J states arising from the same configuration are connected by lines, and possible E3 and E2 transitions from the isomeric state $\left[(i_{13/2})^{-1}(h_{9/2})\right]^{J=10-}$ are shown by arrows and dashed lines.

E. CONCLUSION

The tensor force has been neglected in most of the past shell-model calculations primarily because of the computational complexity involved, but with the hope that the tensor-force effects are small and may be simulated by an effective central force. That this is not always true is clearly shown in our calculations on Bi^{210} and Po^{210}. The general success of past central-force calculations may be due to the tensor-force matrix elements being small in many cases. From the analysis of various shell-model calculations, the central force alone seems to approximate the residual force very well in most cases, though many of these cases involve like nucleons, where the Pauli principle makes the tensor-even force inoperative. However, the tensor-force contributions are not always negligible, and must be taken seriously in some cases such as in Y^{90}, Bi^{210}, and Po^{210} presented here. Also, we see in Bi^{210} that configurations of high j with parallel or antiparallel alignment of angular momenta can experience appreciable tensor-force effects.

The characteristic of the tensor-force matrix element is that it may be either positive or negative, so that in some cases the tensor-force effects can not be exactly simulated by a linear combination of four central-force components. Also it should be noted that it is very difficult to simulate the finite-shorter-range tensor force by adjusting the strength parameters of the infinite-range tensor force, and that the infinite-range approximation for the tensor force is quite unreliable. Furthermore, inclusion of the tensor force may lead us to a better understanding of the residual force in the nucleus, and we may hope to find a residual force that can be used without alteration for different nuclei.

II. NUCLEAR SPECTROSCOPIC STUDIES OF ISOMERIC STATES IN ODD-ODD YTTRIUM NUCLEI

A. INTRODUCTION

During the past decade, much experimental data has been accumulated in the field of nuclear spectroscopy, and many advances have been made toward the understanding of nuclear structure. Particularily, the nuclear shell model has been very successful in correlating and explaining much of the experimental information, and its successes lead us to hope to understand the effective nuclear force inside the finite nuclei from the detailed theoretical analysis of the experimental spectra. As the theoretical calculations have become more refined, the detailed information of nuclear spectra has become increasingly important as a test of theory.

The greatest successes of the nuclear shell-model in its simplest form have been in explaining the low-energy properties of nuclei near the doubly-closed shells. This group of nuclei is the most important and suitable subject for obtaining much needed information on the nature of the effective residual nuclear force inside the nucleus, because these nuclei involve only a few nucleons outside the inert core which has been assumed to give rise to a central field in which the extra nucleons move. Since the theoretical treatment is the simplest and most basic, the detailed experimental information of these nuclei is extremely important in providing a check to theory and thus leading us to better understanding of the effective nuclear force inside the finite nuclei. This experimental study has been undertaken to add information about the decay schemes of some such odd-odd medium weight nuclei. The results of this investigation have been published previously.[77]

B. EXPERIMENTAL TECHNIQUES

1. Instruments

The various spectroscopic instruments used in this study have all been described in previous publications, and therefore only a summary is given below and references are cited.

a. Permanent-magnet spectrograph. Permanent-magnet spectrographs[78,82] (180-deg) with field strength of 100 gauss were used to detect internal-conversion electrons. This spectrograph has a resolution of about 0.1% and a transmission of the order of 0.01%.

b. Permanent-magnet preaccelerating spectrograph. A permanent-magnet preaccelerating spectrograph[79] was used to study the low-energy electron spectrum of Y^{86m}. This spectrograph has a field strength of 50 gauss.

c. Double-focusing spectrometer. For measuring conversion coefficients by use of the internal-external-conversion method, a flat, double-focusing beta-ray spectrometer[80] of 25-cm mean radius was used. This spectrometer has 0.3% resolution and 0.1% transmission. A special source-holder-converter assembly was used in the spectrometer, and is described elsewhere.

d. Penco gamma analyzer. Photons was detected by the use of a 100-channel pulse-height gamma analyzer[81] coupled with a 3- by 3-in. thallium-activated sodium iodide crystal.

2. Source Production and Chemistry

a. Source production. The neutron-deficient isotope Y^{86} was produced in the Lawrence Radiation Laboratory's 60-in. cyclotron by irradiating RbCl (natural and enriched in Rb^{85}) with alpha particles, and $Sr(NO_3)_2$ (natural and enriched in Sr^{86}) with deuterons. The spectroscopic sample of Y^{90} was also produced in the 60-in. cyclotron by irradiating RbCl (natural and enriched in Rb^{87}) with alpha particles. The Crocker 60-inch cyclotron was capable of accelerating protons, deuterons, and alpha particles to energies of about 12 MeV per nucleon.

b. Cyclotron target. Two general types of cyclotron target are available. The first is the internal target, which uses a single foil of the target material. It is inserted into the cyclotron tank to intercept the beam at any desired radius. Since our target materials were in the powdered form, the internal target was not used in our experiment. The other type is the external target, which is isolated from the main cyclotron tank by a system of aluminum foils. An aluminum foil serves to cover the powdered target material in the target holder, and ion currents of as much as 20 μA have been used on the external targets for short periods of time without apparent damage. One advantage of the external target over the internal probe target is more precise control by the experimenter over the energy of the incident particles. Any desired thickness of aluminum foil can be placed on the top of the target material to degrade the beam energy to a preferred value. This is of particular importance in alpha-particle bombardment, in which it may be desirable to produce one of the (α,xn) reactions with a minimum contamination from other alpha-induced reactions.

c. Chemistry. In most experiments, the pure, carrier-free yttrium sources were prepared as follows: The target was dissolved in concentrated ammonium hydroxide solution and passed through a filter paper, which absorbed the yttrium activity but not the strontium nor the rubidium. After thorough washing of the filter paper with dilute ammonium hydroxide solution, the yttrium was removed with 8N HCl. The details are described step by step in the following:

(i) Dissolve the target in a few ml of distilled water.

(ii) Add a drop of concentrated NH_4OH and adjust the concentration to pH 9.

(iii) Filter the target solution and wash the filter paper with NH_4OH (pH 9) solution several times. The yttrium activity will stick on the filter paper as a hydroxide.

(iv) Remove the activity with a few ml of 8N HCl. The resulting solution might contain NH_4^+ ions. To remove NH_4^+ ions, add a few drops of concentrated HNO_3, and boil to dryness.

d. Source preparation. Samples used in the permanent-magnet spectrograph and in the preaccelerating spectrograph were prepared by electrodeposition onto a 0.010-in.-diam platinum wire from a solution of ammonium oxalate.[78,82] For the double-focusing spectrometer, the sample was electrodeposited onto 0.01-in.-thick copper foil from the ammonium oxalate solution. A plating current of 100 to 150 mA was used for 30 min to 1 h. These sources varied in strength from 0.1 to 50 r/h as measured by a beta-gamma survey meter at a distance of approximately 3 in.

C. DECAY SCHEME STUDIES

1. Yttrium-86m

a. Determination of mass and half life. Following the purification of yttrium from a target of natural RbCl which had been irradiated with 47-MeV helium ions, a 210-keV gamma ray was observed in the scintiallation spectrum, with a decay period of 48±1 min. At the same time, gamma rays known to occur in the decay of the Y^{86} ground state[83,84] were observed to grow into the spectrum and then decay with the characteristic 14.6-h half life of Y^{86}. Similar results were obtained from targets enriched in Rb^{85} and also from bombardments of enriched Sr^{86} irradiated with 15-MeV deuterons. Irradiation of enriched Sr^{86} targets with 5-MeV deuterons failed to produce the activity. From this information, the 48-min activity can be assigned definitely as Y^{86}.

Figure 26 shows a typical decay curve of the 210-keV peak in the scintillation spectrum, and Fig. 27 shows a growth curve of the 1-MeV photon group of Y^{86} (ground state).

b. Energy measurement of the isomeric transition. Additional information about the "210-keV" transition, obtained from measurements in a 100-gauss, 180-deg spectrograph, is summarized in Table XXIII. A more precise value of the energy is chosen to be 208.0±0.3 keV, and it was also verified from the energy differences between the K, L, and M lines that this transition is indeed converted in yttrium, not strontium.

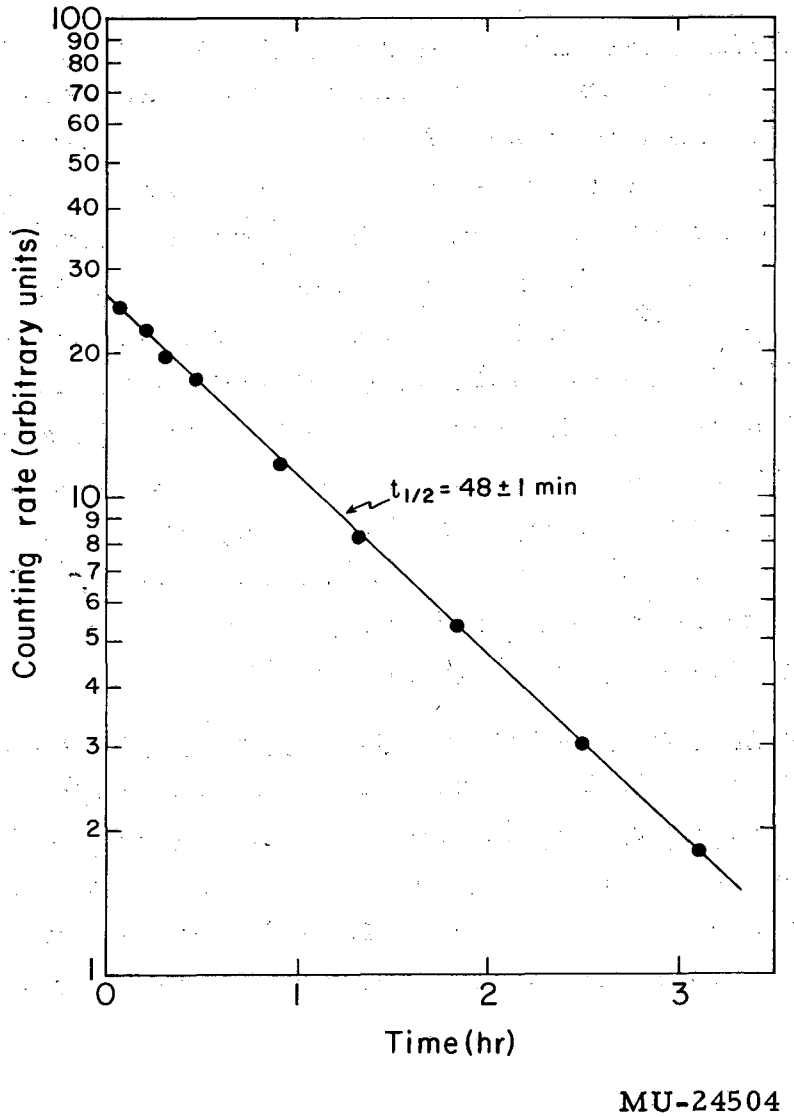

Fig. 26. Decay of the 210-keV photopeak of Y^{86m}.

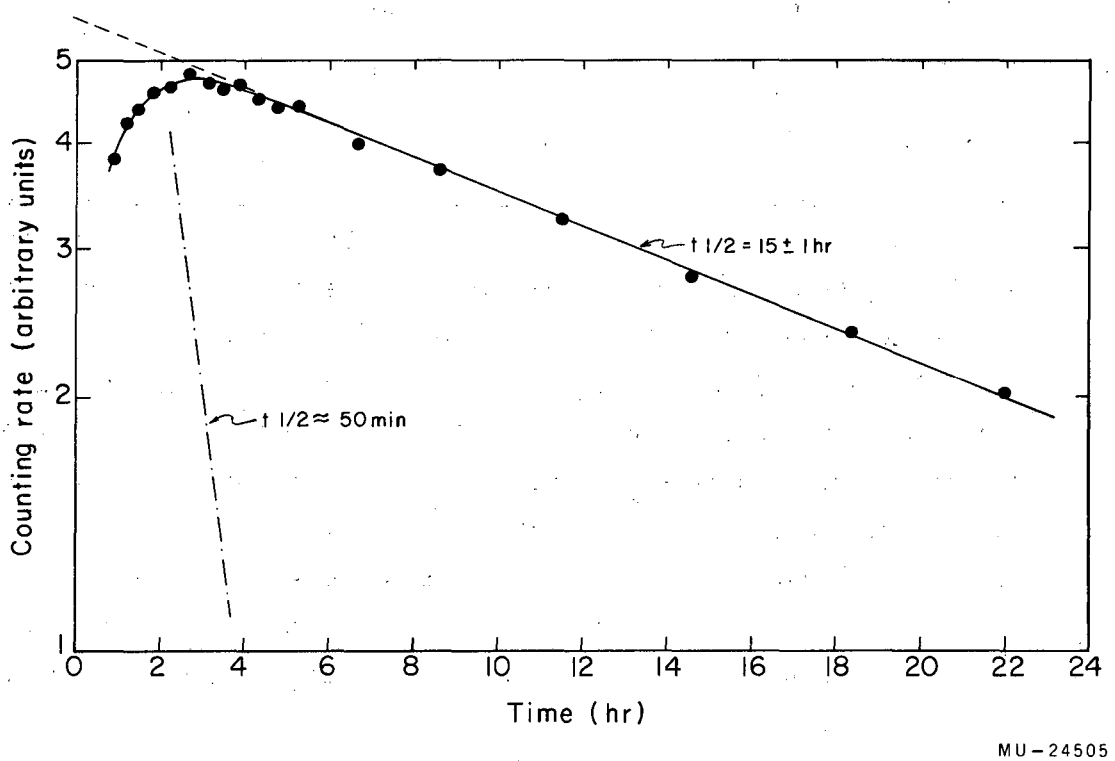

Fig. 27. Growth and decay of the 1.08-MeV photon group of 14.6-h Y^{86} from a sample containing Y^{86} and Y^{86m}.

Table XXIII. Internal conversion data of Y^{86m}

Electron energy (keV)	Shell	Binding energy (Y)	Transition energy (keV)	Intensity ratios
7.98	L_{II}	2.17	10.15	$L_{III}/L_{II}=1.5\pm0.5$
8.06	L_{III}	2.10	10.16	
190.9	K	17.1	208.0	$K/L_I/M_I=100/8.3/1.7$
205.6	L_I	2.39	208.0	
207.5	M_I	0.41	207.9	

A transition of 98.5±0,2 keV was also noted which, on the basis of its K-L electron energy separation, appears to be converted in strontium rather than yttrium. The electron lines decay with a half life of roughly 50 min. Although these data may appear to indicate a direct electron-capture branch of Y^{86m}, we could not observe a 98-keV photon in the scintillation spectrum, and also, no other transitions characteristic of the Sr^{86} levels appeared in the spectrum until the daughter (14.6-h Y^{86}) began to grow into the sample. Experiments with K X-ray-gamma coincidence also failed to indicate any radiations in coincidence with K X-rays. The present evidence on this transition is inconclusive.

c. Internal-conversion-coefficient measurement. The absolute K-conversion coefficient of the 208.0-keV transition was measured in a 25-cm double-focusing spectrometer by use of the internal-external conversion method due to Hultberg and Stockendal.[85] This method utilizes a converter that converts the photons emitted from the source into photoelectrons. If the photoelectric cross section is well known for a given converter material, the photon intensity can be deduced from the intensity of the external-conversion electrons, which can be

measured more accurately with the same spectrometer used for measuring the internal-conversion electrons. The method has been described indetail elsewhere.[85,86]

To accommodate the activity and the photoelectric converter, a special holder assembly was used which allows us to position the converter from outside the spectrometer. By moving a shaft, the converter could be placed either in front of the source or in a position where it did not obstruct the beam of internal-conversion electrons emitted from the source. This arrangement of the assembly is shown in Fig. 28. A 5- by 10-mm^2 rectangular uranium converter with a surface thickness of 2.19±0.02 mg/cm^2 was used. The source was prepared by electrodeposition onto a 0.010-in.-thick copper foil from an ammonium oxalate solution within the 2.0- by 9.0-mm^2 rectangular area.

To calculate the internal-conversion coefficient, we use

$$\epsilon_K = \frac{A_\beta}{A_\gamma} \tau_K f d k b,$$

where A_β is the intensity of internal-conversion electrons, A_γ is the intensity of external-conversion electrons (photoelectrons), τ_K is the absolute photoelectric cross section (in barns/atom) for the K-shell of the converter, f is a correction factor due to the photoelectric angular distribution and the geometric arrangemenet of the source and converter, d is the converter thickness (in mg/cm^2), k is the ratio of intensities of sources used in measurement of the external- and internal-conversion lines, and b is the dimension conversion factor (in atoms - cm^2/barns - mg), which equals $6.025 \times 10^{-4}/M$, where M is the atomic weight of the converter atoms.

The quantities d, k, and b are known prior to the experiment. The intensitites A_β and A_γ are measured in the experiment. The correction factor f corrects the photoelectric angular distribution which depends upon the particular physical parameters of the source and converter, such as the sizes of source and converter and their relative

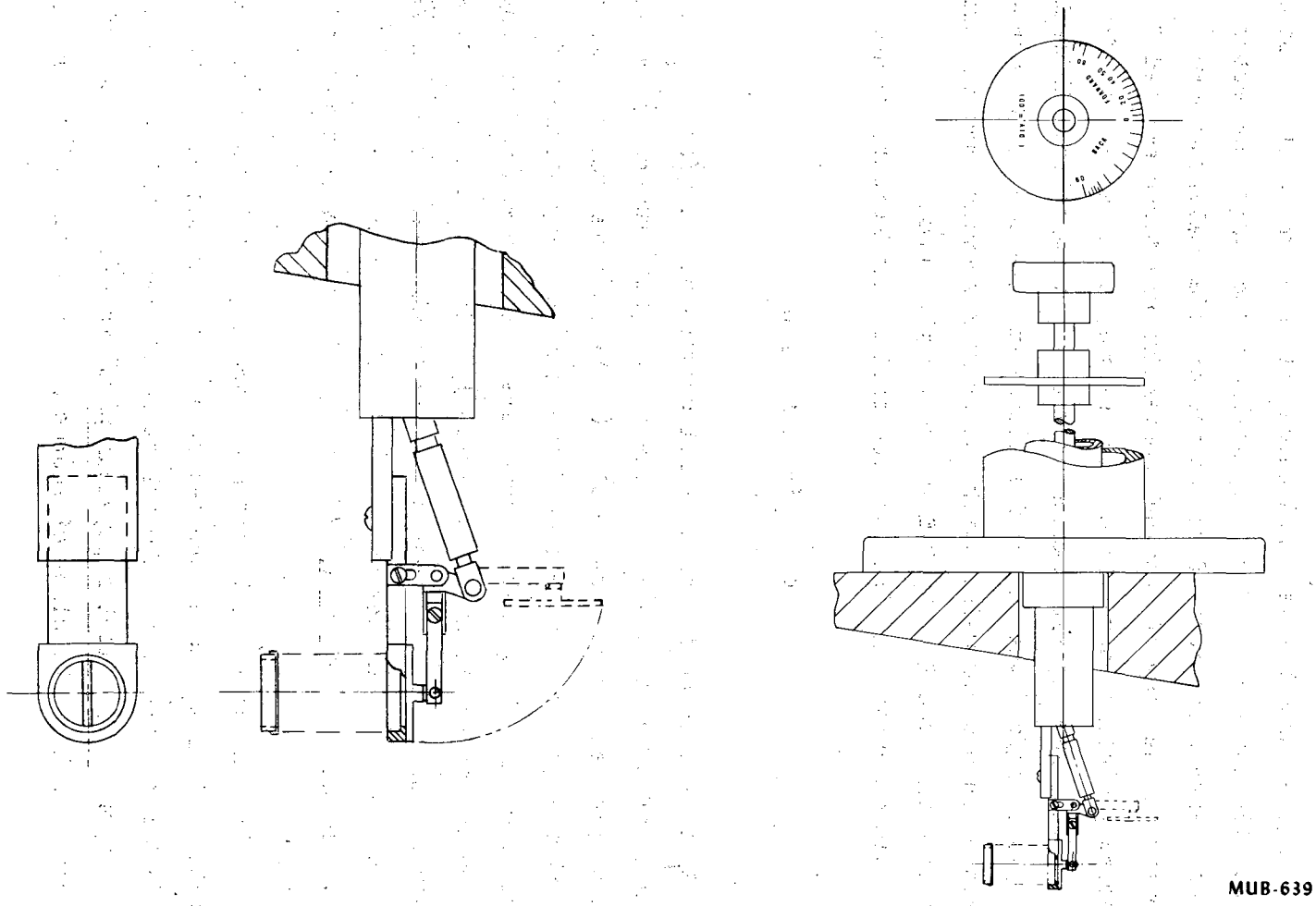

Fig. 28. Sourceholder-converter assembly.

distance apart. Ideally, if we have a point source and a converter which has an infinitely large area, the photoelectric f factor would be a very simple function. This is not the case in the experiment, and therefore evaluation of the f factor is rather complicated. Since the method of calculating the f factor is described in detail by Hultberg,[86] we state only that a computer program was written for this purpose by Hultberg and a courtesy service for computing f factors is available from the BESK computer in Stockholm, Sweden.

For the external-conversion electron measurement, a 1-mm aluminum-foil absorber was used between the source and converter to absorb the internal-conversion electrons. The quantities used in calculating the f factor are summarized below:

Converter half width	0.25 cm
Converter half height	0.50 cm
Source half width	0.10 cm
Source half height	0.45 cm
Source-to-converter distance	0.15 cm
Converter-to-aperture distance	19.00 cm
Absorber thickness	0.10 cm
Z value (atomic number) of absorber	13
Energy of gamma-transition	208 keV

Of course, the atomic shell must be specified. The result obtained from the "BESK service" was f = 0.705 for the source used in the experiment and f = 0.795 for the ideal case of a point source.

The absolute photoelectric cross section for the K-shell of uranium has been studied experimentally as a function of the energy of incident photons and is taken to be 318 barns/atom at 208 keV from an extrapolation of the experimental points.[86]

The intensities of the internal and external electrons are measured by a flow-type methane proportional counter as a function of electron energy, which is proportional to the magnetic field of the

spectrometer. The decrease in intensity due to the short half life (48 min) is corrected at each measured point. The experimental spectra for the internal- and external-conversion lines are shown in Figs. 29 and 30, respectively. The relative intensity, k, was taken to be unity because the same source was used for both the internal- and external-conversion-electron measurements.

Final values used for obtaining the conversion coefficient ϵ_K of the 208-keV transition are:

$$A_\beta/A_\gamma = 33.0$$
$$\tau_K = 318 \text{ barns/atom}$$
$$f = 0.705$$
$$d = 2.19 \text{ mg/cm}^2$$
$$k = 1.0$$
$$b = 6.025 \times 10^{-4}/218 \text{ atom} \times \text{cm/barns} \times \text{mg}.$$

These values yield $\epsilon_K = 0.04 \pm 0.01$, which corresponds to a mixed M1-E2 transition (about 40% E2).[87,88]

d. Preaccelerating spectrograph results. Although only the 208.0-keV transition could be assigned to Y^{86m} on the basis of the photon or initial electron spectra, obviously the observed 48-min half life is much too long to be compatible with an E2 or M1-E2 transition. Therefore a search was made for a low-energy transition. A 50-gauss preaccelerating spectrograph was used, with an accelerating voltage of 9.82 kV. Two electron lines which decayed with a half life of about 50 min were observed with an energy separation of 0.08±0.01 keV (see Table XXIII and Fig. 31). This spacing is in good agreement with the characteristic L_{II}-L_{III} energy difference of yttrium, 0.075 keV,[89] and indicates an isomeric transition of 10.15±0.1 keV.

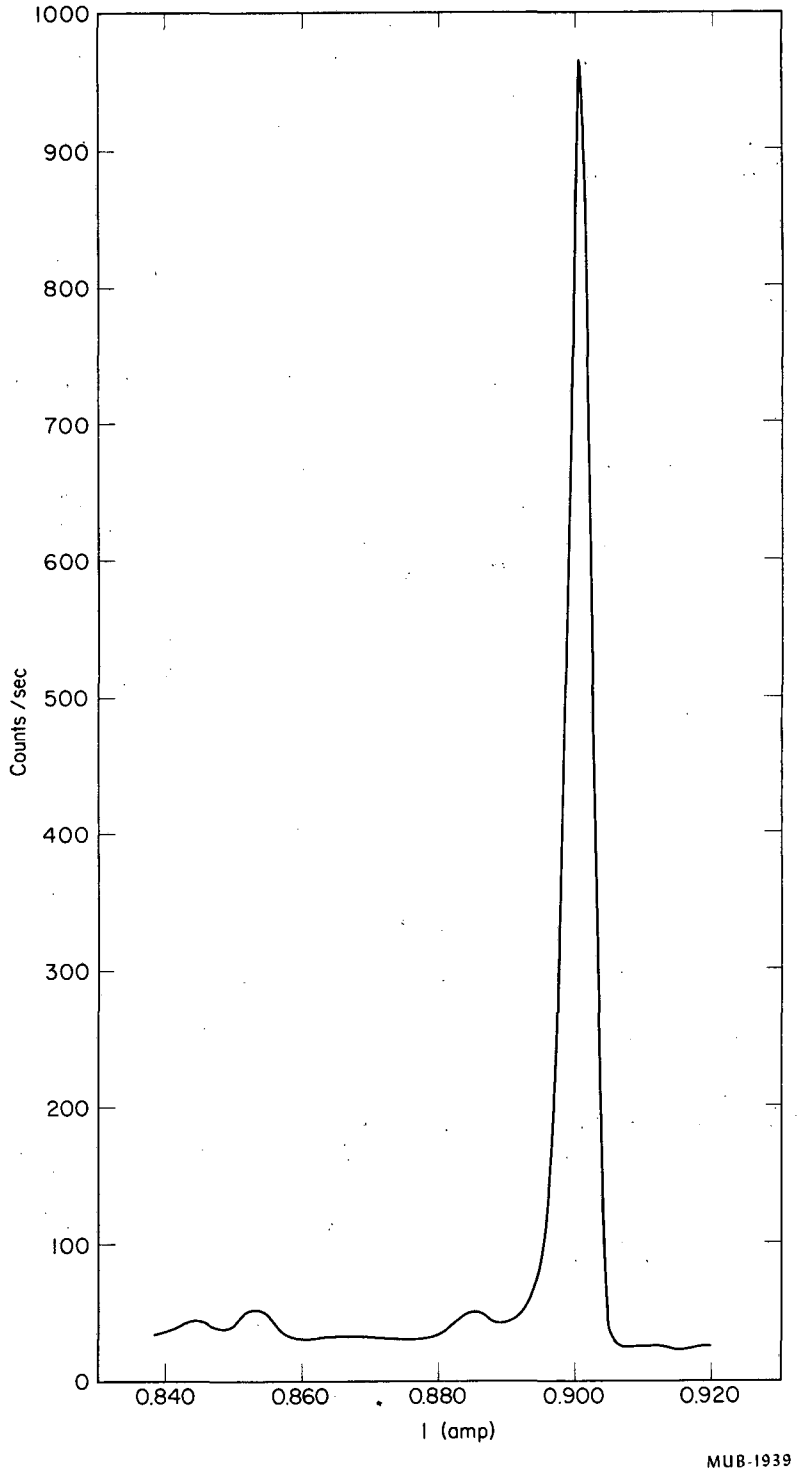

Fig. 29. Internal-conversion spectrum of 208-keV transition in Y^{86}.

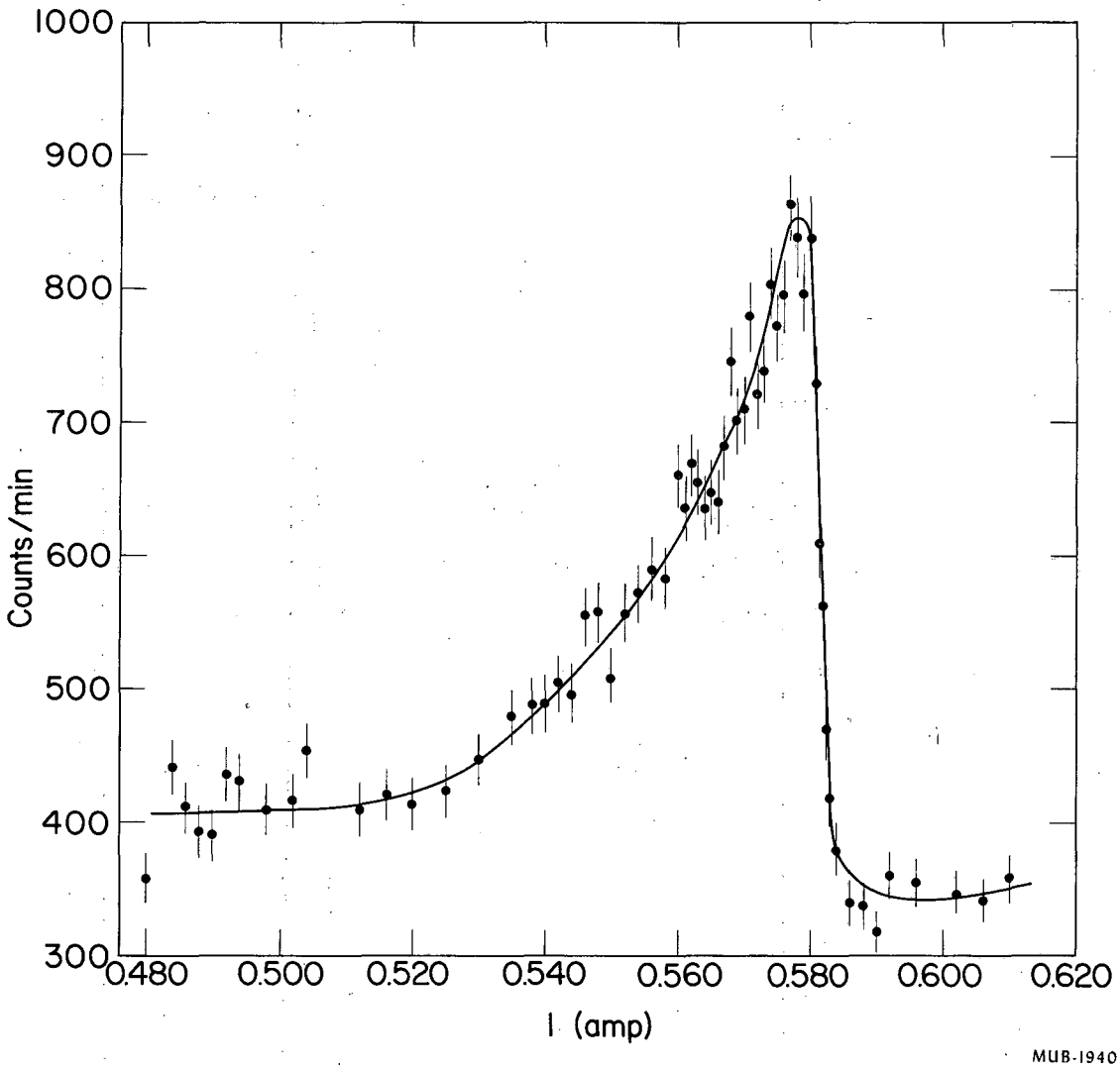

Fig. 30. External-conversion spectrum of 208-keV transition in Y^{86}.

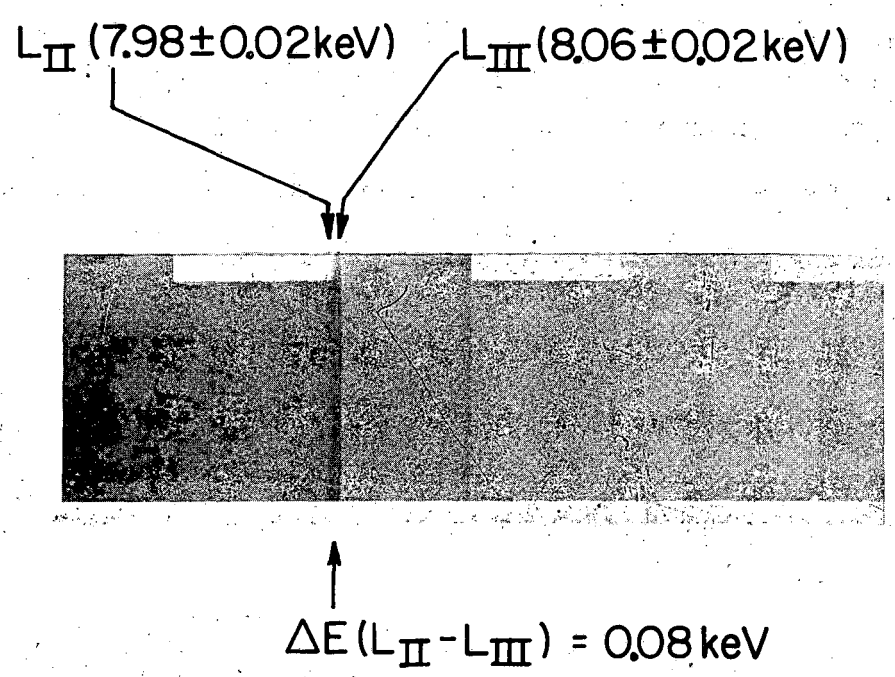

ZN-3808

Fig. 31. Internal-conversion spectrum of 10-keV gamma-ray in Y^{86}.

If we assume that the 10.15-keV transition is responsible for the 48-min half life, it follows that the transition must be of multipole order E3 or M3.[90] These two alternatives are readily distinguishable by an examination of the L-subshell conversion pattern. A straight-line extrapolation to 10 keV on log-log paper of Rose's theoretical L-shell conversion coefficients[88] indicates for M3 radiation the subshell pattern $L_I/L_{II}/L_{III}$= 24/2.6/100, and for E3 radiation the ratios $L_I/L_{II}/L_{III}$= 0.9/49/100 (see Figs. 32 and 33). The experimental observation of only the L_{II} and L_{III} conversions, with the ratio L_{III}/L_{II}= 1.5±0.5, is compatible only with an E3 assignment.

e. Discussion. The 48-min. isomeric state of Y^{86} decays by a 10.15-keV E3 transition followed by a 208.0-keV E2 transition. It is interesting to speculate briefly on the possible nature of the levels in Y^{86} from which these transitions arise.

Yttrium-86, with 39 protons and 47 neutrons, has a ground-state configuration $(p_{1/2})_P^{1}\ (g_{9/2})_N^{-3}$, and hence, according to Norheim's "strong" rule, spin and parity 4-. This assignment is consistent also with the recent results of Yamazaki, Ikegami, and Sakai[84] on the decay of 14.6-h Y^{86}.

The excited states of this odd-odd nucleus are expected to arise as combinations of the neutron states found in ${}_{38}Sr^{85}_{47}$ and proton states in ${}_{39}Y^{85}_{46}$ or ${}_{39}Y^{87}_{48}$. These are shown in Table XXIV.

Preliminary results of a study of the decay of ${}_{40}Zr^{86}_{46}$ being carried on at this laboratory indicate that the 48-min isomeric state of Y^{86} is not populated in Zr^{86} decay. This suggests that the spin of the isomer is higher than the ground-state spin4-. Of those states shown in Table XXIV, a most likely choice for Y^{86m} is the 8+ state arising from $(g_{9/2})_P\ (7/2+)_N$. Thus, the levels of the isomer might be as shown in Fig. 34.

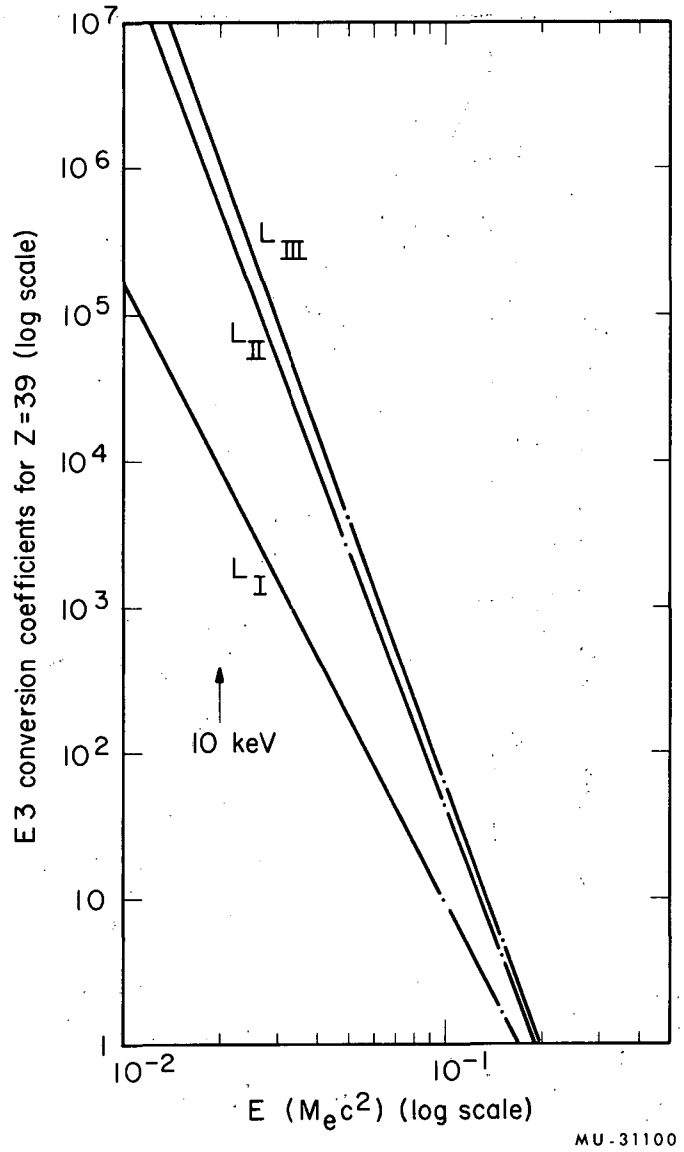

Fig. 32. Straight-line extrapolations to 10-keV on log-log paper of Rose's theoretical E3 L-subshell conversion coefficients.

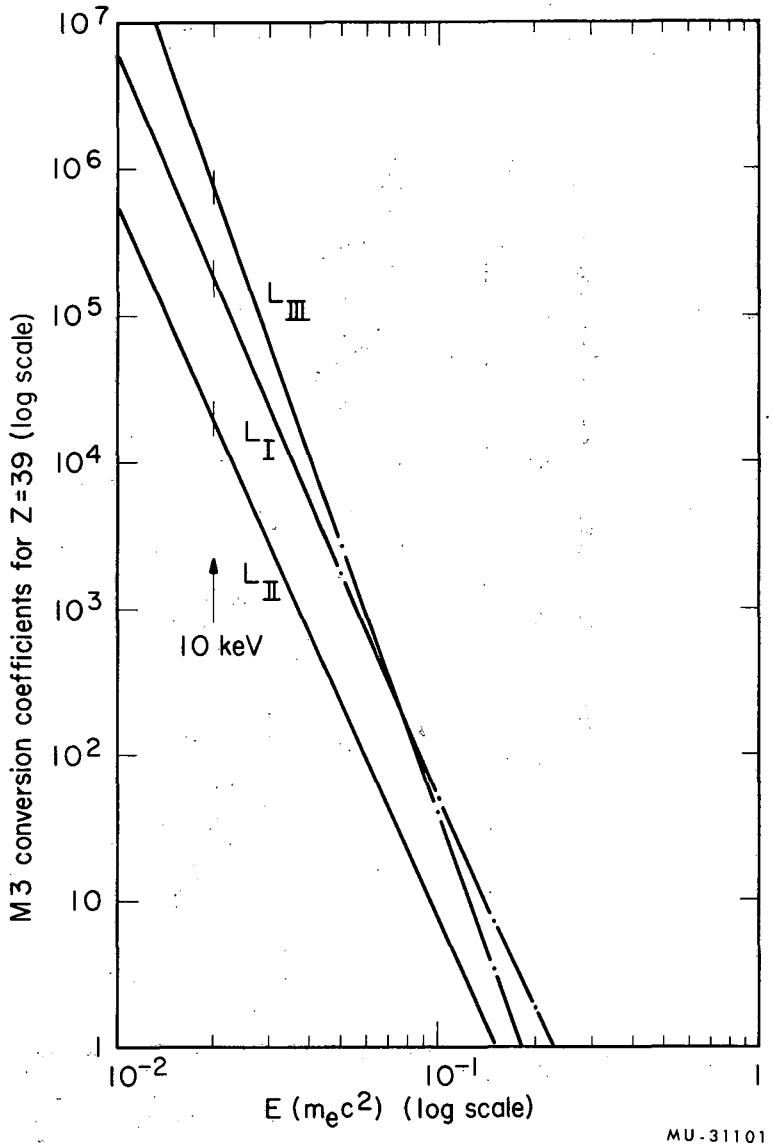

Fig. 33. Straight-line extrapolations to 10-keV on log-log paper of Rose's theoretical M3 L-subshell conversion coefficients.

Table XXIV. Expected configurations of Y^{86}

Proton state (Y^{87})	Neutron state (Sr^{85})	Resultant spins	Resultant parity
$p_{1/2}$	$g_{9/2}$	4,5	-
$p_{1/2}$	7/2+	3,4	-
$p_{1/2}$	$p_{1/2}$	0,1	+
$g_{9/2}$	$g_{9/2}$	0,1,2....9	+
$g_{9/2}$	7/2+	1,2,3....8	+
$g_{9/2}$	$p_{1/2}$	4,5	

2. Yttrium-90m.

In the course of the investigation of Y^{86m}, an isomeric state in Y^{90} was detected. The isomeric state was produced by irradiating RbCl (natural and enriched in Rb^{87}) with 15-MeV alpha particles in the 60-in. cyclotron. An 202 keV photopeak was observed, which decayed with a half life of 3 h. A more accurate value of the transition energy was measured to be 202.4±0.3 keV by use of a 100-gauss permanet-magnet spectrograph. Concurrently with this work, other investigators studied Y^{86m} and this isomeric state,[91-94] and since several groups reported their results on Y^{90m}, we did not pursue this investigation further. We note here only that our results agree with reported data, which is summarized in Fig. 1, and that the measured energy of the isomeric transition, 202.4±0.3 keV, is identical with the result obtained by Bartholomew et al.[40] by use of a flat crystal spectrometer at Chalk River. The more complete decay scheme including energy levels populated by the thermal-neutron capture $Y^{89}(n,\gamma)Y^{90}$ is presented in Section C of part I.

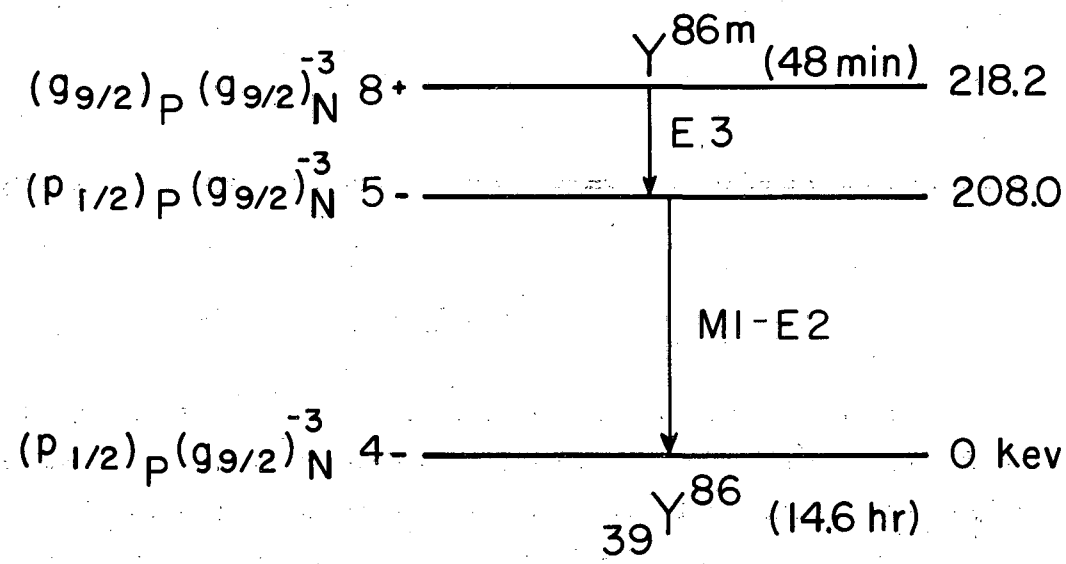

Fig. 34. Suggested level scheme of Y^{86m}.

D. CONCLUSION

The experimental techniques presented here are some of the typical methods of nuclear spectroscopy. On the other hand, there are many other experimental techniques that prove to be very useful in nuclear-strucutre studies, such as the high-resolution nuclear reaction which may be able to resolve the low-energy states of nuclei near doubly closed shells. Accumulation of more, very detailed nuclear spectra should give us some insight into the nature of the effective nuclear force inside the finite nucleus, thus stimulating progress in the theory. Increased theoretical understanding, in turn, may suggest new experiments and new directions to explore, and help to understand nuclear structure better. A close interplay of theory and experiments is very essential in the development of our understanding of nuclear structure.

ACKNOWLEDGMENTS

I wish to express my sincere gratitude to Professor John O. Rasmussen for his constant encouragement and thoughtful guidance throughout this work.

Special thanks are due Drs. Jack M. Hollander and Daniel J. Horen for their constant guidance and active participation in the experimental part of this work.

I am grateful to Drs. Paul Concus, Norman K. Glendenning, Brian R. Judd, Hans J. Mang, and William W. True for their helpful discussions of the theoretical problems of this study.

Contacts and acquaintances with many associates and colleagues at the Lawrence Radiation Laboratory have been a most stimulating and pleasant experience for me.

The critical reading of this manuscript by Kenneth Poggenburg is greatly appreciated.

This work was done under the auspices of the U. S. Atomic Energy Commission.

APPENDICES

A. The Central-Force Matrix Element

Our interest here is to evaluate the spin-dependent part of the central-force matrix element $\langle a|V(r_{12})\underset{\sim}{\sigma}_1 \cdot \underset{\sim}{\sigma}_2|a\rangle$. It is convenient to consider the singlet projection operator P_S and write the matrix element of $V(\underline{r}_{12})P_S$,

$$\langle a|V(\underline{r}_{12})P_S|a'\rangle = \frac{1}{4}\langle a|V(\underline{r}_1 - \underline{r}_2)(1 - \underset{\sim}{\sigma}_1 \cdot \underset{\sim}{\sigma}_2)|a'\rangle. \tag{1}$$

Here, $V(\underline{r}_1 - \underline{r}_2)$ can be expanded in terms of the angle ω between $\underline{r}_1$ and $\underline{r}_2$:

$$V(\underline{r}_1 - \underline{r}_2) = \sum_k v_k(r_1, r_2)P_k(\cos\omega),$$

where $P_k(\cos\omega)$ is the Legendre polynomial of order k. We write $\langle a|V(r_{12})P_s|a'\rangle$ as

$$\langle a\ V(\underline{r}_{12})P_S|a'\rangle = \frac{1}{4}\sum_{n,k} f_{nk}\ F_k, \tag{2}$$

where

$$f_{nk} = (-1)^n(2k + 1)\langle j_1 j_2 JM|\underset{\sim}{\sigma}_1^{(n)} \cdot \underset{\sim}{\sigma}_2^{(n)} P_k(\cos\omega)|\ j_1' j_2' J'M'\rangle, \tag{3}$$

and

$$F_k = \frac{1}{2k+1}\iint R_1^*(r_1)R_2^*(r_2)v_k(r_1,r_2)R_1'(r_1)R_2'(r_2)r_1^2 r_2^2 dr_1 dr_2. \tag{4}$$

By addition theorem for spherical harmonics, we may write $P_k(\cos\omega)$ as

$$P_k(\cos\omega) = \sum_{\kappa} (-1)^{\kappa} C_{\kappa}^{(k)}(1) C_{-\kappa}^{(k)}(2),$$

where

$$C_{\kappa}^{(k)}(\theta_i) = \left[\frac{4\pi}{2k+1}\right]^{1/2} Y_{\kappa}^{(k)}(\theta_i, \phi_i),$$

so that

$$f_{nk} = \sum_{\kappa,\gamma} (-1)^{n+\kappa+\gamma} (2k+1)$$

$$\times \langle j_1 j_2 JM | \sigma_{\gamma}^{(n)}(1) C_{\kappa}^{(k)}(1) \cdot \sigma_{-\gamma}^{(n)}(2) C_{-\kappa}^{(k)}(2) | j_1' j_2' J'M' \rangle. \quad (5)$$

The angular part f_{nk} can be evaluated by using the tensor-operator algebra developed by Racah,[95] and de-Shalit has obtained the expression of f_{nk} for the diagonal case in the zero-range limit.[2] The similar expression including the off-diagonal case can be calculated easily and is given in terms of the usual 6-j and 9-j symbols by

$$f_{nk} = (-1)^{j_1' + j_2' + J} \delta_{J,J'} \delta_{M,M'} (2k+1) [j,j']^{1/2}$$

$$\times \left(\tfrac{1}{2}\|\sigma^{(n)}\|\tfrac{1}{2}\right)^2 (\ell_1 \|C^{(k)}\| \ell_1') (\ell_2 \|C^{(k)}\| \ell_2') \quad (6)$$

$$\times \sum_{r} (-1)^{k+r} (2r+1) \begin{Bmatrix} j_1 & j_2 & J \\ j_2' & j_1' & r \end{Bmatrix} \begin{Bmatrix} n & k & r \\ \frac{1}{2} & \ell_1 & j_1 \\ \frac{1}{2} & \ell_1' & j_1' \end{Bmatrix} \begin{Bmatrix} n & k & r \\ \frac{1}{2} & \ell_2 & j_2 \\ \frac{1}{2} & \ell_2' & j_2' \end{Bmatrix}$$

where

$$[j,j'] = [(2j_1+1)(2j_1'+1)(2j_2+1)(2j_2'+1)],$$

and $(\frac{1}{2}\|\sigma^{(n)}\|\frac{1}{2})$ and $(\ell'\|C^{(k)}\|\ell')$ are the usual reduced matrix elements. Here the summation over r is restricted by $|k-n| \leqslant r \leqslant k+n$. Obviously, we have

$$\langle a|V(\underline{r}_1 - \underline{r}_2)|a'\rangle = \sum_k f_{0k}F_k,$$

$$\langle a|V(\underline{r}_1 - \underline{r}_2)\underset{\sim}{\sigma}_1 \cdot \underset{\sim}{\sigma}_2|a'\rangle = -\sum_k f_{1k}F_k, \tag{7}$$

and

$$\langle a|V(\underline{r}_{12})P_S|a'\rangle = \frac{1}{4}[\langle a|V(\underline{r}_1 - \underline{r}_2)|a'\rangle - \langle a|V(\underline{r}_1 - \underline{r}_2)\underset{\sim}{\sigma}_1 \cdot \underset{\sim}{\sigma}_2|a'\rangle],$$

where $\langle a|V(\underline{r}_{12})|a'\rangle$ is just the matrix element for the Wigner force $(n = 0)$, whereas $\langle a|V(\underline{r}_1 - \underline{r}_2)\underset{\sim}{\sigma}_1 \cdot \underset{\sim}{\sigma}_2|a'\rangle$ is the contribution from the spin-dependent force $(n = 1)$. Instead of evaluating $\langle a|V(r_{12})\underset{\sim}{\sigma}_1 \cdot \underset{\sim}{\sigma}_2|a'\rangle$ directly, we shall find it easier to evaluate $\langle a|V(\underline{r}_{12})P_S|a'\rangle$ first and then obtain $\langle a|V(\underline{r}_{12})\underset{\sim}{\sigma}_1 \cdot \underset{\sim}{\sigma}_2|a'\rangle$ by subtracting the contribution due to $\langle a|V(\underline{r}_{12})|a'\rangle$ from $\langle a|V(\underline{r}_{12})P_S|a'\rangle$.

Because n can take only two values, 0 and 1, we find it convenient to sum over n first. We may sum over n in Eq. (6) by using

$$\sum_y (2y+1)\begin{Bmatrix} d & q & e \\ p & c & b \\ a & f & y \end{Bmatrix}\begin{Bmatrix} h & r & e \\ s & g & b \\ a & f & y \end{Bmatrix} = \sum_x (2x+1)\begin{Bmatrix} a & b & x \\ c & d & p \end{Bmatrix}\begin{Bmatrix} c & d & x \\ e & f & q \end{Bmatrix}\begin{Bmatrix} e & f & x \\ g & h & r \end{Bmatrix}\begin{Bmatrix} g & h & x \\ a & b & x \end{Bmatrix}, \tag{8}$$

which is easy to verify. Summation over r can also be easily performed, yielding a simpler expression involving the 3-j symbol:

$$\sum_n f_{nk} = (-1)^{j_1' + j_1 + J+1} \, 2(2k+1)[j,j',\ell,\ell']^{1/2}$$

$$\times \begin{pmatrix} \ell_1 & \ell_1' & k \\ 0 & 0 & 0 \end{pmatrix} \begin{pmatrix} \ell_2 & \ell_2' & k \\ 0 & 0 & 0 \end{pmatrix} \begin{Bmatrix} j_1 & \ell_1 & \frac{1}{2} \\ \ell_2 & j_2 & J \end{Bmatrix} \begin{Bmatrix} \frac{1}{2} & \ell_2' & j_2' \\ J & j_1' & \ell_1' \end{Bmatrix} \begin{Bmatrix} k & \ell_2' & \ell_2 \\ J & \ell_1 & \ell_1' \end{Bmatrix} . \quad (9)$$

Here we have

$$[j,j',\ \ell,\ell'] = [(2j_1+1)(2j_1'+1)\ (2j_2+1)(2j_2'+1)$$

$$\times\ (2\ell_1+1)(2\ell_1'+1)(2\ell_2+1)(2\ell_2'+1)] \ .$$

The final expression for $\langle a|V(\underline{r}_{12})P_S|a'\rangle$ is

$$\langle a|V(\underline{r}_{12})P_S|a'\rangle = \frac{1}{2}\sum_k F_k(-1)^{j_2'+j_2+J+1}[j,j',\ell.\ell]$$

$$\times\ (\ell_1 0 \ell_1' 0|k0)(\ell_2 0 \ell_2' 0|k0)W(\ell_1 j_1 \ell_2 j_2\ ;\ \tfrac{1}{2}J) \qquad (10)$$

$$\times\ W(\ell_1' j_1' \ell_2' j_2'\ ;\ \tfrac{1}{2}J)W(\ell_1 \ell_1' \ell_2 \ell_2'\ ;\ kJ)\ ,$$

where the symbols $(\ \ |\ )$ and W are the usual Clebsch-Gordan and Racah coefficients.

Now we evaluate $\langle a|V(\underline{r}_{12})|a'\rangle$. Noting

$$\begin{Bmatrix} 0 & k & r \\ s & \ell & j \\ s' & \ell' & j' \end{Bmatrix} = (-1)^{k+s+j+\ell'} [2(2k+1)]^{-1/2} \begin{Bmatrix} j' & j & k \\ \ell & \ell' & s \end{Bmatrix} \delta_{k,r} ,$$

we can easily verify

$$\langle a|V(\underline{r}_{12})|a'\rangle = \sum_k F_k (-1)^{j_2'+j_2+J} [j,j']^{1/2} (j_1' \tfrac{1}{2} j_1 - \tfrac{1}{2} |k0)(j_2' \tfrac{1}{2} j_2 - \tfrac{1}{2} |k0)$$

$$\times \; W(j_1 j_1' j_2 j_2' ; kJ) , \tag{11}$$

with the restriction that it vanishes unless both $\ell_1 + \ell_1' + k$ and $\ell_2 + \ell_2' + k$ are even. From Eqs. (7), (10), and (11), we get

$$\langle a|V(\underline{r}_{12})\underset{\sim}{\sigma}_1 \cdot \underset{\sim}{\sigma}_2|a'\rangle = 2 \sum_k F_k (-1)^{j_2+j_2'+J} [j,j',\ell,\ell']^{1/2} (\ell_1 0 \ell_1' 0|k0)(\ell_2 0 \ell_2' 0|k0)$$

$$\times W(\ell_1 j_1 \ell_2 j_2; \tfrac{1}{2} J) W(\ell_1' j_1' \ell_2' j_2' ; \tfrac{1}{2} J) \; W(\ell_1 \ell_1' \ell_2 \ell_2' ; kJ) + \langle a|V(\underline{r}_{12})|a'\rangle ,$$

where $\langle a|V(\underline{r}_{12}) \mid a'\rangle$ is given by Eq. (11).

Now that we have obtained the explicit forms of the spin-dependent matrix element for the finite-range case, we obtain the corresponding expressions in the limit of zero range. For the zero-range force, we have $F_k \equiv F_0$ for every k, so that the summation over k can be easily carried out analytically. The final results for the zero-range force are

$$\langle a|V^0(r_{12})|a'\rangle = \frac{1}{2(2J+1)} F_0 \, [j,j']^{1/2} (j_1 \tfrac{1}{2} j_2 - \tfrac{1}{2} | J0)$$

$$\times (j_1' \tfrac{1}{2} j_2' - \tfrac{1}{2} | J0)[(-1)^{j_1+j_1'+\ell_1+\ell_1'+1} + (-1)^{j_1+j_1'+j_2+j_2'} \frac{AA'}{4J(J+1)}] \tag{13}$$

and

$$\langle a|V^0(\underline{r}_{12})\underset{\sim}{\sigma}_1 \cdot \underset{\sim}{\sigma}_2|a'\rangle = \frac{1}{2(2J+1)} F_0 \, [j,j']^{1/2} (j_1 \tfrac{1}{2} j_2 - \tfrac{1}{2} | J0)$$

$$\times (j_1' \tfrac{1}{2} j_2' - \tfrac{1}{2} | 0) \left\{ (-1)^{j_1+j_1'+\ell_1+\ell_1'} [1+2(-1)^{\ell_1+\ell_1'+J}] + (-1)^{j_1+j_1'+j_2+j_2'} \frac{AA'}{4J(J+1)} \right\} , \tag{14}$$

where the superscript zero refers to the zero-range limit, and

$$A = (2j_1+1)+(-1)^{j_1+j_2+J} (2j_2+1) .$$

In Eq. (13) $\langle a|V^0(\underline{r}_{12})|a'\rangle$ vanishes unless $\ell_1+\ell_1'+\ell_2+\ell_2'$ is even. Likewise $\langle a|V^0(\underline{r}_{12})\underset{\sim}{\sigma}_1 \cdot \underset{\sim}{\sigma}_2|a'\rangle$ vanishes unless both $\ell_1 + \ell_2 + J$ and $\ell_1' + \ell_2' + J$ are even. The diagonal cases of both Eqs. (13) and (14) agree with the results obtained by de-Shalit.[2] An almost identical expression for (13) is given by Newby and Konopinski,[51] and a similar expression by Noya et al.[6] Equations (10) and (11) are also given by Newby and Konopinski.

B. The Tensor-Force Matrix Element

The tensor-force matrix element is evaluated here in the j-j representation. We may express the tensor force in terms of the orbital and spin tensors as

$$\frac{1}{3} V(\underline{r}_{12}) S_{12} = (\underset{\sim}{S}^{(2)} \cdot \underset{\sim}{L}^{(2)}) ,$$

where $\underset{\sim}{S}^{(2)}$ is the irreducible tensor operator of rank 2 constructed from the spin operators $\underset{\sim}{\sigma}_1$ and $\underset{\sim}{\sigma}_2$, and $\underset{\sim}{L}^{(2)}$ is a product of the scaler $V(r_{12})$ and the irreducible operator of rank 2 constructed from the unit vector $\underset{\sim}{r}_{12}/r_{12}$. The spin and orbital tensors may be obtained from[11]

$$S_m^{(2)} = (8\pi/15)^{1/2} (\underset{\sim}{\sigma}_1 \cdot \nabla)(\underset{\sim}{\sigma}_2 \cdot \nabla) \mathcal{Y}_{2m}(\underset{\sim}{r}_{12})$$

and

$$L_m^{(2)} = (2\pi/15)^{1/2} \frac{V(r_{12})}{r_{12}^2} \mathcal{Y}_{2m}(\underset{\sim}{r}_{12}) ,$$

where $\mathcal{Y}_{\ell m}(\underset{\sim}{r}) = r^{\ell} Y_{\ell m}(\theta,\phi)$ and $Y(\theta,\phi)$ is the spherical harmonics.

The tensor force has been evaluated into spherical tensors by Talmi.[14] Expanding $V(r_{12})/r_{12}^2$ in terms of spherical harmonics,

$$\frac{V(r_{12})}{r_{12}^2} = \sum_k v_k(r_1,r_2) P_k(\cos\omega_{12})$$

$$= \sum_{k=0}^{\infty} v_k(r_1,r_2) \sum_{\kappa} (-1)^{\kappa} C_{\kappa}^{(k)}(1) C_{-\kappa}^{(k)}(2) ,$$

we obtain for the tensor force in terms of spherical tensors

$$V(r_{12})S_{12} = 3 \sum_{K,x,y} F_{xy} W(1x1y;K2) \underset{\sim}{T}_1^{(1x)K} \cdot \underset{\sim}{T}_2^{(1y)K} ,$$

where

$$F_{xy} = -5 \Sigma v_k(r_1,r_2)\{(2/15)^{1/2}[x]^{1/2}(20k0|x0)r_1^{\,2}$$

$$+ (2/15)^{1/2}[y]^{1/2}(20k0|y0)r_2^{\,2}$$

$$+ ([x][y])^{1/2}(10k0|x0)(10k0|y0)W(11xy;2k)r_1r_2\} ,$$

and

$$\underset{\sim}{T}_i^{(1z)K} = [\underset{\sim}{\sigma}^{(1)}(i)\times\underset{\sim}{C}^{(z)}(i)] \text{ for } i = 1 \text{ or } 2.$$

The symbols (|) and W are the usual Clebsch-Gordan and Racah coefficients, and [a] stands for [2a+1] . Now the evaluation of the matrix element for $V(r_{12})S_{12}$ is straightforward by using the similar method of Appendix A. The final result is

$$\langle a|V(r_{12})S_{12}|a'\rangle = \sum_{K,x,y} \langle a|F_{xy}|\alpha'\rangle W(1x1y;K2)$$

$$\times \langle j_1j_2JM|\underset{\sim}{T}^{(1x)K} \cdot \underset{\sim}{T}^{(1y)K}|j_1'j_2'J'M'\rangle ,$$

where

$$\langle a|F_{xy}|\alpha'\rangle = -5 \sum_{k,i,j} \langle\alpha|r_1 r_j|\alpha'\rangle\, X_{ij} \quad \text{for} \quad i,\, j = 1,\, 2,$$

$$X_{11} = (2/15)^{1/2}[x]^{1/2}\,(20k0|x0)\ ,$$

$$X_{22} = (2/15)^{1/2}[y]^{1/2}\,(20k0|y0)\ ,$$

$$X_{12} = ([x][y])^{1/2}(10k0|x0)(10k0|y0)W(11xy;2k)\ ,$$

and

$$\langle\alpha|r_1 r_j|\alpha'\rangle = (2k+1)\int_0^\infty dr_1 r_1^{\,2} R_1 R_1' \int_0^\infty dr_2 r_2^{\,2} R_2 R_2' r_i r_j$$

$$\times \int_{-1}^{1} d\left(\frac{\cos\omega_{12}}{2}\right) P_k(\cos\omega_{12})\ \frac{V(r_{12})}{r_{12}^{\,2}}\ .$$

The angular part is given in terms of 3-, 6-, and 9-j symbols as

$$\langle j_1 j_2 JM|\underset{\sim}{T}_1{}^{(1x)K}\cdot\underset{\sim}{T}_2{}^{(1y)K}|j_1' j_2' J'M'\rangle = (-1)^{j_1'+j_2+\ell_1+\ell_2+J}\, 6\,\delta_{JJ'}\delta_{MM'} \begin{Bmatrix} J & j_2 & j_1 \\ k & j_1' & j_2' \end{Bmatrix}$$

$$\times\ ([j_1][j_2][j_1'][j_2'])^{1/2}([\ell_1][\ell_2][\ell_1'][\ell_2'])^{1/2}$$

$$\times \begin{pmatrix} \ell_1 & x & \ell_1' \\ 0 & 0 & 0 \end{pmatrix} \begin{pmatrix} \ell_2 & y & \ell_2 \\ 0 & 0 & 0 \end{pmatrix} \begin{Bmatrix} \frac{1}{2} & \frac{1}{2} & 1 \\ \ell_1' & \ell_1 & x \\ j_1' & j_1 & K \end{Bmatrix} \begin{Bmatrix} \frac{1}{2} & \frac{1}{2} & 1 \\ \ell_2' & \ell_2 & y \\ j_2' & j_2 & K \end{Bmatrix}\ .$$

An almost identical result for the diagonal case only is given by de-Shalit and Walecka.[15] The radial integral $\langle\alpha|r_i r_j|\alpha'\rangle$ can be evaluated by expanding it into a linear combination of Talmi integrals:

$$\langle\alpha|r_i r_j|\alpha'\rangle = \sum_{m,m'} f_k(m,m')$$

$$= \sum_{m,m'} (1/2\pi)^{1/2} 2^{-(m+m')-3} \sum_{\sigma} (m+m'-2\sigma+1)!!\, T_k^{2\sigma}(m,m') J_{2\sigma} ,$$

where f_k is the double integral of the form

$$f_k = \iint x_1^m x_2^{m'} v_k(r_1,r_2) \exp(-x_1^2-x_2^2) x_1^2 dx_1 x_2^2 dx_2$$

the variable x_i is defined here as $r_i\sqrt{\nu}$ and $(\nu)^{-1/2}$ is the length parameter appearing in the harmonic oscillator radial wave functions, and

$$v_k(r_1,r_2) = (2k+1)\int_{-1}^{1} d\left(\frac{\cos\omega_{12}}{2}\right) P_k(\cos\omega_{12}) \frac{V(r_{12})}{r_{12}^2} .$$

The Talmi integral $J_{2\sigma}$ is the single integral defined as

$$J_{2\sigma} = \int_0^\infty x^{2\sigma} \exp\left(-\frac{x^2}{2}\right) \frac{V(\sqrt{\nu}\, x)}{\nu x^2} x^2 dx .$$

The expansion coefficient T is the Talmi coefficient defined by Ford and Konopinski,[18] and the explicit expressions along with several recursion relations for the Talmi coefficients are given in detail by Ford and Konopinski.

C. Fortran Programs

The FORTRAN programs used in this paper are presented here. Detailed information for inputs and outputs of the programs is summarized whenever necessary. Four separate main programs are described below. All matrix element are computed with the use of Gaussian radial-dependence and harmonic-oscillator wave functions.

1. Tensor-Force Matrix Elements

a. For the particle-particle interaction. This FORTRAN program calculates the tensor-force matrix elements for the particle-particle interaction. The FORTRAN listing is in Appendix D.

i. Input

The first card contains OSC (F10.5), where OSC is the harmonic oscillator parameter $(\nu)^{-1/2}$ in units of fermis.

The second card contains, VTTE, VTTO, RTF(1), RTF(2) (4F10.5), where VTTE and VTTO are the strength parameters for the tensor triplet-even and triplet-odd forces, respectively (in units of MeV), and RTF(1) and RTF(2) are the ranges for the tensor triplet-even and triplet-odd forces, respectively (in units of Fermi).

The third card contains MAXN (I5), where MAXN is the total number of configurations for which the tensor-force matrix elements are to be computed in a single run.

The fourth card contains LLT (I5), where LLT is the number of various spin-J states arising from a given configuration. This number is adjustable according to the desired number of J states of a given configuration to be computed.

The fifth card contains N11, L1, N22, L2, MN33, ML3, MN44, ML4 (8I5), where these parameters correspond to the radial quantum numbers n_1, ℓ_1, n_2, ℓ_2, n_1', ℓ_1', n_2', ℓ_2' , respectively.

The sixth card contains AL1F, AL2F, BL1I, BL2I, AJ1F, AJ2F, BJ2I, BJ, ZERO (9F5.1, F10.5),

where these parameters correspond to the quantum numbers, $\ell_1, \ell_2, \ell_1', \ell_2'$, j_1, j_2, j_1', j_2', J_{max}, and the zeroth-order energy in MeV, respectively.

The program computes the tensor-force matrix elements for J (BJ) state of a given configuration, and proceeds to compute for the (J_{max} - 1) state, (J_{max} - 2), etc. until it repeats LLT times (see the fourth card). After a given configuration is completed, it proceeds to another configuration by going back to the fourth card, and repeats this process MAXN times (see the third card). After a set of configurations is finished, another set of configruations can be computed if more data cards are added, starting from the second card.

ii. Output

The output consists of:

tensor-force direct radial integrals with various possible k values

corresponding quantum numbers

tensor-force direct matrix elements

tensor-force exchange radial integrals with various possible k values

corresponding quantum numbers

tensor-force exchange matrix elements

$$\beta_{TE}^{T}, \langle a | P_{TE} S_{12} \exp(-\beta_{TE}^{T} r^2) | a' \rangle,$$

$$\langle a | V_{TE}^{T} P_{TE} S_{12} \exp(-\beta_{TE}^{T} r^2) | a' \rangle ,$$

$$\langle a | P_{TO} S_{12} \exp(-\beta_{TE}^{T} r^2) | a' \rangle$$

and

$$\langle a | V_{TO}^{T} P_{TO} S_{12} \exp(-\beta_{TE}^{T} r^2) | a' \rangle$$

for various J states of a given configuration.

$$\beta^T_{TO}\ ,\ \langle a|P_{TE}S_{12}\ \exp\ (-\beta^T_{TO}r^2)|a'\rangle\ ,$$

$$\langle a|V^T_{TE}P_{TE}S_{12}\ \exp\ (-\beta^T_{TO}\ r^2)|a'\rangle\ ,$$

$$\langle a|P_{TO}S_{12}\exp\ (-\beta^T_{TO}\ r^2)|a'\rangle\ ,$$

and

$$\langle a|V^T_{TO}P_{TO}S_{12}\ \exp\ (-\beta^T_{TO}\ r^2)|a'\rangle$$

for various J states of a given configuration.

In addition, the following output is punched on cards:

FTTE, FTTO, AJ (2F10.7, F5.1),

where

FTTE and FTTO are $\langle a|V^T_{TE}\ P_{TE}S_{12}\ \exp(-\beta r^2)|a'\rangle$ and

$\langle a|V^T_{TO}\ P_{TO}S_{12}\ \exp\ (-\beta r^2)|a'\rangle$, respectively, and AJ

is the total angular momentum J.

iii. Subprograms

The following five subprograms and three functions are necessary (pages for FORTRAN listings are shown in parenthesis):

(a) subroutine TFORCE which calculates the angular part of the tensor-force matrix elements (p. 145)

(b) subroutine TENSOR which calculates the radial parts of the tensor-force matrix elements (p. 149)

(c) subroutine TFMOD which calculates all the common factors for the various J states of a given configuration (p. 151)

(d) subroutine TALMI which calculates the Talmi coefficients defined in Appendix B (p. 153)

(e) subroutine RADIAL which calculates the expansion coefficients f(m,m') defined in Appendix B (p. 154)

(f) function VEC which calculates the numerical values of the 9-j symbols (p. 155)

(g) function RACAH which calculates the Racah coefficients (obtained from Los Alamos Laboratory, and hence not shown here)

(h) function CLEBSH which calculates the Clebsch-Gordan coefficients (also obtained from Los Alamos Laboratory, and hence not shown here).

b. For the particle-hole interaction. This program converts the tensor-force matrix element of the particle-particle interaction (B3) into the matrix element for the particle-hole interaction (B2). In addition, it can convert the punched output cards of program la into input data cards of the tensor-force matrix elements for the next program 2 and 3. The FORTRAN listing is in Appendix E.

i. Input

The first card contains TTEC and TTOC (2F10.5), which are arbitrary constants that may be multiplied by the strength parameters V^T_{TE} and V^T_{TO}, respectively.

The second card contains NE, ND, JAMIN, JAMAX (4I5), where:

NE is the total number of configurations under consideration. This corresponds to the maximum dimension of the matrix.

ND is a control number. If we have ND < 0, the program is for the particle-particle case, and if we have ND $\geqslant$ 0, it is for the particle-hole case.

JAMIN and JAMAX are $(J_{min} + 1)$ and $(J_{max} + 1)$, respectively, where J_{min} and J_{max} are the smallest and largest J, respectively, for all configurations under consideration.

The third card contains BJ1F, BJ2F, BJ1I, BJ2I (4F5.1) where these parameters correspond to j_1, j_2, j_1', j_2', respectively, for both the particle-particle case and the particle-hole case.

Starting from the fourth card, a series of cards follows as shown below:

The fourth card: TTE(JMNC), DUM(JMNC) (2F10.7)

The fifth card: TTE(JMNC + 1), DUM(JMNC + 1) (2F10.7)

.....

The last card: TTE(JMXC), DUM(JMXC) (2F10.7)

where

TTE(JMNC) and TTE(JMXC) are the triplet-even tensor-force matrix elements for the J_{min} and J_{max} states of a given configuration, respectively, which have been calculated in 1 a, and DUM is a dummy variable which does not enter into the calculation. This set of cards is followed by another similar set of cards for the triplet-odd, i.e.

DUM(JMNC), TTO(JMNC) (2F10.7)

.....

etc.,

where TTO(JMNC) has the obvious meaning similar to TTE(JMNC).

After these two sets of cards, the input is repeated from the third card with following sequence:

$$\begin{array}{lllll} (1,1), & (1,2), & \cdot & \cdot\ \cdot\ \cdot & (1, NE) \\ & (2,2), & \cdot & \cdot\ \cdot\ \cdot & (2, NE) \\ & & & \cdot\ \cdot\ \cdot & \cdot \\ & & & \cdot\ \cdot & \cdot \\ & & & & (NE, NE) \end{array},$$

where the indices designate the configurations under consideration.

ii. Output

The output consists of the total angular momentum J, the initial matrix, and the final matrix. In addition, the following output is punched on cards:

J(I5).

For ND = 0, A(1,1), A(2,2), ..., etc. (8F10.7), i.e., only the diagonal matrix elements are punched.

For ND ≠ 0, A(1,1), A(1,2), ..., etc. (8F10.7), i.e., the entire matrix elements are punched.

iii. Subprogram

The only subprogram needed is FUNCTION RACAH [1 a (g)] .

2. Particle-Particle Interaction

This program computes the central-force matrix elements for the particle-particle interaction. Optionally, it can take the tensor-force matrix elements as inputs. If the dimension of the resulting matrix is greater than 2 by 2, this program will automatically diagonalize the matrix and compute the eigenvalues and eigenfunctions. The FORTRAN listing is in Appendix F.

i. Input

The first card contains NTE (I5), where NTE is a control number. For NTE ≠ 0, the tensor-force matrix elements can be read in as input. In addition, for NTE < 0, the initial matrix will be printed out. For NTE = 0, the tensor-force matrix elements are not read in.

The second card contains OCS, VTEN (2F10.5), where OSC is already defined in 1a, and VTEN is any arbitrary constant that can be multipled into the tensor-force matrix.

The third card contains VTE, SE, TO, SO, RCF(1), RCF(2), RCF(3), and RCF(4) (8F10.5), where VTE, SE, TO, and SO are strength parameters in MeV for the central triplet-even, singlet-even, triplet-odd, and singlet-odd forces respectively. The corresponding force ranges in Fermi are RCF(1), RCF(2), RCF(3), and RCF(4).

The fourth card contains NE, ND, JAMIN, JAMAX (4I5), where NE has been defined in 1b, and ND is a control number. For ND = 0, only the diagonal tensor-force matrix elements are to be read in as input. Otherwise, the tensor-force matrix elements, including the off-diagonal case are to be included.

JAMIN and JAMAX have the same meanings as defined in 1b. The fifth card contains MN11, ML1, MN22, ML2, MN33, ML3, MN44, and ML4 (8I5), where these parameters correspond to the radial quantum numbers, n_1, ℓ_1, n_2, ℓ_2, n_1', ℓ_1', n_2', ℓ_2', respectively.

The sixth card contains BL1F, BL2F, BL1I, BL2I, BJ1F, BJ2F, BJ1I, BJ2I, and ZERO (8F5.1, F10.5), where these parameters correspond to the quantum numbers, $\ell_1, \ell_2, \ell_1', \ell_2'$, j_1, j_2, j_1', j_2', and the zeroth-order energy in MeV, respectively.

After the sixth card, input is repeated again starting from the fifth card in the following sequence:

$$
\begin{array}{lllll}
(1,1), & (1,2), & \cdots & \cdots & (1,NE) \\
 & (2,2), & \cdots & \cdots & (2,NE) \\
 & & \cdots & \cdots & \\
 & & & \cdots & \\
 & & & & (NE,NE)\ ,
\end{array}
$$

where indices denote the configurations under consideration.

Next comes the input for the tensor-force matrix elements. For NTE = 0, there is no input for these matrix elements. For NTE $\neq$ 0 , and ND = 0, then only the diagonal tensor-force matrix elements for J_{min}(JAMIN) states must be read in with the format (8F10.7) in the following sequence:

(1,1), (2,2), . . . , etc.

This process repeats for successive J-states until it reaches the J_{max} (JAMAX) states. For NTE $\neq$ 0, and ND $\neq$ 0, the entire tensor-force matrix including off-diagonal elements must be read in with format (8F10.7) in the following triangular sequence:

(1,1), (1,2), ...

(2,2), ...

etc.

This process repeats for successive J states until it reaches the J_{max} (JAMAX) states.

ii. Output

The output consists of:

OCS, VTEN

VTE, SE, TO, SO, RCF(1), RCF(2), RCF(3), and RCF(4).

For NTE < 0, the initial matrix is printed out.

angular momentum J

central-force matrix.

For NTE = 0, the tensor-force matrix elements are printed out.

final matrix

eigenvalues in MeV and eigenfunctions.

iii. Subprograms

(a) Subroutine CFORCE calculates the angular part of the central-force matrix elements.

(b) Subroutine SLATED calculates the radial part of the central-force matrix elements.

(c) Subroutine EIGEN diagonalizes the matrix and calculates eigenvalues and eigenfunctions. IBM SHARE PROGRAM F2 AN F022 was slightly modified to obtain this program.

In addition, subroutines TALMI and RADIAL, and functions RACAH and CLEBSH are necessary. All of these subprograms are described in la.

3. Particle-Hole Interaction

This program calculates the central-force matrix elements for the particle-hole interaction. The tensor-force matrix elements for the particle-hole interaction are to be computed separately by use of program lb, and are to be read in as input in this program. Again, as in the particle-particle program, the resulting matrix is diagonalized to obtain the eigenvalues and eigenfunctions. The FORTRAN listing is given in Appendix G.

i. Input

The input is the same as for program 2, except that subscripts 1 and 2 always refer to the hole and particle states, respectively.

ii. Output

The output is the same as for program 2.

iii. Subprograms

The subprograms are the same as those for program 2.

D. FORTRAN Listing (1a)

```
C       MATRIX ELEMENTS OF TENSOR FORCE (IV)
D       DIMENSION T(20),BI(20,20),BIN(20,20),DBI(20,20),P(20),Q(20),SQ(20)
D      1,SQF(20),DF(20),GJ(20),SQ2(20),FACT(20),RT(25,5),VPN(20,20),VP(20)
D      2,VN(20),R(20),BK(20),B1K(20),B2K(20)
        DIMENSION COM(20),RTF(2) ,TLLL(20,20,2),TLL(20,20)
        COMMON T,BI,BIN,DBI,P,Q,N1,N2,N3,N4,L1,L2,L3,L4,SQ,SQ2,SQF,DF,FACT
       1,GJ,N13,N24,N11,N22,N33,N44,L11,L22,L33,L44,K1U,K2U,K3U,K1L,K2L,K3
       2L,      KL,KU,      AL1F,AL2F,AL1I,AL2I,AJ1F,AJ2F,AJ1I,AJ2I,AJ
       3,BK,B1K,B2K
  117 FORMAT(I5)
D       BI(1,1)=1.0
D       DBI(1,1)=1.0
        DO 10 J=2,19
D       BI(J,1)=1.
D       DBI(J,1)=1.
        K=J
        DO 10 M=2,K
D       BI(J,M)=(FLOATF(J-M+1)/FLOATF(M-1))*BI(J,M-1)
D   10 DBI(J,M)=((FLOATF(J-M)*2.+3.)/(FLOATF(M)*2.-1.D)*DBI(J,M-1)
        DO 11 J=1,19
D       BIN(J,1)=1.
        K=J+1
        DO 11 M=2,K
D   11 BIN(J,M)=((FLOATF(J-M+2)-0.5)/FLOATF(M-1))*BIN(J,M-1)
D       P(1)=1.
D       Q(1)=1.
D       SQ(1)=1.
D       DF(1)=1.
D       SQ2(1)=1.
D       SQF(1)=1.
        DO 12 I=1,19
D       P(I+1)=-1.*P(I)
D       SQ(I+1)=-2.*SQ(I)
D       SQF(I+1)=4.*SQF(I)
D       DF(I+1)=(2.*FLOATF(I)+1.)*DF(I)
D       SQ2(I+1)=2.*SQ2(I)
D   12 Q(I+1)=-4.*Q(I)
D       FACT(1)=1.
        DO 129 M=2,19
D  129 FACT(M)=FLOATF(M-1)*FACT(M-1)
        READ INPUT TAPE 2,212 ,OSC
  212 FORMAT(F10.5)
        WRITE OUTPUT TAPE 3,211,OSC
  211 FORMAT(1X11HOSCILLATOR=F10.5)
  118 READ INPUT TAPE2,14,VTTE,VTTO,(RTF(I),I=1,2)
   14 FORMAT(4F10.5)
        WRITE OUTPUT TAPE 3,14,VTTE,VTTO,(RTF(I),I=1,2)
        READ INPUT TAPE 2,280,MAXN
  280 FORMAT(I5)
        DO 305 KX=1,MAXN
        READ INPUT TAPE 2,117,LLT
        READ INPUT TAPE 2,2,N11,L1,N22,L2,MN33,ML3,MN44,ML4
    2 FORMAT(8I5)
        READ INPUT TAPE 2,119,AL1F,AL2F,BL1I,BL2I,AJ1F,AJ2F,BJ1I,BJ2I,BJ,
       1ZERO,KM
  119 FORMAT(9F5.1,F10.5,I5)
        DO 112 L=1,2
        BT=(OSC/RTF(L))**2
D       GJ(1)=1.
```

```
      DO 13 I=1,19
D  13 GJ(I+1)=(FLOATF(I)-0.5)*GJ(I)/(0.5+BT)
      DO 400 II=1,LLT
      AJ=BJ-FLOATF(II-1)
      AL1I=BL1I
      AL2I=BL2I
      AJ1I=BJ1I
      AJ2I=BJ2I
      IF (II-1) 201,201,202
  202 DO 205 I=1,20
      DO 205 J=1,20
  205 TLL(I,J)=TLLL(I,J,1)
      CALL TFMOD( ET,TLL)
      GO TO 203
  201 N33=MN33
      L3=ML3
      N44=MN44
      L4=ML4
      CALL TENSOR(RT,BT)
      WRITE OUTPUT TAPE 3,3,(I,RT(I,1),I=1,K1U)
      WRITE OUTPUT TAPE 3,3,(I,RT(I,2),I=1,K2U)
      WRITE OUTPUT TAPE 3,3,(I,RT(I,3),I=1,K3U)
    3 FORMAT(I5,E20.8)
      CALL        TFORCE( ET,RT,TLL,TMM1,TMM2,TMM3,CO,TL1)
      DO 204 I=1,20
      DO 204 J=1,20
  204 TLLL(I,J,1)=TLL(I,J)
  203 WRITE OUTPUT TAPE 3,35,AL1F,AL2F,AL1I,AL2I,AJ1F,AJ2F,AJ1I,AJ2I,AJ,
     1ET
   35 FORMAT(9F5.1,4F20.8)
      AL1I=BL2I
      AL2I=BL1I
      AJ1I=BJ2I
      AJ2I=BJ1I
      IF (II-1) 501,501,502
  502 DO 505 I=1,20
      DO 505 J=1,20
  505 TLL(I,J)=TLLL(I,J,2)
      CALL TFMOD(QET,TLL)
      GO TO 503
  501 N33=MN44
      L3=ML4
      N44=MN33
      L4=ML3
      CALL TENSOR(RT,BT)
      WRITE OUTPUT TAPE 3,3,(I,RT(I,1),I=1,K1U)
      WRITE OUTPUT TAPE 3,3,(I,RT(I,2),I=1,K2U)
      WRITE OUTPUT TAPE 3,3,(I,RT(I,3),I=1,K3U)
      CALL        TFORCE(QET,RT,TLL,TMM1,TMM2,TMM3,CO,TL1)
      DO 504 I=1,20
      DO 504 J=1,20
  504 TLLL(I,J,2)=TLL(I,J)
  503 WRITE OUTPUT TAPE 3,35,AL1F,AL2F,AL1I,AL2I,AJ1F,AJ2F,AJ1I,AJ2I,AJ,
     1QET
      MA=AJ1I+AJ2I+AJ
      MM=XMODF(MA,2)
      IF (MM) 71,71,72
   71 QP=1.
```

```
      GO TO 252
   72 QP=-1.
  252 CONTINUE
      TTE=0.5*(ET+QP*QET)
      TTO=0.5*(ET-QP*QET)
      FTTE=TTE*VTTE
      FTTO=TTO*VTTO
      WRITE OUTPUT TAPE 3,301,RTF(L),TTE,FTTE,TTO,FTTO
  301 FORMAT(1X6HRANGE=F10.5,1X4HTTE=E15.8,1X5HFTTE=E15.8,1X4HTTO=E15.8,
     11X5HFTTO=E15.8)
      WRITE OUTPUT TAPE 14,284,FTTE,FTTO,AJ
  284 FORMAT(2F10.7,F5.1)
  400 CONTINUE
  112 CONTINUE
  305 CONTINUE
      GO TO 118
      END
```

```
      SUBROUTINE TFORCE(QET,RT,TLL,TMM1,TMM2,TMM3,COS,TL1)
D     DIMENSION T(20),BI(20,20),BIN(20,20),DBI(20,20),P(20),Q(20),SQ(20)
D    1,SQF(20),DF(20),GJ(20),SQ2(20),FACT(20),RT(25,5),VPN(20,20),VP(20)
D    2,VN(20),R(20)
      DIMENSION TLL(20,20),COM(20),CB1(20),CC1(20),CD3(20,20),VX(20,20)
     1,VR(6),V(9),W(9), A12(6),B1(6), X(9),C1(6),CA12(20,20),D3(6),E3(6)
      COMMON T,BI,BIN,DBI,P,Q,N1,N2,N3,N4,L1,L2,L3,L4,SQ,SQ2,SQF,DF,FACT
     1,GJ,N13,N24,N11,N22,N33,N44,L11,L22,L33,L44,K1U,K2U,K3U,K1L,K2L,K3
     2L,     KL,KU,      AL1F,AL2F,AL1I,AL2I,AJ1F,AJ2F,AJ1I,AJ2I,AJ
     3,BK,B1K,B2K
      DO 666 M=1,20
  666 COM(M)=SQRTF(2.*FLOATF(M-1)+1.)
      LU=AJ+2.
      L121=AL1F+AL2F+1.
      L341=AL1I+AL2I+1.
      L13=AL1F+AL1I
      L24=AL2F+AL2I
      L131=L13+1
      L132=L13+2
      L241=L24+1
      L242=L24+2
      L133=L13+3
      L243=L24+3
      LUF =XMINOF(L121,LU)
      LUI =XMINOF(L341,LU)
      KL1U=XMINOF(L241,L133)
      KL2U=XMINOF(L243,L131)
      KL3U=XMINOF(L242,L132)
      KLU =XMINOF(L133,L243)
      ML24=XMODF(L24,2)
      ML13=XMODF(L13,2)
      AJ12I=(2.*AJ1I+1.)*(2.*AJ2I+1.)
      AJ12F=(2.*AJ1F+1.)*(2.*AJ2F+1.)
      AL12I=(2.*AL1I+1.)*(2.*AL2I+1.)
      TL1=0.0
      DO 61 I=1,20
      DO 61 J=1,20
   61 TLL(J,I)=0.0
      IF(ML24-ML13) 71,72,71
   71 GO TO 200
   72 IF(ML24) 151,151,152
  151 KL1L=1
      KL3L=2
      XP=1.
      GO TO 73
  152 KL1L=2
      KL3L=1
      XP=-1.
   73 DO 425 IX=KL1L,L131,2
      B1(1)=IX-1
      B1(2)=AL1I
      B1(3)=AL1F
      B1(4)=0.0
      B1(5)=0.0
      B1(6)=0.0
  425 CB1(IX)=CLEBSH(B1)
      DO 245 IX=KL1L,L241,2
      C1(1)=IX-1
      C1(2)=AL2I
```

```
      C1(3)=AL2F
      C1(4)=0.0
      C1(5)=0.0
      C1(6)=0.0
  245 CC1(IX)=CLEBSH(C1)
      DO 445 K=KL1L,KLU,2
      K2=K+2
      KLUU=XMINOF(K2,KLU)
      IF(K-3) 401,401,402
  401 KLLL=KL1L
      GO TO 403
  402 KLLL=K-2
  403 DO 445 IX=KLLL,KLUU,2
      A12(1)=K-1
      A12(2)=2
      A12(3)=IX-1
      A12(4)=0.0
      A12(5)=0.0
      A12(6)=0.0
  445 CA12(K,IX)=CLEBSH(A12)
      DO 145 K=KL3L,KL3U,2
      K1=K+1
      KLUU=XMINOF(K1,KLU)
      IF(K-2) 501,501,502
  501 KLLL=KL1L
      GO TO 503
  502 KLLL=K-1
  503 DO 145 IX=KLLL,KLUU,2
      D3(1)=K-1
      D3(2)=1
      D3(3)=IX-1
      D3(4)=0.0
      D3(5)=0.0
      D3(6)=0.0
  145 CD3 (K,IX)=CLEBSH(D3)
      DO 41 I=1,LUI
      I2=I+2
      LUFF=XMINOF(I2,LUF)
      IF(I-3) 51,51,52
   51 LLF=1
      GO TO 53
   52 LLF=I-2
   53 DO 41 J=LLF,LUFF
      DO 345 K=KL1L,KL1U,2
      K2=K+2
      KLUU=XMINOF(K2,KL2U)
      IF (K-3) 81,81,82
   81 KLLL=KL1L
      GO TO 83
   82 KLLL=K-2
   83 DO 345 IX=KLLL,KLUU,2
      X(1)=AL1I
      X(2)=AL2I
      X(3)=I-1
      X(4)=IX-1
      X(5)=K-1
      X(6)=2
      X(7)=AL1F
```

```
      X(8)=AL2F
      X(9)=J-1
  345 VX(IX,K)=VEC(X)
      VR(1)=J-1
      VR(2)=I-1
      VR(3)=1
      VR(4)=1
      VR(5)=2
      VR(6)=AJ
      V(1)=AL1I
      V(2)=AL2I
      V(3)=I-1
      V(4)=0.5
      V(5)=0.5
      V(6)=1.0
      V(7)=AJ1I
      V(8)=AJ2I
      V(9)=AJ
      W(1)=AL1F
      W(2)=AL2F
      W(3)=J-1
      W(4)=0.5
      W(5)=0.5
      W(6)=1.0
      W(7)=AJ1F
      W(8)=AJ2F
      W(9)=AJ
      VI=VEC(V)
      VF=VEC(W)
      RVR=RACAH(VR)
      ALI=(2.*FLOATF(I-1)+1.)
      ALF=(2.*FLOATF(J-1)+1.)
      JJ=AJ
      MJ=JJ+J
      MJJ=XMODF(MJ,2)
      IF (MJJ) 42,42,43
   42 PHASE=1.
      GO TO 44
   43 PHASE =-1.
   44 CO =PHASE*   ALF*ALI*                RVR*VF*VI
      TMM1=0.0
      DO 110 K=KL1L,KL1U,2
      K2=K+2
      KLUU=XMINOF(K2,KL2U)
      IF (K-3) 101,101,102
  101 KLLL=KL1L
      GO TO 103
  102 KLLL=K-2
  103 DO 110 IX=KLLL,KLUU,2
  113 EXK=(2.*FLOATF(K-1)+1.)
      TTM1=XP*COM(IX)*CA12(K,IX)*CB1(IX)*CC1(K)*VX(IX,K)*RT(K,1)*EXK*SQR
     1TF(2./3.)
  110 TMM1=TMM1+TTM1
      TMM2=0.0
      DO 120 K=KL1L,KL2U,2
      K2=K+2
      KLUU=XMINOF(K2,KL1U)
      IF (K-3) 201,201,202
```

```
201 KLLL=KL1L
    GO TO 203
202 KLLL=K-2
203 DO 120 IX=KLLL,KLUU,2
123 EXK=(2.*FLOATF(K-1)+1.)
    TTM2=XP*COM(IX)*CA12(K,IX)*CB1(K)*CC1(IX)*VX(K,IX)*RT(K,2)*EXK*SQR
   1TF(2./3.)
120 TMM2=TMM2+TTM2
    TMM3=0.0
    DO 130 K=KL3L,KL3U,2
    K1=K+1
    KL1UU=XMINOF(K1,KL2U)
    IF (K-2) 91,91,92
 91 KL1LL=KL1L
    GO TO 93
 92 KL1LL=K-1
 93 DO 130 IX=KL1LL,KL1UU,2
    IX2=IX+2
    KL2UU=XMINOF(IX2,KL1U)
    IF (IX-3) 301,301,302
301 KL2LL=KL1L
    GO TO 303
302 KL2LL=IX-2
303 DO 130 IY=KL2LL,KL2UU,2
    E3(1)=1
    E3(2)=1
    E3(3)=IX-1
    E3(4)=IY-1
    E3(5)=2
    E3(6)=K-1
    RE3=RACAH(E3)
133 EXK=(2.*FLOATF(K-1)+1.)
    TTM3=XP*COM(IX)*COM(IY)*CD3(K,IX)*CD3(K,IY)*CB1(IX)*CC1(IY)*RE3*VX
   1(IX,IY)*RT(K,3)*EXK*SQRTF(5.)
130 TMM3=TMM3+TTM3
    TLL(J,I)=TMM1+TMM2+2.*TMM3
 41 TL1=TL1+TLL(J,I)*CO
200 QET=TL1*6.*SQRTF(AJ12F*AJ12I*AL12I*5.)
    RETURN
    END
```

```
      SUBROUTINE TENSOR(RT,BT)
D     DIMENSION T(20),BI(20,20),BIN(20,20),DBI(20,20),P(20),Q(20),SQ(20)
D    1,SQF(20),DF(20),GJ(20),SQ2(20),FACT(20),RT(25,5),VPN(20,20),VP(20)
D    2,VN(20)
      COMMON T,BI,BIN,DBI,P,Q,N1,N2,N3,N4,L1,L2,L3,L4,SQ,SQ2,SQF,DF,FACT
     1,GJ,N13,N24,N11,N22,N33,N44,L11,L22,L33,L44,K1U,K2U,K3U,K1L,K2L,K3
     2L,KL,KU
      N1=N11-1
      N2=N22-1
      N3=N33-1
      N4=N44-1
      L11=L1+1
      L22=L2+1
      L33=L3+1
      L44=L4+1
      N13=N1+N3+1
      N24=N2+N4+1
      NL1=N1+L1+1
      NL2=N2+L2+1
      NL3=N3+L3+1
      NL4=N4+L4+1
      L112=L11+2
      L222=L22+2
      L332=L33+2
      L442=L44+2
D     RNL1=SQRTF((SQ2(L112)*DF(NL1))/(SQ2(N11)*FACT(N11)*(DF(L11)**2)))
D     RNL2=SQRTF((SQ2(L222)*DF(NL2))/(SQ2(N22)*FACT(N22)*(DF(L22)**2)))
D     RNL3=SQRTF((SQ2(L332)*DF(NL3))/(SQ2(N33)*FACT(N33)*(DF(L33)**2)))
D     RNL4=SQRTF((SQ2(L442)*DF(NL4))/(SQ2(N44)*FACT(N44)*(DF(L44)**2)))
D     RNL=RNL1*RNL2*RNL3*RNL4
      L24=L2+L4
      L241=L2+L4+1
      L242=L2+L4+2
      L243=L2+L4+3
      L13=L1+L3
      L131=L1+L3+1
      L132=L1+L3+2
      L133=L1+L3+3
D     CALL RADIAL (VPN,VP,VN)
      K1U=XMINOF(L241,L133)
      K2U=XMINOF(L131,L243)
      K3U=XMINOF(L132,L242)
      ML24=XMODF( L24,2)
      ML13=XMODF( L13,2)
      DO 101 I=1,20
      DO 101 J=1,3
D 101 RT(I,J)=0.0
      IF (ML24-ML13) 71,72,71
   71 GO TO 200
   72 IF (ML24) 51,51,52
   51 K1L=1
      GO TO 73
   52 K1L=2
   73 DO 111 K=K1L,K1U,2
D     TRR=0.0
      DO 121 M=1,N13
      DO 121 N=1,N24
      IT=0.5*FLOATF(L13+2*M-(K-1))+1.
      JT=0.5*FLOATF(L24+2*(N-1)-(K-1))+1.
```

```
      KT=K
      MT=0.5*FLOATF(L13+2*M+L24+2*(N-1))+1.
D     CALL TALMI (T,IT,JT,KT,MT)
D     TTR=0.0
      DO 131 I=1,MT
      MTT=MT-I+1
D     TT =DF(MTT)*T(I)*GJ(I)
D 131 TTR=TTR+TT
D     TR=TTR*VPN(M,N)/(SQF(MT)*SQRTF(2.*(0.5+BT))*16.)
D 121 TRR=TRR+TR
D 111 RT(K,1)=TRR*RNL
      IF (ML24) 61,61,62
   61 K2L=1
      GO TO 63
   62 K2L=2
   63 DO 112 K=K2L,K2U,2
D     TRR=0.0
      DO 122 M=1,N13
      DO 122 N=1,N24
      IT=0.5*FLOATF(L13+2*(M-1)-(K-1))+1.
      JT=0.5*FLOATF(L24+2*N-(K-1))+1.
      KT=K
      MT=0.5*FLOATF(L13+2*N+L24+2*(M-1))+1.
D     CALL TALMI (T,IT,JT,KT,MT)
D     TTR=0.0
      DO 132 I=1,MT
      MTT=MT-I+1
D     TT =DF(MTT)*T(I)*GJ(I)
D 132 TTR=TTR+TT
D     TR=TTR*VPN(M,N)/(SQF(MT)*SQRTF(2.*(0.5+BT))*16.)
D 122 TRR=TRR+TR
D 112 RT(K,2)=TRR*RNL
      IF (ML24) 91,91,92
   91 K3L=2
      GO TO 93
   92 K3L=1
   93 DO 113 K=K3L,K3U,2
D     TRR=0.0
      DO 123 M=1,N13
      DO 123 N=1,N24
      IT=0.5*FLOATF(L13+2*(M-1)+1-(K-1))+1.
      JT=0.5*FLOATF(L24+2*(N-1)+1-(K-1))+1.
      KT=K
      MT=0.5*FLOATF(L13+2  +L24+2*(M-1)+2*(N-1))+1.
D     CALL TALMI (T,IT,JT,KT,MT)
D     TTR=0.0
      DO 133 I=1,MT
      MTT=MT-I+1
D     TT =DF(MTT)*T(I)*GJ(I)
D 133 TTR=TTR+TT
D     TR=TTR*VPN(M,N)/(SQF(MT)*SQRTF(2.*(0.5+BT))*16.)
D 123 TRR=TRR+TR
D 113 RT(K,3)=TRR*RNL
  200 RETURN
      END
```

```
      SUBROUTINE TFMOD(QET,TLL)
D     DIMENSION T(20),BI(20,20),BIN(20,20),DBI(20,20),P(20),Q(20),SQ(20)
D    1,SQF(20),DF(20),GJ(20),SQ2(20),FACT(20),RT(25,5),VPN(20,20),VP(20)
D    2,VN(20),R(20)
      DIMENSION TLL(20,20),COM(20),CB1(20),CC1(20),CD3(20),VX(20,20)
     1,VR(6),V(9),W(9), A12(6),B1(6), X(9),C1(6),CA12(20,20),D3(6),E3(6)
      COMMON T,BI,BIN,DBI,P,Q,N1,N2,N3,N4,L1,L2,L3,L4,SQ,SQ2,SQF,DF,FACT
     1,GJ,N13,N24,N11,N22,N33,N44,L11,L22,L33,L44,K1U,K2U,K3U,K1L,K2L,K3
     2L,      KL,KU,      AL1F,AL2F,AL1I,AL2I,AJ1F,AJ2F,AJ1I,AJ2I,AJ
     3,BK,B1K,B2K
      LU=AJ+2.
      L121=AL1F+AL2F+1.
      L341=AL1I+AL2I+1.
      L13=AL1F+AL1I
      L24=AL2F+AL2I
      L131=L13+1
      L132=L13+2
      L241=L24+1
      L242=L24+2
      L133=L13+3
      L243=L24+3
      LUF =XMINOF(L121,LU)
      LUI =XMINOF(L341,LU)
      KL1U=XMINOF(L241,L133)
      KL2U=XMINOF(L243,L131)
      KL3U=XMINOF(L242,L132)
      KLU =XMINOF(L133,L243)
      KL33U=XMINOF(L131,L241)
      KMAX=XMAXOF(L131,L241)
      ML24=XMODF(L24,2)
      ML13=XMODF(L13,2)
      AJ12I=(2.*AJ1I+1.)*(2.*AJ2I+1.)
      AJ12F=(2.*AJ1F+1.)*(2.*AJ2F+1.)
      AL12I=(2.*AL1I+1.)*(2.*AL2I+1.)
      TL1=0.0
      DO 41 I=1,LUI
      I2=I+2
      LUFF=XMINOF(I2,LUF)
      IF(I-3) 51,51,52
   51 LLF=1
      GO TO 53
   52 LLF=I-2
   53 DO 41 J=LLF,LUFF
      VR(1)=J-1
      VR(2)=I-1
      VR(3)=1
      VR(4)=1
      VR(5)=2
      VR(6)=AJ
      V(1)=AL1I
      V(2)=AL2I
      V(3)=I-1
      V(4)=0.5
      V(5)=0.5
      V(6)=1.0
      V(7)=AJ1I
      V(8)=AJ2I
      V(9)=AJ
      W(1)=AL1F
```

```
      W(2)=AL2F
      W(3)=J-1
      W(4)=0.5
      W(5)=0.5
      W(6)=1.0
      W(7)=AJ1F
      W(8)=AJ2F
      W(9)=AJ
      VI=VEC(V)
      VF=VEC(W)
      RVR=RACAH(VR)
      ALI=(2.*FLOATF(I-1)+1.)
      ALF=(2.*FLOATF(J-1)+1.)
      JJ=AJ
      MJ=JJ+J
      MJJ=XMODF(MJ,2)
      IF (MJJ) 42,42,43
   42 PHASE=1.
      GO TO 44
   43 PHASE =-1.
   44 CO =PHASE*   ALF*ALI*                RVR*VF*VI
      IF(ML24-ML13) 71,72,71
   71 GO TO 200
   72 CONTINUE
   41 TL1=TL1+TLL(J,I)*CO
  200 QET=TL1*6.*SQRTF(AJ12F*AJ12I*AL12I*5.)
      RETURN
      END
```

```
      SUBROUTINE  TALMI(T,I,J,K,M)
D     DIMENSION T(20),BI(20,20),BIN(20,20),DBI(20,20D,P(20),Q(20),SQ(20)
D    1,SQF(20),DF(20),GJ(20),SQ2(20),FACT(20),RT(25,5),VPN(20,20),VP(20)
D    2,VN(20)
      COMMON T,BI,BIN,DBI,P,Q,N1,N2,N3,N4,L1,L2,L3,L4,SQ,SQ2,SQF,DF,FACT
     1,GJ,N13,N24,N11,N22,N33,N44,L11,L22,L33,L44,K1U,K2U,K3U,K1L,K2L,K3
     2L,BT,B,KL,KU
      DO 8 IS=1,M
D     TF=0.0
      IJ=XMINOF(I,J)
      DO 9 IQ=1,IJ
      DO 9 IP=1,K
D     TT=0.0
      N=IS-IQ-IP+2
      L=M-K-IQ-IQ+3
      IF (N) 4,4,5
D   4 TT=0.0
      GO TO 3
    5 IF (L-N) 1,2,2
D   1 TT=0.0
      GO TO 3
D   2 TT=DBI(M,IS)*P(IP)*Q(IQ)*BI(I,IQ)*BI(J,IQ)*BI(K,IP)*BI(L,N)/BIN(M,
D    1IQ)
    3 CONTINUE
D   9 TF=TF+TT
D   8 T(IS)=TF
      RETURN
      END
```

```
      SUBROUTINE RADIAL(VPN,VP,VN)
D     DIMENSION T(20),BI(20,20),BIN(20,20),DBI(20,20D,P(20),Q(20),SQ(20)
D    1,SQF(20),DF(20),GJ(20),SQ2(20),FACT(20),RT(25,5),VPN(20,20),VP(20)
D    2,VN(20),V1(20),V2(20),V3(20),V4(20),V13(20,20),V24(20,20)
      COMMON T,BI,BIN,DBI,P,Q,N1,N2,N3,N4,L1,L2,L3,L4,SQ,SQ2,SQF,DF,FACT
     1,GJ,N13,N24,N11,N22,N33,N44,L11,L22,L33,L44,K1U,K2U,K3U,K1L,K2L,K3
     2L,BT,B,KL,KU
      DO 14 I=1,N11
      J1=I+L1
D  14 V1(I)=SQ(I)*BI(N11,I)*DF(L11)/DF(J1)
      DO 15 I=1,N22
      J2=I+L2
D  15 V2(I)=SQ(I)*BI(N22,I)*DF(L22)/DF(J2)
      DO 16 I=1,N33
      J3=I+L3
D  16 V3(I)=SQ(I)*BI(N33,I)*DF(L33)/DF(J3)
      DO 17 I=1,N44
      J4=I+L4
D  17 V4(I)=SQ(I)*BI(N44,I)*DF(L44)/DF(J4)
      DO 18 I=1,N11
      DO 18 M=1,N33
D  18 V13(I,M)=V1(I)*V3(M)
      DO 19 K=1,N13
D     VPP=0.0
      DO 20 I=1,N11
      DO 20 J=1,N33
      NP=(I-1)+(J-1)+1
      IF(NP-K) 1,2,1
    1 GO TO 20
D   2 VPP=VPP+V13(I,J)
   20 CONTINUE
D  19 VP(K)=VPP
      DO 22 I=1,N22
      DO 22 M=1,N44
D  22 V24(I,M)=V2(I)*V4(M)
      DO 23 K=1,N24
D     VNN=0.0
      DO 24 I=1,N22
      DO 24 J=1,N44
      NN=(I-1)+(J-1)+1
      IF (NN-K) 3,4,3
    3 GO TO 24
D   4 VNN=VNN+V24(I,J)
   24 CONTINUE
D  23 VN(K)=VNN
      DO 25 M=1,N13
      DO 25 N=1,N24
D  25 VPN(M,N)=VP(M)*VN(N)
      RETURN
      END
```

```
      FUNCTION VEC(X)
      DIMENSION X(9),R(6),S(6),T(6)
      A=X(4)+X(8)
      B=X(2)+X(6)
      C=X(1)+X(9)
      D=MIN1F(A,B,C)
      L=2.*(D+1.)
      VECTOR =0.0
      Y=-0.5
      DY=0.5
      DO 10 K=1,L
      Y=Y+DY
      R(1)=X(1)
      R(2)=X(4)
      R(3)=X(9)
      R(4)=X(8)
      R(5)=X(7)
      R(6)=Y
      S(1)=X(2)
      S(2)=X(5)
      S(3)=Y
      S(4)=X(4)
      S(5)=X(8)
      S(6)=X(6)
      T(1)=X(3)
      T(2)=X(6)
      T(3)=X(1)
      T(4)=Y
      T(5)=X(9)
      T(6)=X(2)
      RR=RACAH(R)
      RS=RACAH(S)
      RT=RACAH(T)
      VECT=(2.*Y+1.)*RR*RS*RT
   10 VECTOR=VECTOR+VECT
      NA=2.*(X(1)+X(4))+X(2)+X(3)+X(5)+X(6)+X(8)+X(9)
      NM=XMODF(NA,2)
      IF (NM) 1,1,2
    1 VEC=VECTOR
      GO TO 3
    2 VEC=-VECTOR
    3 RETURN
      END
```

E. FORTRAN Listing (1b)

```
C     MATRIX ELEMENTS OF THE TENSOR FORCE FOR THE PA-TICLE-PARTICLE OR
C     PARTICLE-HOLE INTERACTION
      DIMENSION X(6), CF(16),FME(20,20,16),TTE(16),TTO(16),A(20,20)
     1,DUM(16)
      READ INPUT TAPE 2,9,TTEC,TTOC
    9 FORMAT(2F10.5)
   80 READ INPUT TAPE 2,70,NE,ND,JAMIN,JAMAX
   70 FORMAT(4I5)
      DO 31 JJ=1,16
      DO 31 M=1,20
      DO 31 L=1,20
   31 FME(L,M,JJ)=0.0
      DO 32 M=1,20
      DO 32 L=1,20
   32 A(L,M)=0.0
      DO 33 L=1,16
   33 CF(L)=0.0
      IF (ND) 71,72,72
   71 CONTINUE
      DO 276 L=1,NE
      DO 272 M=L,NE
      READ INPUT TAPE 2,119,                    BJ1F,BJ2F,BJ1I,BJ2I
      CJFL=BJ1F-BJ2F
      CJIL=BJ1I-BJ2I
      CJFU=BJ1F+BJ2F
      CJIU=BJ1I+BJ2I
      CJFA=ABSF(CJFL)
      CJIA=ABSF(CJIL)
      JMCX=XMIN1F(CJFU,CJIU)
      JMCN=XMAX1F(CJIA,CJFA)
      JMNC=JMCN+1
      JMXC=JMCX+1
      IF (JMCX-JMCN) 161,162,162
  161 GO TO 272
  162 CONTINUE
      READ INPUT TAPE 2,8, (TTE(J),DUM(J),J=JMNC,JMXC)
      READ INPUT TAPE 2,8, (DUM(J),TTO(J),J=JMNC,JMXC)
      DO 174  JJ=JMNC,JMXC
      CF(JJ)=TTE(JJ)*TTEC+TTO(JJ)*TTOC
      FME(L,M,JJ)=CF(JJ)
  174 FME(M,L,JJ)=FME(L,M,JJ)
  272 CONTINUE
  276 CONTINUE
      GO TO 277
   72 CONTINUE
      DO 176 L=1,NE
      DO 172 M=L,NE
  118 READ INPUT TAPE 2,119,                    BJ1F,BJ2F,BJ1I,BJ2I
  119 FORMAT(4F5.1)
      AJFL=BJ1I-BJ2F
      AJIL=BJ1F-BJ2I
      AJFU=BJ1I+BJ2F
      AJIU=BJ1F+BJ2I
      AJFA=ABSF(AJFL)
      AJIA=ABSF(AJIL)
      JMAX=XMIN1F(AJFU,AJIU)
      JMIN=XMAX1F(AJFA,AJIA)
      JMN=JMIN+1
      JMX=JMAX+1
```

```
      CJFL=BJ1F-BJ2F
      CJIL=BJ1I-BJ2I
      CJFU=BJ1F+BJ2F
      CJIU=BJ1I+BJ2I
      CJFA=ABSF(CJFL)
      CJIA=ABSF(CJIL)
      JMCX=XMIN1F(CJFU,CJIU)
      JMCN=XMAX1F(CJIA,CJFA)
      JMNC=JMCN+1
      JMXC=JMCX+1
      IF (JMCX-JMCN) 61,62,62
   61 GO TO 172
   62 CONTINUE
      READ INPUT TAPE 2,8, (TTE(J),DUM(J),J=JMN,JMX)
      READ INPUT TAPE 2,8, (DUM(J),TTO(J),J=JMN,JMX)
    8 FORMAT(2F10.7)
      DO 173 JJ=JMN,JMX
  173 CF(JJ)=TTE(JJ)*TTEC+TTO(JJ)*TTOC
      DO 177 JJ=JMNC,JMXC
      MAP=AJFU+AJIU
      MAM=XMODF(MAP,2)
      IF (MAM) 771,771,772
  771 AP=1.
      GO TO 773
  772 AP=-1.
  773 CONTINUE
      PHME=0.0
      X(1)=BJ2I
      X(2)=BJ1F
      X(3)=BJ1I
      X(4)=BJ2F
      X(6)=JJ-1
      DO 51 K=JMN,JMX
      X(5)=K-1
      RAC=RACAH(X)
      PHM=AP*FLOATF(2*(K-1)+1)*RAC*CF(K)
   51 PHME=PHME+PHM
      FME(L,M,JJ)=-PHME
  177 FME(M,L,JJ)=FME(L,M,JJ)
  172 CONTINUE
  176 CONTINUE
  277 CONTINUE
      DO 20 JJ=JAMIN,JAMAX
      JA=JJ-1
      WRITE OUTPUT TAPE 3,301,JA
      WRITE OUTPUT TAPE   14,301,JA
  301 FORMAT(1X2HJ=I2)
   66 WRITE OUTPUT TAPE 3,69
   69 FORMAT(1X14HINITIAL MATRIX)
      DO 68 M=1,NE
   68 WRITE OUTPUT TAPE 3,303,(FME(L,M,JJ),L=1,NE)
   67 CONTINUE
      K=0
   28 DO 30 L=1,NE
      IF (FME(L,L,JJ)) 25,26,25
   26 K=K+1
      GO TO 30
   25 N=0
```

```
      DO 29 M=L,NE
      IF (FME(M,M,JJ)) 39,22,39
   22 N=N+1
      GO TO 29
   39 LL=L-K
      MM=M-K-N
      A(LL,MM)=FME(L,M,JJ)
      A(MM,LL)=A(LL,MM)
   29 CONTINUE
   30 CONTINUE
      NK=NE-K
      IF (NK) 601,601,602
  601 GO TO 603
  602 CONTINUE
  303 FORMAT(13F10.5)
      WRITE OUTPUT TAPE 3, 378
  378 FORMAT(1X12HFINAL MATRIX)
      DO 333 J=1,NK
  333 WRITE OUTPUT TAPE 3,303,(A(I,J),I=1,NK)
      IF (ND) 101,102,101
  102 WRITE OUTPUT TAPE 14,284,(A(I,I),I=1,NK)
      GO TO 20
  101 WRITE OUTPUT TAPE 14,284,((A(L,M),M=L,NK),L=1,NK)
  284 FORMAT (8F10.7)
  603 CONTINUE
   20 CONTINUE
   81 GO TO 80
      END
```

F. FORTRAN Listing (2)

```
C     EIGENVALUES AND VECTORS FOR THE PARTICLE-PARTICLE INTERACTION
D     DIMENSION T(20),BI(20,20),BIN(20,20),DBI(20,20),P(20),Q(20),SQ(20)
D    1,SQF(20),DF(20),GJ(20),SQ2(20),FACT(20),RT(25,5),VPN(20,20),VP(20)
D    2,VN(20),R(20),BK(20),B1K(20),B2K(20)
      DIMENSION RR(20,2,4)   ,RCF(4),X(6),VALU(20)  ,A(20,20),E(4),QV(4),
     1VPS(4),QVPS(4),ATEN(20,20),TENS(20,20),FME(20,20,16),CF(16)
      COMMON T,BI,BIN,DBI,P,Q,N1,N2,N3,N4,L1,L2,L3,L4,SQ,SQ2,SQF,DF,FACT
     1,GJ,N13,N24,N11,N22,N33,N44,L11,L22,L33,L44,K1U,K2U,K3U,K1L,K2L,K3
     2L,      KL,KU,      AL1F,AL2F,AL1I,AL2I,AJ1F,AJ2F,AJ1I,AJ2I,AJ
     3,BK,B1K,B2K
      READ INPUT TAPE 2,280,NTE
  280 FORMAT(I5)
      READ INPUT TAPE 2,202 ,OSC,VTEN
  202 FORMAT(2F10.5)
      WRITE OUTPUT TAPE 3,201,OSC,VTEN
  201 FORMAT(1X11HOSCILLATOR=F10.5,10X5HVTEN=F10.5)
      READ INPUT TAPE 2,4,      VTE,SE,TO,SO,(RCF(I),I=1,4)
    4 FORMAT(8F10.5)
      WRITE OUTPUT TAPE 3,4,      VTE,SE,TO,SO,(RCF(I),I=1,4)
D     BI(1,1)=1.0
D     DBI(1,1)=1.0
      DO 10 J=2,19
D     BI(J,1)=1.
D     DBI(J,1)=1.
      K=J
      DO 10 M=2,K
D     BI(J,M)=(FLOATF(J-M+1)/FLOATF(M-1))*BI(J,M-1)
D   10 DBI(J,M)=((FLOATF(J-M)*2.+3.)/(FLOATF(M)*2.-1.D)*DBI(J,M-1)
      DO 11 J=1,19
D     BIN(J,1)=1.
      K=J+1
      DO 11 M=2,K
D   11 BIN(J,M)=((FLOATF(J-M+2)-0.5)/FLOATF(M-1))*BIN(J,M-1)
D     P(1)=1.
D     Q(1)=1.
D     GJ(1)=1.
D     SQ(1)=1.
D     DF(1)=1.
D     SQ2(1)=1.
D     SQF(1)=1.
      DO 12 I=1,19
D     P(I+1)=-1.*P(I)
D     SQ(I+1)=-2.*SQ(I)
D     SQF(I+1)=4.*SQF(I)
D     DF(I+1)=(2.*FLOATF(I)+1.)*DF(I)
D     GJ(I+1)=(FLOATF(I)-0.5)*GJ(I)/(0.5+BT)
D     SQ2(I+1)=2.*SQ2(I)
D   12 Q(I+1)=-4.*Q(I)
D     FACT(1)=1.
      DO 129 M=2,19
D  129 FACT(M)=FLOATF(M-1)*FACT(M-1)
   80 READ INPUT TAPE 2,70,NE,ND,JAMIN,JAMAX
   70 FORMAT(4I5)
      ME=1
      DO 171 I=1,20
  171 VALU(I)=0.0
      DO 77 J=1,20
      DO 77 I=1,20
   77 A(I,J)=0.0
```

```
      DO 31 J=1,16
      DO 31 M=1,NE
      DO 31 L=1,NE
   31 FME(L,M,J)=0.0
      DO 32 J=1,16
   32 CF(J)=0.0
      DO 174 L=1,NE
  118 DO 172 M=L,NE
      READ INPUT TAPE 2,2,MN11,ML1,MN22,ML2,MN33,ML3,MN44,ML4
      READ INPUT TAPE 2,119,BL1F,BL2F,BL1I,BL2I,BJ1F,BJ2F,BJ1I,BJ2I,
     1ZERO
  119 FORMAT(8F5.1,F10.5)
    2 FORMAT(8I5)
      CJFL=BJ1F-BJ2F
      CJIL=BJ1I-BJ2I
      CJFU=BJ1F+BJ2F
      CJIU=BJ1I+BJ2I
      CJFA=ABSF(CJFL)
      CJIA=ABSF(CJIL)
      JMCX=XMIN1F(CJFU,CJIU)
      JMCN=XMAX1F(CJIA,CJFA)
      JMNC=JMCN+1
      JMXC=JMCX+1
      IF (JMCX-JMCN) 61,62,62
   61 GO TO 172
   62 CONTINUE
      DO 210 N=1,4
      B=(OSC/RCF(N))**2
D     BK(1)=1.0
D     B1K(1)=1.0
D     B2K(1)=1.0
      DO 231 I=1,19
D     BK(I+1)=B*BK(I)
D     B1K(I+1)=(1.+B)*B1K(I)
D 231 B2K(I+1)=(1.+B*2.)*B2K(I)
      N11=MN11
      L1=ML1
      N22=MN22
      L2=ML2
      N33=MN33
      L3=ML3
      N44=MN44
      L4=ML4
D     CALL SLATED(R,B)
      DO 41 I=1,20
   41 RR(I,1,N)=R(I)
      N33=MN44
      L3=ML4
      N44=MN33
      L4=ML3
D     CALL SLATED(R,B)
      DO 42 I=1,20
   42 RR(I,2,N)=R(I)
  210 CONTINUE
      DO 173 JJ=JMNC,JMXC
      AJ=JJ-1
      DO 177 N=1,4
      DO 115 I=1,20
```

```
115 R(I)=RR(I,1,N)
    AL1F=BL1F
    AL2F=BL2F
    AL1I=BL1I
    AL2I=BL2I
    AJ1F=BJ1F
    AJ2F=BJ2F
    AJ1I=BJ1I
    AJ2I=BJ2I
    CALL CFORCE( EWF, ESF,R)
    E(N)=EWF
    VPS(N)=ESF
    DO 116 I=1,20
116 R(I)=RR(I,2,N)
    AL1I=BL2I
    AL2I=BL1I
    AJ1I=BJ2I
    AJ2I=BJ1I
    CALL CFORCE(QEWF,QESF,R)
    QV(N)=QEWF
    QVPS(N)=QESF
177 CONTINUE
    MA=AJ1I+AJ2I+AJ
    MM=XMODF(MA,2)
    IF (MM) 71,71,72
 71 QP=1.
    GO TO 252
 72 QP=-1.
252 CONTINUE
    FTE    =0.5*          (E(1)+QP*QV(1)-VPS(1)-QP*-VPS(1))
    FTO    =0.5*          (E(3)-QP*QV(3)-VPS(3)+QP*-VPS(3))
    FSE    =0.5*          (VPS(2)-QP*QVPS(2))
    FSO    =0.5*          (VPS(4)+QP*QVPS(4))
    CE=(FTE*VTE    +FSE*SE+FTO*TO+FSO*SO)
    CF(JJ)=CE
    FME(L,M,JJ)=CF(JJ)+ZERO
173 FME(M,L,JJ)=FME(L,M,JJ)
172 CONTINUE
174 CONTINUE
    DO 20 JJ=JAMIN,JAMAX
    IF (NTE) 66,67,67
 66 WRITE OUTPUT TAPE 3,69
 69 FORMAT(1X14HINITIAL MATRIX)
    DO 68 M=1,NE
 68 WRITE OUTPUT TAPE 3,303,(FME(L,M,JJ),L=1,NE)
 67 CONTINUE
    K=0
 28 DO 30 L=1,NE
    IF (FME(L,L,JJ)) 25,26,25
 26 K=K+1
    GO TO 30
 25 N=0
    DO 29 M=L,NE
    IF (FME(M,M,JJ)) 39,22,39
 22 N=N+1
    GO TO 29
 39 LL=L-K
    MM=M-K-N
```

```
      A(LL,MM)=FME(L,M,JJ)
      A(MM,LL)=A(LL,MM)
   29 CONTINUE
   30 CONTINUE
      NK=NE-K
      IF (NK) 601,601,602
  601 GO TO 603
  602 CONTINUE
      JA=JJ-1
      WRITE OUTPUT TAPE 3,301,JA
  301 FORMAT(1X2HJ=I2)
      WRITE OUTPUT TAPE 3, 374
  374 FORMAT(1X20HCENTRAL FORCE MATRIX)
      DO 302 J=1,NK
  302 WRITE OUTPUT TAPE 3,303,(A(I,J),I=1,NK)
  303 FORMAT(13F10.5)
      IF (NTE) 281,282,281
  281 GO TO 283
  282 IF (ND) 55,56,55
   55 READ INPUT TAPE 2,284,((ATEN(L,M),M=L,NK),L=1,NK)
      GO TO 57
   56 READ INPUT TAPE 2,284, (ATEN(L,L),L=1,NK)
  284 FORMAT(8F10.7)
   57 CONTINUE
      DO 285 L=1,NK
      DO 285 M=L,NK
      TENS(L,M)=VTEN*ATEN(L,M)
      TENS(M,L)=TENS(L,M)
      A(L,M)=A(L,M)+TENS(L,M)
  285 A(M,L)=A(L,M)
      WRITE OUTPUT TAPE 3, 377
  377 FORMAT(1X19HTENSOR FORCE MATRIX)
      DO 309 J=1,NK
  309 WRITE OUTPUT TAPE 3,303,(TENS(I,J),I=1,NK)
      WRITE OUTPUT TAPE 3, 378
  378 FORMAT(1X12HFINAL MATRIX)
      DO 333 J=1,NK
  333 WRITE OUTPUT TAPE 3,303,(A(I,J),I=1,NK)
  283 CONTINUE
      IF (NK-1) 75,75,76
   75 GO TO 20
   76 CALL EIGEN(A,VALU,NK,ME)
      WRITE OUTPUT TAPE 3,305
  305 FORMAT(11HEIGENVALUES,2X12HEIGENVECTORS)
      DO 304 J=1,NK
      WRITE OUTPUT TAPE 3,303,VALU(J),(A(I,J),I=1,NK)
  304 CONTINUE
  603 CONTINUE
   20 CONTINUE
   81 GO TO 80
      END
```

```
      SUBROUTINE CFORCE(EWF,ESF,R)
D     DIMENSION T(20),BI(20,20),BIN(20,20),DBI(20,20),P(20),Q(20),SQ(20)
D    1,SQF(20),DF(20),GJ(20),SQ2(20),FACT(20),RT(25,5),VPN(20,20),VP(20)
D    2,VN(20),R(20),BK(20),B1K(20),B2K(20)
     3,CK(20),  S(6),D(6),U(6),V(6),W(6),X(6),Y(6),Z(6),EW(16),ES(16)
     4,F(34),   VF(100),AM(100),VFF(100),WA(100),BA(100),SA(100),HA(100)
      COMMON T,BI,BIN,DBI,P,Q,N1,N2,N3,N4,L1,L2,L3,L4,SQ,SQ2,SQF,DF,FACT
     1,GJ,N13,N24,N11,N22,N33,N44,L11,L22,L33,L44,K1U,K2U,K3U,K1L,K2L,K3
     2L,     KL,KU,      AL1F,AL2F,AL1I,AL2I,AJ1F,AJ2F,AJ1I,AJ2I,AJ
     3,BK,B1K,B2K
      CJ=SQRTF((2.*AJ1F+1.)*(2.*AJ1I+1.)*(2.*AJ2F+1.)*(2.*AJ2I+1.))
      CL=SQRTF((2.*AL1F+1.)*(2.*AL1I+1.)*(2.*AL2F+1.)*(2.*AL2I+1.))
      V(1)=AL1F
      V(2)=AJ1F
      V(3)=AL2F
      V(4)=AJ2F
      V(5)=0.5
      V(6)=AJ
      W(1)=AL1I
      W(2)=AJ1I
      W(3)=AL2I
      W(4)=AJ2I
      W(5)=0.5
      W(6)=AJ
      RV=RACAH(V)
      RW=RACAH(W)
      EWS=0.0
      ESS=0.0
      LA=AL2F+AL2I
      LB=AL1F+AL1I
      L=XMINOF(LA,LB)
      K=L+1
      DO 101 M=1,K
      I=M-1
      S(1)=AJ1I
      S(2)=AJ1F
      S(3)=I
      S(4)=0.5
      S(5)=-0.5
      S(6)=0.0
      D(1)=AJ2I
      D(2)=AJ2F
      D(3)=I
      D(4)=0.5
      D(5)=-0.5
      D(6)=0.0
      U(1)=AJ1F
      U(2)=AJ1I
      U(3)=AJ2F
      U(4)=AJ2I
      U(5)=I
      U(6)=AJ
      EW(M)=R(M)*CLEBSH(S)*CLEBSH(D)*RACAH(U)
      EWS=EWS+EW(M)
      X(1)=AL1F
      X(2)=AL1I
      X(3)=I
      X(4)=0.0
      X(5)=0.0
```

```
      X(6)=0.0
      Y(1)=AL2F
      Y(2)=AL2I
      Y(3)=I
      Y(4)=0.0
      Y(5)=0.0
      Y(6)=0.0
      Z(1)=AL1F
      Z(2)=AL1I
      Z(3)=AL2F
      Z(4)=AL2I
      Z(5)=I
      Z(6)=AJ
      ES(M)=R(M)*CLEBSH(X)*CLEBSH(Y)*RACAH(Z)
  101 ESS=ESS+ES(M)
      NA=AJ2I+AJ2F+AJ
      NM=XMODF(NA,2)
      IF (NM) 31,31,51
   31 EWF=CJ*EWS
      ESF=2.*CJ*CL*RV*RW*ESS/(-4.)
      GO TO 251
   51 EWF=(-1.)*CJ*EWS
      ESF=(-2.)*CJ*CL*RV*RW*ESS/(-4.)
  251 CONTINUE
      RETURN
      END
```

```
      SUBROUTINE SLATED(R,B)
D     DIMENSION T(20),BI(20,20),BIN(20,20),DBI(20,20D,P(20),Q(20),SQ(20)
D    1,SQF(20),DF(20),GJ(20),SQ2(20),FACT(20),RT(25,5),VPN(20,20),VP(20)
D    2,VN(20),R(20),BK(20),B1K(20),B2K(20)
      COMMON T,BI,BIN,DBI,P,Q,N1,N2,N3,N4,L1,L2,L3,L4,SQ,SQ2,SQF,DF,FACT
     1,GJ,N13,N24,N11,N22,N33,N44,L11,L22,L33,L44,K1U,K2U,K3U,K1L,K2L,K3
     2L,      KL,KU,      AL1F,AL2F,AL1I,AL2I,AJ1F,AJ2F,AJ1I,AJ2I,AJ
     3,BK,B1K,B2K
      N1=N11-1
      N2=N22-1
      N3=N33-1
      N4=N44-1
      L11=L1+1
      L22=L2+1
      L33=L3+1
      L44=L4+1
      N13=N1+N3+1
      N24=N2+N4+1
      NL1=N1+L1+1
      NL2=N2+L2+1
      NL3=N3+L3+1
      NL4=N4+L4+1
      L112=L11+2
      L222=L22+2
      L332=L33+2
      L442=L44+2
D     RNL1=SQRTF((SQ2(L112)*DF(NL1))/(SQ2(N11)*FACT(N11)*(DF(L11)**2)))
D     RNL2=SQRTF((SQ2(L222)*DF(NL2))/(SQ2(N22)*FACT(N22)*(DF(L22)**2)))
D     RNL3=SQRTF((SQ2(L332)*DF(NL3))/(SQ2(N33)*FACT(N33)*(DF(L33)**2)))
D     RNL4=SQRTF((SQ2(L442)*DF(NL4))/(SQ2(N44)*FACT(N44)*(DF(L44)**2)))
D     RNL=RNL1*RNL2*RNL3*RNL4
      L24=L2+L4
      L241=L2+L4+1
      L242=L2+L4+2
      L243=L2+L4+3
      L13=L1+L3
      L131=L1+L3+1
      L132=L1+L3+2
      L133=L1+L3+3
D     CALL RADIAL (VPN,VP,VN)
      KU=XMIN0F(L241,L131)
      ML24=XMODF( L24,2)
      ML13=XMODF( L13,2)
      DO 101 I=1,20
D 101 R(I)=0.0
      IF (ML24-ML13) 71,72,71
   71 GO TO 200
   72 IF (ML24) 51,51,52
   51 KL=1
      GO TO 73
   52 KL=2
   73 DO 111 K=KL,KU,2
D     TRR=0.0
      DO 121 M=1,N13
      DO 121 N=1,N24
      IT=0.5*FLOATF(L13+2*(M-1)-(K-1))+1.
      JT=0.5*FLOATF(L24+2*(N-1)-(K-1))+1.
      IM=0.5*FLOATF(L13+2*(M-1)+(K-1))+1.
      MT=0.5*FLOATF(L13+2*(M-1)+L24+2*(N-1))+1.
```

```
      MU=XMINOF(IT,JT)
D     TTR=0.0
      DO 131 I=1,MU
      MTI=MT-I+1
      JT1=JT-I+1
      KI2=K+2*I-2
D     TTSD=P(I)* BI(IT,I)*BIN(MTI,JT1)*BK(K)*B1K(MT)MB2K(I)/(B1K(KI2)*B2
     1K(MT))
D 131 TTR=TTR+TTSD
D     TR=TTR*VPN(M,N)*DF(IM)*FACT(JT)/(SQ2(IM)*(1.+2.*B)*SQRTF(1.+2.*B)*
     116.)
D 121 TRR=TRR+TR
D 111 R(K)=TRR*RNL
  200 CONTINUE
      RETURN
      END
```

```
      SUBROUTINE EIGEN(A,VALU,N,M)
      DIMENSION A(20,20), B(20,20), VALU(20), DIAG(20), SUPERD(19),
     1          V(19), VALL(20), S(19), C(19), D(20), IND(20), U(20),
     2          DUMMY(478)
      EQUIVALENCE (DIAG,DUMMY), (SUPERD,DUMMY(21)), (VALL,D,DUMMY(40)),
     1            (V,S,DUMMY( 60)), (B,DUMMY( 79)), (IND,U), (II,MATCH),
     2            (TAU,BETA), (W,PRODS), (X,SMALLD), (ANORM,ANORM2)
C
C     CALCULATE NORM OF MATRIX
C
    3 ANORM2=0.0
    4 DO 6 I=1,N
    5 DO 6 J=1,N
    6 ANORM2=ANORM2+A(I,J)**2
    7 ANORM=SQRTF(ANORM2)
C
C     GENERATE IDENTITY MATRIX
C
    9 IF (M) 10, 45, 10
   10 DO 40 I=1,N
   12 DO 40 J=1,N
   20 IF(I-J) 35, 25, 35
   25 B(I,J)=1.0
   30 GO TO 40
   35 B(I,J)=0.0
   40 CONTINUE
C
C     PERFORM ROTATIONS TO REDUCE MATRIX TO JACOBI FORM
C
   45 IEXIT=1
   50 NN=N-2
   52 IF (NN) 890, 170, 55
   55 DO 160 I=1,NN
   60 II=I+2
   65 DO 160 J=II,N
   70 T1=A(I,I+1)
   75 T2=A(I,J)
   80 GO TO 900
   90 DO 105 K=I,N
   95 T2=COS*A(K,I+1)+SIN*A(K,J)
  100 A(K,J)=COS*A(K,J)-SIN*A(K,I+1)
  105 A(K,I+1)=T2
  110 DO 125 K=I,N
  115 T2=COS*A(I+1,K)+SIN*A(J,K)
  120 A(J,K)=COS*A(J,K)-SIN*A(I+1,K)
  125 A(I+1,K)=T2
  128 IF (M) 130, 160, 130
  130 DO 150 K=1,N
  135 T2=COS*B(K,I+1)+SIN*B(K,J)
  140 B(K,J)=COS*B(K,J)-SIN*B(K,I+1)
  150 B(K,I+1)=T2
  160 CONTINUE
C
C     MOVE JACOBI FORM ELEMENTS AND INITIALIZE EIGENVALUE BOUNDS
C
  170 DO 200 I=1,N
  180 DIAG(I)=A(I,I)
  190 VALU(I)=ANORM
  200 VALL(I)=-ANORM
```

```
  210 DO 230 I=2,N
  220 SUPERD(I-1)=A(I-1,I)
  230 V(I-1)=(SUPERD(I-1))**2
C
C     DETERMINE SIGNS OF PRINCIPAL MINORS
C
  235 TAU=0.0
  240 I=1
  260 MATCH=0
  270 T2=0.0
  275 T1=1.0
  277 DO 450 J=1,N
  280 W=DIAG(J)-TAU
  290 IF(T2) 300, 330, 300
  300 IF(T1) 310, 370, 310
  310 X=W*T1-V(J-1)*T2
  320 GO TO 410
  330 IF(T1) 335, 350, 350
  335 T1=-1.0
  340 X=-W
  345 GO TO 410
  350 T1=1.0
  355 X=W
  360 GO TO 410
  370 IF(V(J-1)) 380, 350, 380
  380 IF(T2) 400, 390, 390
  390 X=-1.0
  395 GO TO 410
  400 X=1.0
C
C     COUNT AGREEMENTS IN SIGN
C
  410 IF(T1) 425, 420, 420
  420 IF(X) 440, 430, 430
  425 IF(X) 430, 440, 440
  430 MATCH=MATCH+1
  440 T2=T1
  450 T1=X
C
C     ESTABLISH TIGHTER BOUNDS ON EIGENVALUES
C
  460 DO 530 K=1,N
  465 IF (K-MATCH) 470, 470, 520
  470 IF(TAU-VALL(K)) 530, 530, 480
  480 VALL(K)=TAU
  490 GO TO 530
  520 IF(TAU-VALU(K)) 525, 530, 530
  525 VALU(K)=TAU
  530 CONTINUE
  540 IF(VALU(I)-VALL(I)-5.0E-8) 570, 570, 550
  550 IF(VALU(I)) 560, 580, 560
  560 IF(ABSF(VALL(I)/VALU(I)-1.0)-5.0E-8) 570, 570, 580
  570 I=I+1
  575 IF(I-N) 540, 540, 590
  580 TAU=(VALL(I)+VALU(I))/2.0
  585 GO TO 260
C
C     JACOBI EIGENVECTORS BY ROTATIONAL TRIANGULARIZATION
```

```
C
  590 IF (M) 593, 890, 593
  593 IEXIT=2
  595 DO 610 I=1,N
  600 DO 610 J=1,N
  610 A(I,J)=0.0
  615 DO 850 I=1,N
  620 IF (I-1) 625, 625, 621
  621 IF (VALU(I-1)-VALU(I)-5.0E-7) 730, 730, 622
  622 IF (VALU(I-1)) 623, 625, 623
  623 IF (ABSF(VALU(I)/VALU(I-1)-1.0)-5.0E-7) 730, 730, 625
  625 COS=1.0
  628 SIN=0.0
  630 DO 700 J=1,N
  635 IF(J-1) 680, 680, 640
  640 GO TO 900
  650 S(J-1)=SIN
  660 C(J-1)=COS
  670 D(J-1)=T1*COS+T2*SIN
  680 T1=(DIAG(J)-VALU(I))*COS-BETA*SIN
  690 T2=SUPERD(J)
  700 BETA=SUPERD(J)*COS
  710 D(N)=T1
  720 DO 725 J=1,N
  725 IND(J)=0
  730 SMALLD=ANORM
  735 DO 780 J=1,N
  740 IF (IND(J)-1) 750, 780, 780
  750 IF (ABSF(SMALLD)-ABSF(D(J)))780, 780, 760
  760 SMALLD=D(J)
  770 NN=J
  780 CONTINUE
  790 IND(NN)=1
  800 PRODS=1.0
  805 IF (NN-1) 810, 850, 810
  810 DO 840 K=2,NN
  820 II=NN+1-K
  830 A(II+1,I)=C(II)*PRODS
  840 PRODS=-PRODS*S(II)
  850 A(1,I)=PRODS
C
C     FORM MATRIX PRODUCT OF ROTATION MATRIX WITH JACOBI VECTOR MATRIX
C
  855 DO 885 J=1,N
  860 DO 865 K=1,N
  865 U(K)=A(K,J)
  870 DO 885 I=1,N
  875 A(I,J)=0.0
  880 DO 885 K=1,N
  885 A(I,J)=B(I,K)*U(K)+A(I,J)
  890 RETURN
C
C     CALCULATE SINE AND COSINE OF ANGLE OF ROTATION
C
  900 IF (T2) 910, 940, 910
  910 X=SQRTF(T1**2+T2**2)
  920 COS=T1/X
  925 SIN=T2/X
```

```
930 GO TO (90,650), IEXIT
940 GO TO (160,910), IEXIT
950 END
```

G. FORTRAN Listing (3)

```
C     EIGENVALUES AND VECTORS FOR THE PARTICLE-HOLE INTERACTION
D     DIMENSION T(20),BI(20,20),BIN(20,20),DBI(20,20),P(20),Q(20),SQ(20)
D    1,SQF(20),DF(20),GJ(20),SQ2(20),FACT(20),RT(25,5),VPN(20,20),VP(20)
D    2,VN(20),R(20),BK(20),B1K(20),B2K(20)
      DIMENSION RR(20,2,4)  ,RCF(4),X(6),VALU(20) ,A(20,20),E(4),QV(4),
     1VPS(4),QVPS(4),ATEN(20,20),TENS(20,20),FME(20,20,16),CF(16)
      COMMON T,BI,BIN,DBI,P,Q,N1,N2,N3,N4,L1,L2,L3,L4,SQ,SQ2,SQF,DF,FACT
     1,GJ,N13,N24,N11,N22,N33,N44,L11,L22,L33,L44,K1U,K2U,K3U,K1L,K2L,K3
     2L,     KL,KU,     AL1F,AL2F,AL1I,AL2I,AJ1F,AJ2F,AJ1I,AJ2I,AJ
     3,BK,B1K,B2K
      READ INPUT TAPE 2,280,NTE
  280 FORMAT(I5)
      READ INPUT TAPE 2,202 ,OSC,VTEN
  202 FORMAT(2F10.5)
      WRITE OUTPUT TAPE 3,201,OSC,VTEN
  201 FORMAT(1X11HOSCILLATOR=F10.5,10X5HVTEN=F10.5)
      READ INPUT TAPE 2,4,     VTE,SE,TO,SO,(RCF(I),I=1,4)
    4 FORMAT(8F10.5)
      WRITE OUTPUT TAPE 3,4,     VTE,SE,TO,SO,(RCF(I),I=1,4)
D     BI(1,1)=1.0
D     DBI(1,1)=1.0
      DO 10 J=2,19
D     BI(J,1)=1.
D     DBI(J,1)=1.
      K=J
      DO 10 M=2,K
D     BI(J,M)=(FLOATF(J-M+1)/FLOATF(M-1))*BI(J,M-1)
D   10 DBI(J,M)=((FLOATF(J-M)*2.+3.)/(FLOATF(M)*2.-1.D)*DBI(J,M-1)
      DO 11 J=1,19
D     BIN(J,1)=1.
      K=J+1
      DO 11 M=2,K
D   11 BIN(J,M)=((FLOATF(J-M+2)-0.5)/FLOATF(M-1))*BIN(J,M-1)
D     P(1)=1.
D     Q(1)=1.
D     GJ(1)=1.
D     SQ(1)=1.
D     DF(1)=1.
D     SQ2(1)=1.
D     SQF(1)=1.
      DO 12 I=1,19
D     P(I+1)=-1.*P(I)
D     SQ(I+1)=-2.*SQ(I)
D     SQF(I+1)=4.*SQF(I)
D     DF(I+1)=(2.*FLOATF(I)+1.)*DF(I)
D     GJ(I+1)=(FLOATF(I)-0.5)*GJ(I)/(0.5+BT)
D     SQ2(I+1)=2.*SQ2(I)
D   12 Q(I+1)=-4.*Q(I)
D     FACT(1)=1.
      DO 129 M=2,19
D  129 FACT(M)=FLOATF(M-1)*FACT(M-1)
   80 READ INPUT TAPE 2,70,NE,ND,JAMIN,JAMAX
   70 FORMAT(4I5)
      ME=1
      DO 171 I=1,20
  171 VALU(I)=0.0
      DO 77 J=1,20
      DO 77 I=1,20
   77 A(I,J)=0.0
```

```
      DO 31 J=1,16
      DO 31 M=1,NE
      DO 31 L=1,NE
   31 FME(L,M,J)=0.0
      DO 32 J=1,16
   32 CF(J)=0.0
      DO 172 L=1,NE
  118 DO 172 M=L,NE
      READ INPUT TAPE 2,2,N11,L1,N22,L2,MN33,ML3,MN44,ML4
      READ INPUT TAPE 2,119,AL1F,AL2F,BL1I,BL2I,AJ1F,AJ2F,BJ1I,BJ2I,
     1ZERO
  119 FORMAT(8F5.1,F10.5)
    2 FORMAT(8I5)
      AJFL=AJ1F-AJ2F
      AJIL=BJ1I-BJ2I
      AJFU=AJ1F+AJ2F
      AJIU=BJ1I+BJ2I
      AJFA=ABSF(AJFL)
      AJIA=ABSF(AJIL)
      JMAX=XMIN1F(AJFU,AJIU)
      JMIN=XMAX1F(AJFA,AJIA)
      JMN=JMIN+1
      JMX=JMAX+1
      IF (JMAX-JMIN) 61,62,62
   61 GO TO 172
   62 CONTINUE
      DO 210 N=1,4
      B=(OSC/RCF(N))**2
D     BK(1)=1.0
D     B1K(1)=1.0
D     B2K(1)=1.0
      DO 231 I=1,19
D     BK(I+1)=B*BK(I)
D     B1K(I+1)=(1.+B)*B1K(I)
D 231 B2K(I+1)=(1.+B*2.)*B2K(I)
      N33=MN33
      L3=ML3
      N44=MN44
      L4=ML4
D     CALL SLATED(R,B)
      DO 41 I=1,20
   41 RR(I,1,N)=R(I)
      N33=MN44
      L3=ML4
      N44=MN33
      L4=ML3
D     CALL SLATED(R,B)
      DO 42 I=1,20
   42 RR(I,2,N)=R(I)
  210 CONTINUE
      DO 173 JJ=JMN,JMX
      AJ=JJ-1
      DO 177 N=1,4
      DO 115 I=1,20
  115 R(I)=RR(I,1,N)
      AL1I=BL1I
      AL2I=BL2I
      AJ1I=BJ1I
```

```
      AJ2I=BJ2I
      CALL CFORCE( EWF, ESF,R)
      E(N)=EWF
      VPS(N)=ESF
      DO 116 I=1,20
  116 R(I)=RR(I,2,N)
      AL1I=BL2I
      AL2I=BL1I
      AJ1I=BJ2I
      AJ2I=BJ1I
      CALL CFORCE(QEWF,QESF,R)
      QV(N)=QEWF
      QVPS(N)=QESF
  177 CONTINUE
      MA=AJ1I+AJ2I+AJ
      MM=XMODF(MA,2)
      IF (MM) 71,71,72
   71 QP=1.
      GO TO 252
   72 QP=-1.
  252 CONTINUE
      FTE    =0.5*            (E(1)+QP*QV(1)-VPS(1)-QP*-VPS(1))
      FTO    =0.5*            (E(3)-QP*QV(3)-VPS(3)+QP*-VPS(3))
      FSE    =0.5*            (VPS(2)-QP*QVPS(2))
      FSO    =0.5*            (VPS(4)+QP*QVPS(4))
      CE=VTE*(FTE    +FSE*SE+FTO*TO+FSO*SO)
  173 CF(JJ)=CE
      DO 172 JJ=JMN,JMX
      MAP=AJFU+AJIU
      MAM=XMODF(MAP,2)
      IF (MAM) 771,771,772
  771 AP=1.
      GO TO 773
  772 AP=-1.
  773 CONTINUE
      PHME=0.0
      X(1)=AJ2I
      X(2)=AJ1F
      X(3)=AJ1I
      X(4)=AJ2F
      X(6)=JJ-1
      DO 51 K=JMN,JMX
      X(5)=K-1
      RAC=RACAH(X)
      PHM=AP*FLOATF(2*(K-1)+1)*RAC*CF(K)
   51 PHME=PHME+PHM
      FME(L,M,JJ)=PHME+ZERO
  172 CONTINUE
      DO 20 JJ=JAMIN,JAMAX
      JA=JJ-1
      WRITE OUTPUT TAPE 3,301,JA
  301 FORMAT(1X2HJ=I2)
   66 WRITE OUTPUT TAPE 3,69
   69 FORMAT(1X14HINITIAL MATRIX)
      DO 68 M=1,NE
   68 WRITE OUTPUT TAPE 3,303,(FME(L,M,JJ),L=1,NE)
   67 CONTINUE
   28 DO 30 L=1,NE
```

```
      DO 29 M=L,NE
      A(L,M)=FME(L,M,JJ)
      A(M,L)=A(L,M)
   29 CONTINUE
   30 CONTINUE
      NK=NE
      WRITE OUTPUT TAPE 3, 374
  374 FORMAT(1X20HCENTRAL FORCE MATRIX)
      DO 302 J=1,NK
  302 WRITE OUTPUT TAPE 3,303,(A(I,J),I=1,NK)
  303 FORMAT(21F6.3)
      IF (NTE) 281,282,281
  281 GO TO 283
  282 IF (ND) 55,56,55
   55 READ INPUT TAPE 2,284,((ATEN(L,M),M=L,NK),L=1,NK)
      GO TO 57
   56 READ INPUT TAPE 2,284, (ATEN(L,L),L=1,NK)
  284 FORMAT(8F10.7)
   57 CONTINUE
      DO 285 L=1,NK
      DO 285 M=L,NK
      TENS(L,M)=VTEN*ATEN(L,M)
      TENS(M,L)=TENS(L,M)
      A(L,M)=A(L,M)+TENS(L,M)
  285 A(M,L)=A(L,M)
      WRITE OUTPUT TAPE 3, 377
  377 FORMAT(1X19HTENSOR FORCE MATRIX)
      DO 309 J=1,NK
  309 WRITE OUTPUT TAPE 3,303,(TENS(I,J),I=1,NK)
      WRITE OUTPUT TAPE 3, 378
  378 FORMAT(1X12HFINAL MATRIX)
      DO 333 J=1,NK
  333 WRITE OUTPUT TAPE 3,303,(A(I,J),I=1,NK)
  283 CONTINUE
      IF (NK-1) 75,75,76
   75 GO TO 81
   76 CALL EIGEN(A,VALU,NK,ME)
      WRITE OUTPUT TAPE 3,305
  305 FORMAT(11HEIGENVALUES,2X12HEIGENVECTORS)
      DO 304 J=1,NK
      WRITE OUTPUT TAPE 3,303,VALU(J),(A(I,J),I=1,NK)
  304 CONTINUE
   20 CONTINUE
   81 GO TO 80
      END
```

REFERENCES

1. L. W. Nordheim, Phys. Rev. 78, 294 (1950).
2. A. De-Shalit, Phys. Rev. 91, 1479 (1953).
3. D. Kurath, Phys. Rev. 91, 1430 (1953); D. M. Brink, Proc. Phys. Soc. (London) A67, 757 (1954); S. P. Pandya, Phys. Rev. 108, 1312 (1957).
4. N. D. Newby, Jr., and E. J. Konopinski, Phys. Rev. 115, 434 (1959).
5. S. G. Nilsson, Kgl. Danske Videnskab. Selskab, Mat.-fys. Medd. 29, No. 16 (1955).
6. H. Noya, A. Arima, and H. Horie, Suppl. Progr. Theoret. Phys. (Kyoto) 8, 33 (1958).
7. D. M. Brink and G. R. Satchler, Nuovo cimento 4, 549 (1956).
8. P. A. M. Dirac, Principles of Quantum Mechanics (Oxford University Press, Oxford, 1958), Ch. X.
9. J. C. Carter, W. T. Pinkston, and W. W. True, Phys. Rev. 120, 504 (1960).
10. S. S. Schweber, An Introduction to Relativistic Quantum Field Theory (Row, Peterson & Company, New York, 1961), Ch. 6., and references given in this book.
11. A. R. Edmonds, Angular Momentum in Quantum Mechanics (Princeton University Press, Princeton, 1957).
12. G. Racah, Phys. 63, 367 (1943).
13. M. E. Rose, Elementary Theory of Angular Momentum (John Wiley & Sons, Inc., New York, 1957), Ch. VI.
14. I. Talmi, Phys. Rev. 89, 1065 (1953).
15. A. de-Shalit and J. D. Walecka, Nucl. Phys. 22, 184 (1961).
16. Y. E. Kim, The Low-Energy States in Y^{90}, UCRL-10329, Feburary 22, 1963, submitted to Phys. Rev.
17. I. Talmi, Helv. Phys. Acta 25, 185 (1952).
18. K. W. Ford and E. J. Konopinski, Nucl. Phys. 9, 218 (1958/59).
19. N. Zeldes, Nucl. Phys. 2, 1 (1956/57).

20. W. M. Visscher and R. A. Ferrell, Phys. Rev. 107, 781 (1957).
21. K. A. Brueckner and J. L. Gammel, Phys. Rev. 109, 1023 (1958).
22. H. Bethe and J. Goldstone, Proc. Roy. Soc. (London) A238, 551 (1957).
23. W. W. True and K. W. Ford, Phys. Rev. 109, 1675 (1958).
24. J. F. Dawson, I. Talmi, and J. D. Walecka, Ann. Phys. (N. Y.) 18, 339 (1962).
25. H. Yukawa, Proc. Phys. Math. Soc. Japan 17, 48 (1935).
26. P. Cziffra and M. J. Moravcsik, Phys. Rev. 116, 226 (1959).
27. T. D. Spearman, Nuovo cimento 15, 147 (1960); Nuclear Phys. 16, 402 (1960); G. Breit, M. H. Hull, K. Lassila, and K. D. Pyatt, Phys. Rev. Letters 4, 79 (1960).
28. M. H. MacGregor, M. J. Moravcsik, and H. P. Stapp, Phys. Rev. 116, 1249 (1959).
29. J. Iwadare, S. Otsuki, R. Tamagaki, and W. Watari, Progr. Theoret. Phys. (Tokyo) 15, 86 (1956).
30. For references to the original literature see M. J. Moravcsik and H. P. Noyes, Ann. Rev. Nuclear Sci. 11, 95 (1961).
31. J. M. Blatt and M. H. Kalos, Phys. Rev. 92, 1563 (1953); S. Gartenhaus, ibid. 100, 900 (1955).
32. P. S. Signell and R. E. Marshak, Phys. Rev. 106, 832 (1957).
33. J. L. Gammel and R. M. Thaler, Phys. Rev. 107, 1337 (1957).
34. T. Hamada, Progr. Theoret. Phys. (Kyoto) 24, 126 (1960).
35. N. K. Glendenning and G. Kramer, Phys. Rev. 126, 2159 (1962).
36. J. L. Gammel and R. M. Thaler, Progr. Cosmic Ray Phys. 5, 99 (1960).
37. J. M. Blatt and J. D. Jackson, Phys. Rev. 76, 18 (1949).
38. M. H. Kalos, L. C. Biedenharn, and J. M Blatt, Nucl. Phys. 1, 233 (1956).
39. W. L. Alford, D. R. Kochler, and C. E. Mandeville, Phys. Rev. 123, 1365 (1961); L. Haskin and R. Vandenbosch, Phys. Rev. 123, 184 (1961); R. L. Heath, J. E. Cline, C. W. Reich, E. C. Yates, and E. H. Turk Phys. Rev. 123, 903 (1961); W. S. Lyon, J. S. Eldridge, and L. C. Bate, Phys. Rev. 123, 1747 (1961).

40. G. A. Bartholomew, P. J. Campion, J. W. Knowles, and G. Manning, Nucl. Phys. 10, 590 (1959).

41. K. W. Ford, Phys. Rev. 98, 1516 (1955); J. P. Elliot and A. M. Lane, Handbuch der Physik (Springer-Verlag, Berlin, 1957), Vol. 39, p. 241; R. K. Sheline, Physica 23, 923 (1957); N. H. Lazar, G. D. O'Kelley, J. H. Hamilton, L. M. Langer, and W. G. Smith, Phys. Rev. 110, 513 (1958).

42. B. F. Bayman, A. S. Reiner, and R. K. Sheline, Phys. Rev. 115, 1627 (1959); V. K. Thankappan and Y. R. Wagmare, Progr. Theoret. Phys. (Kyoto) 22, 459 (1959); I. Talmi and I. Unna, Nucl. Phys. 19, 225 (1960); V. K. Thankappan, Y. R. Waghmare, and S. P. Pandya, Progr. Theoret. Phys. 26, 22 (1961).

43. D. Strominger, J. M. Hollander, and G. T. Seaborg, Revs. Modern Phys. 30, 585 (1958).

44. F. R. Petersen and H. A. Shugart, Phys. Rev. 128, 1740 (1962).

45. F. R. Petersen and H. A. Shugart, Phys. Rev. 125, 284 (1962).

46. M. Bouten, M. Demeur, and H. Pollak, Phys. Radium 22, 697 (1961).

47. M. H. Brennan and A. M. Bernstein, Phys. Rev. 120, 927 (1960).

48. R. L. Preston, H. J. Martin, Jr. and M. B. Sampson, Phys. Rev. 121, 1741 (1961).

49. Y. E. Kim and J. O. Rasmussen, Energy Levels of Bi^{210} and Po^{210} and the Nuclear-Shell-Model Residual Force, UCRL-10707, March 11, 1963, submitted to Nucl. Phys.

50. J. R. Erskine, W. W. Buechner, and H. A. Enge, Phys. Rev. 128, 720 (1962).

51. M. H. L. Price, Proc. Phys. Soc. (London) A65, 773 (1952); N. Newby and E. J. Konopinski, Phys. Rev. 115, 434 (1959); J. Flores and P. A. Mello, Bull. Am. Phys. Soc. 8, 129 (1963), Abstract W5.

52. Yu. I. Kharitonov, L. A. Sliv, and G. A. Sogomonova, Nucl. Phys. 28, 210 (1961).

53. J. R. Erskine, Massachusetts Institute of Technology, private communication.

54. R. W. Hoff and J. M. Hollander, Phys. Rev. 109, 447 (1958).

55. P. Mukherjee and B. L. Cohen, Phys. Rev. 127, 1284 (1962).

55a. G. E. Lee-Whiting, Phys. Rev. 97, 463 (1955).

56. Jun-Ichi Fujita, Phys. Rev. 126, 202 (1962).

57. R. Feynman and M. Gell-Mann, Phys. Rev. 109, 193 (1958).

58. R. M. Spector, Nucl. Phys. 40, 338 (1963).

59. H. J. Mang, Lawrence Radiation Laboratory, private communication.

60. M. Redlich, Lawrence Radiation Laboratory, private communication.

61. S. S. Alpert, E. Lipworth, M. B. White, and K. F. Smith, Phys. Rev. 125, 256 (1962).

62. E. G. Funk, Jr., H. J. Prask, F. Schima, J. McNulty, and J. W. Mihelich, Phys. Rev. 129, 757 (1962).

63. B. Mottelson, Nordita Publ. No. 20 (1959), Cours de l'Ecole d'Ete de Physique Théorique des Houches (Dunod, Paris, 1959).

64. Z. Szymanski, Bull. Acad. Polon, Sci., Ser. Sci. Math. Astron. Phys. 7, 233 (1959).

65. J. Horton and R. Sherr, Phys. Rev. 90, 388(A) (1958).

66. J. W. Weale, Proc. Phys. Soc. (London) 68 A, 35 (1955).

67. L. G. Elliott, R. L. Graham, J. Walker, and J. L. Wolfson, Phys. Rev. 93, 356 (1954).

68. G. Schupp, H. Daniel, G. W. Eakins, and E. N. Jensen, Phys. Rev. 120, 189 (1960).

69. R. L. Graham and R. E. Bell, Can. J. Phys. 31, 377 (1953).

70. O. B. Nielsen, Kgl. Danske Videnskab. Selskab, Mat.-fys. Medd. 30, No. 16 (1955).

71. G. T. Emery and W. R. Kane, Phys. Rev. 118, 755 (1960).

72. W. C. Cobb submitted to Phys. Rev.

73. J. Hope and L. W. London, Phys. Rev. 101, 710 (1956).

74. R. B. Duffield and S. H. Vegors, Jr., Phys. Rev. 112, 1958 (1958).

75. S. Wahlborn, Nucl. Phys. 3, 644 (1957). Also see Proceedings of the International Conference on Nuclear Structure at Weizmann Institute of Science, Rehovoth, Israel, 1957, (North-Holland Publishing Co., Amsterdam, 1958).

76. D. E. Alburger and A. W. Sunyar, Phys. Rev. 99, 695 (1955).

77. Y. E. Kim, D. J. Horen, and J. M. Hollander, Nucl. Phys. 31, 447 (1962).

78. Warren G. Smith, I. Neutron-Deficient Isotopes in the Noble Metal Region. II. Conversion-Electron Spectra of Some Heavy Elements (Thesis), UCRL-2974, June 1955.

79. Royal G. Albridge, Jr., I. Nuclear Spectroscopic Studies in the Heaviest Element Region. II. An Accelerating Electron Spectrograph (Thesis), UCRL-8642, April 1960.

80. G. D. O'Kelly, The Spectrometric Determination of Some Beta-Particle and Conversion-Electron Energies (Thesis), UCRL-1243, May 1951.

81. Manufactured by the Pacific Electro-Nuclear Company, Culver City, California.

82. W. G. Smith and J. M. Hollander, Phys. Rev. 99, 42 (1955).

83. E. K. Hyde, M. G. Florence, and F. S. Stephens, Jr., UCRL-2813, December 1954.

84. T. Yamazaki, H. Ikegami, and M. Sakai, University of Tokyo Institute for Nuclear Study Report INS-32, May 1961.

85. S. Hultberg and R. Stockendal, Arkiv Fysik 14, 565 (1959).

86. S. Hultberg, Arkiv Fysik 15, 307 (1959).

87. L. A. Sliv and I. M. Band, Coefficients of the Internal Conversion of Gamma Radiation, Part I, K Shell. (USSR Academy of Sciences, Leningrad, 1956.)

88. M. E. Rose, Internal Conversion Coefficients (North-Holland Publishing Co., Amsterdam; Interscience Publishers Inc., N. Y., 1958).

89. R. D. Hill, E. Church, and J. W. Mihelich, Rev. Sci. Instr. 23, 523 (1952).

90. A. H. Wapstra, G. J. Nijgh, and R. Van Lieshout, Nuclear Spectroscopy Tables (North-Holland Publishing Co., Amsterdam; Interscience Publishers Inc., N. Y., 1959).

91. W. L. Alford, D. R. Kochler, and C. E. Mandeville, Phys. Rev., to be published.

92. L. Haskin and R. Vandenbosch, Phys. Rev. 123, 184 (1961).

93. R. L. Heath, J. E. Cline, C. W. Réich, E. C. Yates, and E. H. Turk, Phys. Rev. 123, 903 (1961).

94. W. S. Lyon, J. S. Eldridge, and L. C. Bate, Phys. Rev. 123, 1747 (1961).

95. G. Racah, Phys. Rev. 62, 438 (1942).

This report was prepared as an account of Government sponsored work. Neither the United States, nor the Commission, nor any person acting on behalf of the Commission:

A. Makes any warranty or representation, expressed or implied, with respect to the accuracy, completeness, or usefulness of the information contained in this report, or that the use of any information, apparatus, method, or process disclosed in this report may not infringe privately owned rights; or

B. Assumes any liabilities with respect to the use of, or for damages resulting from the use of any information, apparatus, method, or process disclosed in this report.

As used in the above, "person acting on behalf of the Commission" includes any employee or contractor of the Commission, or employee of such contractor, to the extent that such employee or contractor of the Commission, or employee of such contractor prepares, disseminates, or provides access to, any information pursuant to his employment or contract with the Commission, or his employment with such contractor.